APPLICATIONS AND FUNDAMENTAL STUDIES OF SELF-ASSEMBLED MONOLAYERS: CONDUCTING POLYMER DEPOSITION AND CHEMICAL FORCE MICROSCOPY

by

Lawrence Francis Rozsnyai

B. S., Chemistry
University of California, Berkeley
(1991)

Submitted to the Department of Chemistry
in Partial Fulfillment of the Requirements
for the Degree of

DOCTOR OF PHILOSOPHY

at the

MASSACHUSETTS INSTITUTE OF TECHNOLOGY

May, 1995

© 1995, Massachusetts Institute of Technology

Signature of Author_____
Department of Chemistry
May 26, 1995

Certified by_____
Mark S. Wrighton
Thesis Supervisor

Accepted by_____
Dietmar Seyferth
Chairman, Departmental Committee on Graduate Students

ARCHIVES
MASSACHUSETTS INSTITUTE
OF TECHNOLOGY
JUN 12 1995

This doctoral thesis has been examined by a Committee of the Department of Chemistry as follows:

Professor Alan Davisor._____
Chairman

Professor Mark S. Wrighton_____
Thesis Supervisor

Professor Stephen J. Lippard_____

APPLICATIONS AND FUNDAMENTAL STUDIES OF SELF-ASSEMBLED MONOLAYERS: CONDUCTING POLYMER DEPOSITION AND CHEMICAL FORCE MICROSCOPY

by

Lawrence Francis Rozsnyai

Submitted to the Department of Chemistry on May 26, 1995,
in partial fulfillment of the requirements for the
Degree of Doctor of Philosophy in Chemistry

ABSTRACT

Chapter One **An Introduction to Self-Assembled Monolayers**

A brief summary of the formation, structure, and characterization of self-assembled monolayers is given. The use of aryl azide as a photosensitive terminal group in self-assembled monolayers to form surface patterns and the motivations for the studies presented in future chapters are also presented.

Chapter Two **Selective Deposition of Conducting Polymers via Monolayer Photopatterning**

Upon electropolymerization of the corresponding monomer, patterns of polyaniline, poly(3-methylthiophene), or polypyrrole replicate the pattern formed by selective irradiation of a photosensitive monolayer confined to an electrode surface. Irradiation of monolayers of di-11-(4-azidobenzoate)-1-undecyl disulfide, **I**, on Au in the presence of various primary or secondary amines results in the attachment of the amine in very high yields. Irradiation of Au-**I** substrates through a mask results in a patterned monolayer. Electrodeposition of aniline from aqueous solution, or 3-methylthiophene or pyrrole from CH_3CN, results in polymer deposition preferentially on the non-irradiated regions of the surface. Polymer patterns are characterized by optical microscopy and by stylus profilometry. Cyclic voltammetry and X-ray photoelectron spectroscopy are used to measure deposition contrast, and show that under certain electrochemical conditions the ratio of polymer deposition on non-irradiated monolayer regions to irradiated monolayer regions is greater than 1000:1. Cyclic voltammetry of the monomers, $Fe(CN)_6^{3-/4-}$, and N,N,N',N'-tetramethyl-1,4-phenylenediamine$^{2+/+/0}$ shows that electron transfer rates are attenuated in monolayers of Au-**I** compared to bare Au, and are decreased further in monolayers of **I** irradiated in dibutyl- or dioctylamine. Differences in electron transfer through these monolayers agree with the polymer patterning results and are shown to be the principal reason for selective polymer deposition on these photopatterned monolayer substrates.

Chapter Three **Controlling the Adhesion of Conducting Polymer Films with Patterned Self-Assembled Monolayers**

Polyaniline and poly(3-methylthiophene) films may be selectively transferred from metal electrodes to flexible, insulating supports to form high-resolution polymer patterns. Irradiation of self-assembled monolayers (SAMs) of di-11-(4-azidobenzoate)-1-undecyl disulfide, **I**, on Au in the presence of various primary or secondary amines results in the attachment of the amine in very high yields. Irradiation of Au-**I** substrates through a mask results in a patterned monolayer. Electrodeposited polymers of aniline and 3-methylthiophene initially replicate the SAM pattern, and coat the entire substrate as electropolymerization continues. The interfaces between the polymer film and distinct regions of the SAM pattern differ in adhesion and correlate with the surface free energy of the monolayer terminal group, as determined by adhesive tape peel tests. Peeling adhesive tape from polymer films deposited on patterned SAM samples results in transfer of the original polymer pattern from the electrode to the tape. The transferred polymer films are conducting ($\sigma \approx 10^{-4}\ \Omega^{-1}$/cm for polyaniline) and features on the near-micron scale can be transferred successfully.

Chapter Four **An Introduction to Chemical Force Microscopy**

The principals of adhesion and friction forces between solids are reviewed, and a brief introduction to atomic force microscopy (AFM) is given. The ideas behind chemical force microscopy (CFM) are then presented. The placement of known molecules on the AFM probe tip and sample makes it possible to use CFM to study the chemical basis of adhesion and friction, to probe quantitatively the interactions between specific molecular groups, and to acquire high-resolution "chemical maps" of heterogeneous surfaces.

Chapter Five **Functional Group Imaging by Chemical Force Microscopy**

The first example of functional group imaging by chemical force microscopy is presented. Using a force microscope, the adhesive and friction forces have been measured between molecularly modified probe tips and organic monolayers terminating in a lithographically defined pattern of distinct functional groups. The strength of adhesive interactions between CH_3/CH_3, CH_3/COOH and COOH/COOH tip/sample functional groups follows the trend expected chemically, and correlate directly with friction images of surfaces patterned with these groups. Thus, by monitoring the friction between a specifically functionalized tip and sample, it is possible to produce friction images which display predictable contrast and correspond to the spatial distribution of functional groups on the sample surface. Applications of this chemically sensitive imaging technique are discussed.

Chapter Six **Chemical Force Microscopy: Using Chemically-Modified Tips to Quantify Adhesion, Friction, and Functional Group Distributions in Self-Assembled Monolayers**

A detailed account of chemical force microscopy is given. Chemical force microscopy (CFM) has been used to measure adhesion and friction forces between probe tips and substrates covalently modified with self-assembled monolayers (SAMs) that terminate in distinct functional groups. Probe tips have been modified with SAMs using a procedure that involves coating commercial Si_3N_4 cantilever/tip assemblies with a thin

layer of polycrystalline Au followed by immersion in a solution of a functionalized thiol. This methodology provides a reproducible means for endowing the probe with different chemical functional groups. The spring constants and radii of the chemically modified cantilever/tip assemblies have been characterized to allow for quantitative friction and adhesion measurements. Au-coated Si substrates have been treated with functionalized thiols to produce SAM-coated substrates terminating in different chemical groups. A force microscope has been used to characterize the adhesive interactions between probe tips and substrates that have been modified with SAMs which terminate with COOH and CH_3 functional groups in EtOH. Force vs. distance curves recorded in EtOH show that the adhesion force between tip/sample functional groups decreases as follows: COOH/COOH > CH_3/CH_3 > COOH/CH_3. The measured adhesion forces agree well with predictions of the Johnson, Kendall, and Roberts (JKR) theory of adhesive contact, and show that the observed adhesion forces correlate with the surface free energy of the molecular groups in EtOH. The friction force between tips and samples modified with COOH and CH_3 groups has also been measured as a function of applied load. The magnitude of the friction force, and the friction coefficient, were found to decrease with different tip/sample functionalities: COOH/COOH > CH_3/CH_3 > COOH/CH_3. Friction forces between different chemical functional groups thus correlate directly with the adhesion forces between these same groups. Specifically, high friction is observed between groups that adhere strongly, while low friction is observed between weakly interacting functional groups. The dependence of friction forces on the tip and sample functionality is shown to be the basis of CFM in which lateral force images are interpreted in terms of the strength of both adhesive and frictional interactions between different chemical groups.

Chapter Seven **Chemical Force Microscopy: Measuring Adhesion, Friction, and Functional Group Distributions in Aqueous Media**

Chemical force microscopy (CFM) has been used to probe the interactions between acid and base groups in water. The chemical groups are localized on the probe tip and substrate via thiol or silane monolayers. Adhesion forces between CH_3/CH_3, COOH/COOH, and COOH/NH_2 tip/sample functional groups have been measured. Force vs. distance curves recorded between COOH groups on the tip and sample as a function of ionic strength show that the interaction strength decreases with increasing salt concentration. The adhesion force was also measured as a function of solution pH. The observed trend is used to support a recently proposed structural model of COOH-terminated SAMs on Au. In most cases, adhesion between tip/sample functional groups in water correlates with friction. A friction image of a sample patterned with COOH and NH_2 groups taken with a tip terminating in COOH groups is presented. Specific intermolecular interactions account for contrast in this image demonstrating the ability of CFM to generate functional group images in water for the first time.

Thesis Supervisor: Mark S. Wrighton
Title: Provost and CIBA-Geigy Professor of Chemistry

The leading future of American science, however, and that which most distinctly characterizes it, is its utilitarianism....It may readily be conceded that the man who discovers nothing himself, but only applies useful purposes the principles which others have discovered, stands upon a lower plane than the investigator. But when the investigator becomes himself the utilizer; when the same mind that made the discovery contrives also the machine by which it is applied to useful purposes,—the combined achievement must be ranked as superior to either of its separate results.

from "The Future of American Science" *Science* **1883**, *1*, 1.

The value the world sets upon motives is often grossly unjust and inaccurate. Consider, for example, two of them: mere insatiable curiosity and the desire to do good. The latter is put high above the former, and yet it is the former that moves one of the most useful men the human race has yet produced: the scientific investigator. What actually urges him on is not some brummagem idea of Service, but a boundless, almost pathological thirst to penetrate the unknown, to uncover the secret, to find out what has not been found out before. His prototype is not the liberator releasing slaves, the good Samaritan lifting up the fallen, but a dog sniffing tremendously at an infinite series of rat-holes.

"The Scientist" Henry Louis Mencken, 1919.

ACKNOWLEDGMENTS

Since arriving at MIT, I have felt it both a challenge and a privilege to work for Professor Wrighton. I thank Mark for providing me with a well-equipped, sometimes even over-funded laboratory in which to work, a wealth of intriguing research interests from which to choose, and a well-trained though curious collection of students from whom to learn. Over the past years Mark has given me an appreciation of the written and spoken word, as well as a heightened awareness of detail. Most importantly, he has given me tremendous freedom in my graduate studies, with just enough guidance to keep me afloat, and has never doubted in my ability to succeed on my own.

Working in the Wrighton group was seldom easy, and I credit three people in particular for their early contribution to my learning and well-being: Eric Wollman showed me (whether I wanted him to or not) how to do things in lab—from running columns to performing simple reactions (everything in THF?) to preparing my first research reports and group meetings—in an exceedingly practical way. Cantankerous and short on explanation ("Why are we doing this, Eric?" "Why does a dog lick himself?" he would reply), Eric took it upon himself to give me the supervision I needed. For this chore, I am grateful. If Eric taught me how to do things, Dan Frisbie taught me how to think about them. In Dan's mind, no experiment was ever a waste. "Nothing worked today, but I feel good because now we know that something is wrong" seemed to be his maxim in the event of apparent failure. Dan's optimism countered my realism (well, *pessimism* perhaps) and did well to make me realize that all efforts in the lab should be meaningful. His research style and ability to ask probing, insightful questions were genuinely inspiring. Working together in the lab, we would call ourselves the kludge-masters, letting nothing stand in our way and reducing complex set-ups to simple concoctions using often only what was at arm's reach. Such was the spirit of conceptual experiments that exercised our intellect and imagination, and formed the basis of an active collaboration a few years later. I also thank Yoko Kato, who has been a good friend for the past four years. In my first winter, I was almost overcome by the desire to flee MIT's gray, cramped, industrial, burned-out surroundings and return to glorious California. Luckily I met Yoko, and spring had arrived. I value our friendship, admire her ability to cultivate the fine and simple points in life, and hope our friendship remains strong despite our geographic and cultural distance.

Without help and companionship from members of the Wrighton Group, both past and present, I wouldn't have made it through alive. (I was going to write "sane" but I suppose that point is arguable.) Of the odd but inspiring characters I first met in the group, I remember most Tayhas Palmore, and credit (and blame) her for encouraging me to join. Unfortunately she all too efficiently graduated, completed a postdoc at a little-known school down the street, and returned to sunny California. I consider her footsteps as ones to follow in, and only hope I can go as far as she has. Eric Lee, my first and only bench-mate, helped me initially to get to a working speed in the lab, and taught me the details of the daily grind. Though our collaborative project never got off the ground, I'll remember and appreciate his level-headed outlook, cool style, and nuggets of sound, practical advice. To past members and visiting scientists, I thank you for your periodic, well-timed encouragement and tireless technical advice. To Mike Wolf for his practicality, efficiency, and spontaneous stories (especially about RB); Ivan Lorkovic for his scientific analysis, taste in music, scores on vits, and ...uh...um...; Dave Albagli for his teachings both at the chalkboard and on the ice; Chris McCoy for his electrochemistry monologues, unequaled caffeine tolerance, and demonstrations of strapping it on; and Ron Duff for his lingo, dedication to the physical condition and organization of the lab, and cheerful amusement and tunes during the most rancid moments, I salute you all.

Many a time I have felt like the little kid on the block, and I will always appreciate and remember the help you all gave me throughout my graduate years.

The expertise of MIT's technical staff and the ability of MIT to attract truly talented people makes it an excellent place to do research. I especially thank Rich Perilli for his unstoppable help and corny jokes, and Felice Frankel for attending my departmental seminar, giving my work its much wanted artistic advantage, and landing us a cover picture. Frequently Christine Graves, as Mark's assistant for most of his tenure as Provost, helped to squeeze me into his schedule and warn us of his whereabouts. On a daily basis, Dena Groutsis has helped with group administration and finance, and has generally made it very easy to get things done with a minimum amount of hassle or delay (but often with a requisite amount of confusion).

As conspirators in research, bewilderment, and fun, I thank wholeheartedly Dan Frisbie, Alex Noy, and Dmitri Vezenov for a rich, stimulating, and rewarding collaborative research project. In the labs supervised by professor Lieber at Harvard (to whom I am also grateful), long hours, harsh words, giddy grins of disbelief, and countless sandwiches from "the Pain" went towards creating chemical force microscopy. Dan, Alex, and Dmitri all contributed greatly to Part Two of this Thesis, and their help and contribution cannot be underestimated. Collaborations should always be this good! To you all, I owe a big thinks!

The community in academic chemistry is well known to be close. Fittingly, I have shared an apartment with fellow graduate students for the last three years and between one bathroom for the four of us, a separate hot and cold faucet for all but the past few months, and an unexplainable amount of dust, it's a wonder that things worked out so well. Although we don't overlap for more than five minutes a week, I thank Linda Doerrer, who has always been attune to my moods, for never hesitating to giving me a pat on the back when she was probably in need the need of at least two (and for her late-night, almost autonomic lectures about X-ray diffraction, not to mention for putting away the dishes at 5:30 every morning). Jonathan Wilker and I compose a weird study in contrasts—we are in perpetual counterbalance with an eerie mutual understanding. I appreciate his advice about paying attention to the simple joys of everyday life, his pleas to relax and be happy, and will always remember him for being, among chemists, the silliest, most gaudy, and perpetually cheerful ham I ever knew. James White has also given me a new perspective. With an excellent CD collection and the largest assortment of random facts lodged in his brain, he has been enjoyable company—as long as he's not watching that damned TV!

After clinching a postdoctoral position on—of all places—an airplane, it occurred to me that good fortune has been with me at several pivotal moments in my professional life. Call it the influence of God, good luck, or a butterfly's wings in the Sahara; to Him, Her, or It, I am humbly thankful for the past and eagerly hopeful for the future.

I finally and most strongly thank my parents, Jean and Balazs, for their support throughout the years. Though they naturally guided me towards the sciences in my childhood, they pushed me to do my best in whatever I chose to do as I climbed the educational ladder. I hope that I followed their examples well. For their unending encouragement and love, it is to them that I dedicate this Thesis.

TABLE of CONTENTS

ABSTRACT 3

ACKNOWLEDGMENTS 7

LIST of FIGURES 11

LIST of SCHEMES 18

LIST of TABLES 20

PART ONE **An Application of Self-Assembled Monolayers: Selective Electrodeposition of Conducting Polymers** 21

CHAPTER ONE An Introduction to Self-Assembled Monolayers 22

Text 23

References (with titles) 54

CHAPTER TWO Selective Deposition of Conducting Polymers via Monolayer Photopatterning 63

Introduction 64

Experimental Section 67

Results and Discussion 70

Conclusions 99

References 100

CHAPTER THREE Controlling the Adhesion of Conducting Polymer Films with Patterned Self-Assembled Monolayers 103

Introduction 104

Experimental Section 105

Results and Discussion 107

Conclusions 115

References 116

PART TWO **Fundamental Studies of Self-Assembled Monolayers: Measuring Adhesion and Friction at the Molecular Scale** 118

CHAPTER FOUR An Introduction to Chemical Force Microscopy 119
Text 120
References (with titles) 132

CHAPTER FIVE Functional Group Imaging by Chemical Force Microscopy 135
Introduction 136
Results and Discussion 138
Conclusions 149
References 151

CHAPTER SIX Chemical Force Microscopy: Using Chemically-Modified Tips to Quantify Adhesion, Friction, and Functional Group Distributions in Self-Assembled Monolayers 155
Introduction 156
Experimental Section 160
Results and Discussion 163
Conclusions 190
Appendix 192
References 195

CHAPTER SEVEN Chemical Force Microscopy: Measuring Adhesion, Friction, and Functional Group Distributions in Aqueous Media 201
Introduction 202
Experimental Section 204
Results and Discussion 205
Conclusions 221
References 222

PUBLICATIONS 225

BIOGRAPHICAL NOTE 226

LIST of FIGURES

PART ONE

CHAPTER ONE

Figure 1.1 33
A photograph of polyaniline selectively electrodeposited on a large Au-coated Si substrate. The polyaniline pattern (dark green) replicates the pattern initially generated on a photosensitive SAM.

Figure 1.2 44
XPS spectra of the N 1s regions of (a) Au-**I** and (b) Au-**I** irradiated in the presence of $[CH_3(CH_2)_3]_2NH$. Complete loss of the high binding energy peak upon irradiation indicates complete loss of azide. The ratio of total peak area before and after irradiation can be used to estimate the yield of reaction, which is ~80% on this sample.

Figure 1.3 47
An example of electrochemical SAM analysis. Cyclic voltammograms of an Au electrode coated with a SAM of **I** taken (a) before and (b) after irradiation in the presence of an amine attached to ferrocene are shown. Integration of the anodic wave yields a coverage of 3.3×10^{-10} mol/cm^2, roughly a monolayer of ferrocene groups, indicating almost 100% photoattachment of amine on this sample.

Figure 1.4 50
An optical micrograph of a patterned Au-**I** substrate irradiated through a lithographic mask in the presence of $(HOCH_2CH_2)_2NH$. As the sample is cooled in a humid environment, water droplets spread and coalesce on irradiated, OH-terminated areas of the SAM pattern. Condensed water forms beads on the surrounding unirradiated, hydrophobic regions. The hydrophilic lines in the condensation image are 100 μm wide; the features in the middle of the image are 50 μm wide.

CHAPTER TWO

Figure 2.1 72
Optical micrographs of polyaniline, poly(3-methylthiophene) and polypyrrole patterns formed by oxidizing the monomers on patterned SAM substrates, as described in the text. The dark regions correspond to polymer deposited on non-irradiated SAMs of **I**. The light regions contain little or no polymer and correspond to Au-**I** SAMs irradiated in the presence of $[CH_3(CH_2)_7]_2NH$. The microstructures in the bottom micrographs are 4 μm center-to-center.

Figure 2.2 74
Stylus profilometry traces of (three upper traces) the low resolution and (three lower traces) high resolution microline features. The line profiles are taken from the same samples shown in Figure 2.1.

Figure 2.3 77
A comparison of N 1s and Au 4f XPS spectra of a polyaniline pattern: (a) a polyaniline-coated region showing one N peak and strongly attenuated Au peaks; (b), (c) a region without polyaniline showing N and Au peaks, consistent with a monolayer of irradiated aryl azide, respectively. The Au 4f peak of the polyaniline region is completely attenuated and is not shown.

Figure 2.4 81
Cyclic voltammetric plots of (a) polyaniline, (b) poly(3-methylthiophene), and (c) polypyrrole patterns. Solid lines (—) are voltammograms from regions of Au-**I** SAMs; dashed lines (- -) are voltammograms from regions of Au-**I** SAMs irradiated in the presence of $[CH_3(CH_2)_7]_2NH$.

Figure 2.5 85
Current vs. potential curves for aniline (0.11 M in aqueous 0.85 M H_2SO_4, 0.25 M $NaHSO_4$). Each point (taken from a linear sweep voltammogram at 200 mv/s, 0.0-1.2 V vs. SCE) is the average of at least four measurements from freshly prepared samples. Curves are meant to guide the eye only.

Figure 2.6 87
Current vs. potential curves for 3-methylthiophene (0.10 M in CH_3CN, 0.1 M [*n*-$Bu_4N]PF_6$). Each point (taken from a linear sweep voltammogram at 200 mv/s, 0.0-1.7 V vs. Ag wire) is the average of at least two measurements from freshly prepared samples. Curves are meant to guide the eye only.

Figure 2.7 89
Current vs. potential curves for pyrrole (0.14 M in CH_3CN, 0.1 M [*n*-$Bu_4N]PF_6$). Each point (taken from a linear sweep voltammogram at 200 mv/s, 0.0-1.2 V vs. Ag wire) is the average of at least two measurements from freshly prepared samples. Curves are meant to guide the eye only.

Figure 2.8 91
Current vs. potential plots for $Fe(CN)_6^{3-/4-}$ (1.0 mM in aqueous polymerization solution, 200 mV/s) on bare Au and various homogeneous SAM surfaces.

Figure 2.9 93
Current vs. potential plots for $TMPD^{2+/+/0}$ (1.0 mM in CH_3CN polymerization solution, 200 mV/s) on bare Au and various homogeneous SAM surfaces.

Figure 2.10 98
Current vs. potential curves for aniline (0.11 M in aqueous 0.85 M H_2SO_4, 0.25 M $NaHSO_4$) on various SAM surfaces. Each point (taken from a linear sweep voltammogram at 200 mv/s, 0.0-1.2 V vs. SCE) is the average of at least four measurements from freshly prepared samples. Curves are meant to guide the eye only.

CHAPTER THREE

Figure 3.1 112
Micrographs of polyaniline on patterned Au electrodes. Patterns were made by irradiating an Au-**I** SAM in the presence of $(HOCH_2CH_2)_2NH$ for two minutes. The square-shaped features are 10 x 10 μm^2 and terminate in OH. The sample to the left shows polymer selectively depositing on the unirradiated regions of the sample, and beginning to deposit on the irradiated regions. Continued electropolymerization results in complete polymer coverage of these areas. Adhesive tape is applied to the sample to selectively remove polymer from the unirradiated regions, as shown in the sample at the right.

Figure 3.2 114
Patterned Au and adhesive tape samples containing (left) patterned polyaniline and (right) poly(3-methylthiophene) films. The SAM patterns were made using $(HOCH_2CH_2)_2NH$ (see text). The mask used in fabrication of the sample was originally designed for use in the fabrication of microelectrodes; the small features range in size from 2-100 μm. The SAMs in these areas terminate in OH and are hydrophilic. Transfer of polymer film from hydrophobic regions of the Au sample to the adhesive tape is successful for both polymers. Optical microscopy has identified features replicating those of the mask of near-micron resolution (~2 μm) on both adhesive tape samples.

PART TWO

CHAPTER FOUR

Figure 4.1 126
A schematic illustration of an AFM. The sample rests on a piezoelectric crystal which is used to control the separation between the sample and the tip, and to scan the sample laterally. The tip rests at the end of a long, flexible cantilever. Normal forces (height) and lateral forces (friction) are detected by monitoring the deflection of a light beam that is reflected from the backside of the cantilever into a position-sensitive photodiode.

CHAPTER FIVE

Figure 5.1 140
(A) Schematic of the surface modification procedure and a condensation image corresponding to a typical sample. Patterned sample surfaces containing lithographically defined hydrophilic and hydrophobic regions were prepared as previously described.[27] Briefly, Au-coated Si(100) substrates were immersed in 1 mM methylcyclohexane solutions of di-11-(4-azidobenzoate)-1-undecyl disulfide to yield a photosensitive monolayer. Irradiation of these substrates with UV-light ($\lambda > 260$ nm) through a mask and a thin film of ethyl 4-aminobutyrate yielded ethyl ester termination in the irradiated regions of the sample. The sample was then irradiated a second time through a quartz plate and thin film of dioctylamine to yield methyl termination in the previously unreacted areas of the sample. Lastly, the ethyl ester groups were converted to COOH groups by hydrolysis. The condensation image illustrating the spatial pattern of hydrophobic (CH_3) and hydrophilic (COOH) terminated regions in the sample was recorded with an optical microscope while observing the condensation of water vapor onto the cooled sample surface.[28] The water preferentially wets the hydrophilic (COOH) terminated regions of the sample surface. (B) Modification of the cantilever/tip assembly with a specific functional group. Gold-coated Si_3N_4 cantilever/tip assemblies[18] were immersed in 1 mM ethanolic solutions of either octadecylmercaptan or 11-mercapto-undecanoic acid for 2 h to form covalently bound monolayers that were terminated with either hydrophobic (CH_3) or hydrophilic (COOH) functional groups. The specific case of a tip terminating with COOH groups is shown. (C) Schematic views of the experiment. The inset illustrates the interactions between a tip terminating in COOH groups and patterned sample terminating in both CH_3 and COOH groups.

Figure 5.2 142
Typical force vs. displacement curves recorded between a COOH-terminated tip and sample, a CH_3-terminated tip and COOH-terminated sample, and a CH_3-terminated tip and sample in EtOH using a Nanoscope III LFM.

Figure 5.3 146-148
(A) Optical condensation image of a patterned sample. The bright, raised areas in this image correspond to liquid H_2O that has condensed on the hydrophilic (COOH-terminated) regions of the sample. (B) Force microscope image of the sample topography of the same surface pattern as in (A) recorded using a probe-tip terminated with hydrophobic (CH_3) functional groups. As expected, there is little difference in the topography observable between the CH_3- and COOH-terminated regions of the sample. Similar topographic images were also recorded using COOH-terminated tips. (C) Image of the friction force recorded simultaneously with the topography in (B). The bright regions correspond a high friction force, while the dark regions correspond to a lower friction force. In this image, which was recorded with a CH_3-terminated tip, high friction is observed over CH_3-terminated regions of the sample. (D) Image of the friction force recorded between a COOH-terminated tip and a similar region of the sample as in (A-C). In this image, high friction is observed over COOH-terminated regions of the sample. Images (B)-(D) were acquired under EtOH with an applied load of 4 nN and a scan rate

of 3 Hz. Similar results have been obtained using scan rates between 1 and 10 Hz and applied loads from 3-10 nN.

CHAPTER SIX

Figure 6.1 159
Schematic drawing of a CFM setup. The sample rests on a piezoelectric tube which can be finely moved laterally (x and y) and vertically (z). A laser beam is reflected from the backside of the tip into a photodiode to measure two types of tip-surface interactions: As the sample is rastered under the tip, the tip will move up and down in response to surface topography, resulting in the atomic force (height) signal. The tip will also rock back and forth in response to friction, yielding the lateral force (friction) signal. The inset illustrates the chemically specific interactions presented in this report. An Au-coated COOH-terminated tip contacts the boundary of CH_3- and COOH-terminated region of the sample.

Figure 6.2 165
Scanning electron microscopy images of an Au-coated force microscopy probe tip. The inset shows the high magnification image of the area near the end of the tip.

Figure 6.3 167
Plot of the load mass vs. $1/(2\pi\nu)^2$ of tip/cantilever assemblies using adsorbed W balls of varying size. The force constants are 0.07 and 0.12 N/m for native and Au-coated cantilevers, respectively.

Figure 6.4 170
Representative force versus displacement curves recorded for CH_3/COOH, CH_3/CH_3, and COOH/COOH tip/sample termini using sharp tips ($R \approx 60$nm.). All data were obtained in EtOH solution using the fluid cell.

Figure 6.5 172
Histograms showing the number of times that a given adhesion force was observed in repetitive measurements using functionalized samples and "sharp" tips (~60 nm radii) terminating in (a) COOH/COOH, (b) CH_3/CH_3, and (c) CH_3/COOH. Each histogram represents more than 300 repetitive tip-sample contacts for one functionalized tip. All measurements were made in EtOH solution.

Figure 6.6 177
A typical friction loop recorded on a COOH-terminated sample using COOH-modified probe tip in EtOH solution. The applied load was 17 nN.

Figure 6.7 179
Summary of the friction force vs. applied load data recorded for functionalized samples and tips terminating in COOH/COOH, CH_3/CH_3 and COOH/CH_3 in EtOH.

Figure 6.8 183
Condensation image of H_2O on a photopatterned SAM substrate showing the repeat pattern of 10 x 10 μm^2 squares terminating in COOH on a background terminating in CH_3. H_2O condenses only on the hydrophilic COOH-terminated regions of the sample.

Figure 6.9 185
Force microscopy images on one square of a photopatterned sample identical to that shown in Figure 6.8 of (A) topography, (B) friction force using a tip modified with a COOH-terminated SAM, and (C) friction force using a tip modified with a CH_3-terminated SAM. The apparent stretch in vertical direction observed on image (C) is due to the strain of the O-ring in the fluid cell during imaging.

Figure 6.10 188
Histograms of force vs. displacement curves recorded between functionalized samples terminating in COO^- groups and tips terminating in NH_3^+ in (upper histogram) deionized H_2O (18 MΩ·cm, pH = 6.5) and (lower histogram) 0.3 M NaCl aqueous solution (pH = 6.5).

CHAPTER SEVEN

Figure 7.1 208
The adhesion force between COOH groups on the tip and surface is plotted as a function of salt concentration. The lower graph shows that the adhesion force scales linearly with the square root of salt concentration (proportional to reciprocal of the Debye length) for salt concentrations up to 0.05 M.

Figure 7.2 211
Adhesion between COOH groups on the tip and sample as a function of pH using buffered (0.01 M total salt concentration) aqueous solutions. Each adhesion value was taken from an average of at least 200 force-distance measurements.

Figure 7.3 214
Plots of friction force vs. normal load force of the tip between COOH groups at three different pH values. The slope of each line is the friction force coefficient, μ.

Figure 7.4 216
A plot of friction coefficients vs. pH between tips and surfaces terminating in COOH groups. Each point is taken from the slope of a friction force vs. load curve.

Figure 7.5 220
A friction force image of a sample patterned with COOH and NH_2 groups taken with a tip functionalized with COOH groups. Patterns were fabricated by selectively irradiating SAMs terminating in aryl azide in the presence of a liquid film of the appropriate functionalized amine. Light regions indicate high friction and correspond to area on the

surface exposing NH_2 groups. Dark shades indicate low friction forces and represent surface areas ending in COOH. The image was acquired in a buffered solvent at pH 7.

LIST of SCHEMES

PART ONE

CHAPTER ONE

Scheme 1.1 25
An illustration of the self-assembly process. Alkanethiols spontaneously assemble on Au surfaces, energetically driven by covalent attachment of the head groups, S, to the Au substrate and by van der Waals interactions between the alkyl chains, to form a continuous, ordered, two-dimensional molecular film.

Scheme 1.2 29
The alkyl chains of a SAM are close-packed and tilted by an angle θ with respect to the surface normal. Surface properties are determined by the tail groups, X, which are exposed at the outer surface of the SAM.

Scheme 1.3 34
An illustration of several monolayer patterning methods. All methods can be used to fabricate patterns with lateral dimensions on the micron scale. Monolayers are ~30 Å in thickness; substrate thickness ranges from 100-1000 Å (Au supported on Si) to ~1 mm (Si).

Scheme 1.4 37
Solution photochemistry of aryl azide in the presence of a secondary amine trapping agent. **II** and **III** are formed from the singlet; intersystem-crossing to the triplet yields the aniline adduct in the absence of amine.

Scheme 1.5 38
Photochemistry of Au-**I** SAMs. Amines are chosen to alter SAM electron-transfer rate and surface free energy. Ferrocene is used as a redox-active species.

Scheme 1.6 40
A sessile drop in equilibrium an a solid surface forming a contact angle, θ.

CHAPTER TWO

Scheme 2.1 64
Irradiation of Au-**I** SAMs through a mask in the presence of functionalized amines produces a patterned SAM.

Scheme 2.2 96
A structural model of various electrode surfaces.

CHAPTER THREE

Scheme 3.1 108
Photosensitive SAMs of **I** on a flat Au surface are irradiated through a mask in the presence of a functionalized amine. Electrochemical oxidation of aniline or 3-methylthiophene results in selective polymer film (0.1-0.2 μm) after additional electropolymerization. Adhesive tape is applied to the sample and peeled away to selectively remove the polymer film. The original pattern is transferred to the tape while the inverse remains on the sample.

PART TWO

CHAPTER FOUR

Scheme 4.1 127
An illustration of a force-distance measurement. The piezoelectric tube extends and the sample makes contact with the tip (2). As it extends further, the tip bends upward (3). The piezoelectric tube then retracts and the tip continues to adhere to the sample (5) past the point of original contact (4). When the cantilever deflection exceeds the adhesion force, the tip jumps back to its resting position (6).

Scheme 4.2 128
Adhesion is measured by deflection as the sample is retracted from the tip; friction is measured by torsion as the sample is scanned under the tip.

Scheme 4.3 129
A conceptual illustration of chemical force microscopy. Molecules on the probe tip, X, are used to sense specific interactions with chemical groups, Y, on the surface.

CHAPTER SIX

Scheme 6A.1 192
Cantilever/tip geometry showing components of torque.

LIST of TABLES

PART ONE

CHAPTER ONE

Table 1.1 78
XPS analysis of the two regions in the polymer pattern.

CHAPTER FIVE

Table 5.1 143
Summary of adhesive forces (nN) measured between functionalized tips and samples. These data were obtained by averaging the results from at least 300 force vs. displacement curves for each tip/sample combination.

PART ONE

AN APPLICATION OF SELF-ASSEMBLED MONOLAYERS: SELECTIVE ELECTRODEPOSITION OF CONDUCTING POLYMERS

CHAPTER ONE

AN INTRODUCTION TO SELF-ASSEMBLED MONOLAYERS

Many critical materials properties originate in the main body—the bulk—of the material. When considering the stiffness of an I-beam, the optical properties of a lens, or the electrical conductivity of a copper wire, materials properties are largely the result of bulk physical and chemical structure. An increase in analytical sophistication over the past several decades has allowed the surfaces of materials and the interfaces between them to be studied. These experimental investigations have shown that the properties and performance of many materials are controlled at the boundary of materials in addition to the bulk: Metal fatigue occurs as cracks propagate along grain boundaries and coalesce into larger gaps, optical losses occur through reflection and scattering at interfaces, and as circuits become smaller, heat dissipation and local field effects play an increasingly important role in their electrical responses. In addition to materials, research in recent years has also shown that important biological processes occur at surfaces. Cell-cell, cell-protein, and protein-ligand interactions dominate most biological processes and all occur along some type of interface. Our understanding of surface behavior can be increased through chemical investigations of interfaces by relating microscopic chemical structure to macroscopic chemical, physical, or biological function, and by making specific and systematic chemical changes at interfaces to ultimately predict and control these properties at the molecular level.

This thesis describes the use of photosensitive self-assembled monolayers (SAMs) on gold substrates to produce patterns with different physical and chemical properties. Part One describes the use of monolayer patterns of different thickness on gold electrodes to direct the deposition of electropolymerized aniline, 3-methylthiophene, and pyrrole. Once deposited on the surface, these conducting polymers can be selectively removed and transferred to insulating supports. Adhesion to the polymer films is controlled via the terminal chemical groups of the SAM pattern. Part Two describes the development of chemical force microscopy, a new technique derived from conventional atomic force

microscopy. Microscopic probe tips and flat substrates coated with a thin layer of gold followed by SAMs terminating in different chemical groups allows adhesion and friction forces between specific chemical groups to me measured quantitatively on the molecular scale for the first time. The forces are directly related to the strength of the chemical interactions of molecular groups on the surface and tip, and are influenced by the surrounding medium, which is either air or a liquid. Comparisons between adhesion and friction forces on homogeneous monolayer surfaces show that in certain cases adhesion and friction are proportional at the nanometer scale. Images of functional group patterns on the substrate taken with tips ending in different functional groups show that this technique truly probes chemical interactions and may be used to generate "maps" of chemically heterogeneous surfaces.

This introductory chapter offers a brief review of self-assembled monolayers with particular emphasis on monolayers composed of alkanethiols or disulfides on gold surfaces. A wealth of research has been conducted on various monolayer systems.[1] The following review therefore is by no means comprehensive, but rather reflects several principles I feel are important and useful, and introduces some characterization techniques as a background for the remaining chapters. A brief description of the composition, formation, and utility of monolayers is first given, focusing on alkanethiols and disulfides on gold. Next, the techniques of contact angle measurements, ellipsometry, X-ray photoelectron spectroscopy, and cyclic voltammetry are described, along with what information about SAMs is gained from each of these methods. Several methods to generate SAM patterns—two-dimensional monolayer surfaces with different chemical or physical properties—are then briefly reviewed, followed by the fundamentals of our patterning method: alkyl disulfides terminating in aryl azide compose a photosensitive monolayer to which functionalized amines are selectively and covalently attached to generate patterns. The use of monolayers in "molecular architecture", the

fabrication of multilayers, and the possibility using SAMs in several applications are finally discussed.

Self-Assembled Monolayers

A monolayer is a two-dimensional layer of molecules confined to an interface or surface. Self-assembly refers to the spontaneous formation of a monolayer upon introduction of a suitable interface to the appropriate molecules. For example, when a bare Au surface is immersed in a dilute (mM) organic solution of an alkanethiol (such as dodecanethiol in ethanol), a SAM spontaneously forms within minutes or hours, as illustrated in Scheme 1.1. Molecules that form monolayers on solid surfaces are composed of three parts: (1) head groups which covalently attach to the substrate, (2) long alkyl chains, [$(CH_2)_n$ where n ≈ 10-20], which pack tightly because of van der Waals forces, and (3) tail groups which are expressed at the immediate surface. In addition to thiols and disulfides on Au, two other monolayer systems have been studied extensively: one based on silanes on oxide surfaces and another on Langmuir-Blodgett films.

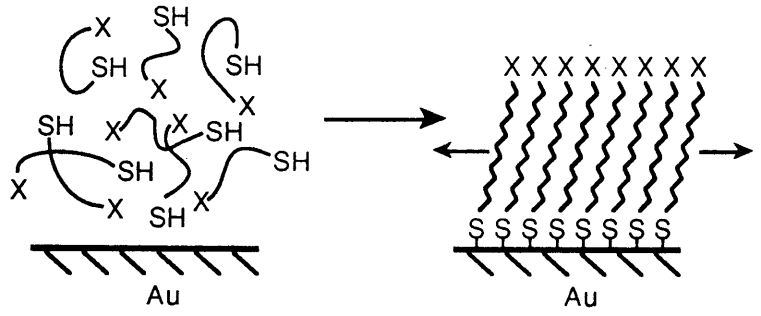

Scheme 1.1. An illustration of the self-assembly process. Alkanethiols spontaneously assemble on Au surfaces, energetically driven by covalent attachment of the head groups, S, to the Au substrate and by van der Waals interactions between the alkyl chains, to form a continuous, ordered, two-dimensional molecular film.

Silane Monolayers and Langmuir-Blodgett Films.[1a,c] Silanes based on $RSiCl_3$ (R = alkyl) and $RSi(OR')_3$ (R = alkyl, R' = methyl or ethyl) react at surfaces with exposed OH groups and with adsorbed water to form an amorphous network of Si–O–Si bonds with R groups projecting normal to the surface. An early demonstration of long chain silanes including *n*-octadecyltrichlorosilane (OTS) discusses the formation of monolayers and mixed monolayers of two different silanes on glass substrates.[2] Long-chain

alkylsilanes such as OTS form stable, uniform monolayers across the entire substrate (as opposed to islands) with a quasi-crystalline structure, as determined by ellipsometry and low-angle X-ray reflectivity.[3] Short alkyl silanes also form monolayers; 3-aminopropyl-triethoxysilane (APS) is commercially available (Hüls) and has been used extensively to fabricate "amine-terminated" surfaces on silicon, silica, and glass.[4] Monolayers of APS have also been formed on electrode surfaces such as platinum, tin oxide (SnO_2), and indium-tin oxide (In_2O_3/SnO_2, ITO), and have been used in subsequent surface reactions with various carboxylic acid derivatives.[5] Because APS does not have a long chain of methylene groups, it is structurally disordered compared to its long-chain counterparts. Recent attempts at forming long-chain silane monolayers with amines and other molecular groups have been developed to overcome this problem,[6] and detailed structural investigations of silane SAMs as a function of deposition temperature and alkyl chain length have been reported.[7] Silane multilayers have also recently been studied at attempts to form more elaborately designed surfaces.[8]

Silane monolayers are distinctly attractive because they readily form on two materials widely used in industry: silicon and glass. Formation of monolayers and multilayers on transparent substrates is especially attractive towards the development of optical devices.[1a,9] Also, silane surfaces are amenable to biological studies. Fluorescence microscopy has been used to detect the recognition of fluorescently labeled ligands to silanes selectively functionalized with DNA,[10] peptides,[11] and antibodies[12] toward the development of ligand binding assay techniques.

Monolayers of silanes have several disadvantages compared to those of thiols on Au, however. The formation of multilayer films is often unavoidable because silanes, especially trialkoxysilanes, are prone to polymerization. Also, because of the reactive nature of SiR_3 and $Si(OR)_3$ groups certain chemical functionalities (i.e., OH and COOH) cannot be incorporated directly into the molecule and must be formed after monolayer assembly in a surface reaction. Methods at performing transformations at the surface to

alter the exposed functionality have been reported,[4-6,13] but these systems have not yet been extensively characterized. Limitations of silane monolayers are now being addressed[14] and have not hindered efforts towards the development of optically or biologically active surfaces, but have probably contributed to the dearth of more detailed structure-property studies.

Langmuir-Blodgett films compose another monolayer system.[1c] In a very crude sense, LB films are similar to films of oil spread on water. These monolayers are composed of "amphiphilic" compounds—long chains similar to fatty acids that have a non-polar end that "likes" oil, and a polar end that "likes" water—and were first studied systematically by Irving Langmuir,[15] who received the Nobel Prize in 1932 for his work in surface chemistry. In this sense, the term "likes" can be interpreted to mean "is soluble in" which is itself a combination of several entropic and enthalpic terms involving the transfer of a solute particle into a solvent.[16] A classic example of an amphiphilic molecule is stearic acid, $CH_3(CH_2)_{16}CO_2H$. The carboxylic acid portion of the molecule is soluble in water, whereas the nonpolar aliphatic chain is insoluble. Amphiphiles therefore aggregate at interfaces of water and air, or water and oil, with the polar portion of the molecule in the water phase. The degree of differential solubility is a critical parameter to the interfacial activity of amphiphiles. Consider stearic acid which forms LB monolayers: if the COOH group is changed to a larger, more polar SO_3^- or $N(CH_3)_4^+$ group, the molecule will become too water soluble for LB film formation. Likewise, monolayers will not form if the alkyl group is not sufficiently long. Propionic acid, with only two methylene groups, will never form well-ordered LB-type monolayers!

In the strictest sense, LB monolayers are not self-assembled monolayers. They lack the highest energy process of formation, the formation of a covalent bond to a solid surface via the head group, and therefore do not spontaneously form well-ordered assemblies. Structurally ordered monolayers may be formed, though, by compressing the amphiphiles at the interface with a moveable barrier. This technique uses what is now

known as a Langmuir trough, and was first demonstrated over 100 years ago.[17] Indeed, the most important indicator of LB monolayer properties is given by surface pressure/area isotherms—plots of the surface pressure as a function of the interface surface area. Films at low pressure are disordered. At high pressures they assume an almost crystalline structure until they collapse at even higher pressures. Well-ordered, compressed films can be transferred from the water/air interface (interfaces between water and organic liquids may also be used) to solid supports, as first demonstrated by Katherine Blodgett.[18]

Langmuir-Blodgett films transferred from a solution interface to a solid support have a monolayer structure similar to SAMs formed directly on solids, but like silane monolayers, suffer in several respects as models for interfacial behavior. Most importantly, the structure of LB films is not well defined, nor is it stable. Films may relax to a second, more stable structure after assuming an initial metastable form. Transferring LB films from the air/water interface to solid supports may also introduce perturbations on the microscopic structure and unlike silanes, transferred LB films have no strong association to the solid support and are not robust. The necessity for a polar end and a non-polar end on the molecule also limits the types of compounds that can be used, and thus limits the types of questions that can be addressed with LB films. Despite these drawbacks, LB films are actively used in fundamental surface science studies and in the development of molecular superstructures, thin-film devices, and optical devices.[1c,19]

Self-Assembled Monolayers of Thiols and Disulfides on Gold

Long-chain alkanethiols (RSH) and dialkyl disulfides (RSSR') spontaneously assemble from solution to form monolayers on Au and compose the best understood monolayer system to date. Most of the thiols and disulfides used are commercially available or easily synthesized. The affinity of sulfur for Au is strong and accounts for the most energetic process in SAM formation (~30 kcal/mol).[20] Though each covalent attachment to the surface is weaker than that for silanes, each alkanethiol is distinct. No

cross-linking occurs between the alkanethiol groups that would compromise the overall SAM structure.

$$\text{thiols:} \quad RS\text{–}H + Au \rightarrow RS^{-}\text{–}Au^{+} + \tfrac{1}{2}H_2 \tag{1.1}$$

$$\text{disulfides:} \quad RS\text{–}SR + Au \rightarrow 2\,RS^{-}\text{–}Au^{+} \tag{1.2}$$

Like the other monolayer systems, van der Waals interactions between the alkyl chains also contribute to the enthalpy of SAM formation. Each additional CH_2–CH_2 interaction contributes ~1 kcal/mol.[21] The combination of covalent attachment to the substrate, van der Waals interactions between the alkyl chains, and the lack of additional structural requirements on the head groups results in the spontaneous formation of well-ordered, stable, rugged SAMs. For example, monolayers of octadecanethiol, $HS(CH_2)_{17}CH_3$, form SAMs within seconds on clean Au substrates immersed in dilute (~1-3 mM) ethanolic solutions. Though clean, freshly evaporated Au substrates give the best results, the adsorption of most alkanethiols to Au is sufficiently strong to displace weakly adsorbed contaminants.

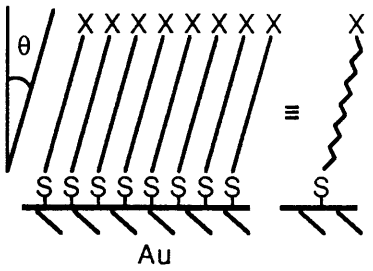

Scheme 1.2. The alkyl chains of a SAM are close-packed and tilted by an angle θ with respect to the surface normal. Surface properties are determined by the tail groups, X, which are exposed at the outer surface of the SAM.

Spectroscopy and diffraction studies have been used to characterize the structure of SAMs on Au in detail. Several important structural features are now well understood:

1. Alkanethiols form ordered SAMs that are epitaxial with the supporting Au substrate. Early electron diffraction studies[22] show that the symmetry of S atoms on Au(111) is hexagonal with a spacing of 4.97Å, which is very close to the spacing of next-nearest Au atoms, 4.99Å. In this $\sqrt{3} \times \sqrt{3}$ R30° structure, each S atom lies in a three-fold-hollow site, and each molecule occupies a surface area of 21.4 Å^2. Recently, X-ray diffraction, helium diffraction, and scanning probe microscopy have been used to investigate superlattices based on this structure and subtle factors such as rotation around the Au–S bond and chain torsion that define

the exact geometry of the unit cell.[23] Additional structures, binding modes, and the migration of thiols on the surface are also being studied with several techniques.

2. The alkyl chains are predominantly trans-extended and tilted with respect to the surface normal (Scheme 1.2). Reflection-absorption (grazing-angle) IR spectroscopy[1a] measures the magnitude and direction of transition dipoles of a thin films on a reflective sample. Used in conjunction with lattice models and molecular dynamics calculations, spectroscopic studies show that alkanethiols adsorb on polycrystalline Au(111) with an average tilt angle of 34° from the surface normal.[24] The cant angle determines the distance between methylene groups and is set to maximize the strength of the van der Waals interactions. Consequently, the cant angle changes according to the bonding and atom spacing of S atoms on the substrate. For instance, alkanethiols adsorb on Ag(111) to form closely packed monolayers with tilt angles of only ~6-7°.
3. Monolayers formed from either alkanethiols, RSH, or dialkyl disulfides, RSSR', have the same structure on Au(111) surfaces, $RS^-–Au^+/Au^0{}_3$, according to eqs 1.1 and 1.2 above.[25,26] In other words, both thiols and disulfides form Au-thiolates, and in the absence of additional steric requirements, SAMs are formed from both compounds at the same rate.[26] Dialkyl sulfides, RSR', also readily adsorb to Au surfaces to form robust SAMs. Due to the C–S–C bond angle however, both alkyl chains cannot extend from the surface to form a close-packed structure. Monolayers formed from dialkyl sulfides thus more closely resemble disordered organic liquids,[27] not the crystalline arrays derived from alkanethiols and dialkyl disulfides.
4. Homogeneous mixed monolayers assemble from solution mixtures of two alkanethiols that differ in their tail groups.[28] If one alkanethiol, $HS(CH_2)_nX$, is used to endow the surface with a certain property (for example X = CF_3 makes the surface

hydrophobic) and another alkanethiol is used to endow the surface with a different property (such as X = OH, which makes the surface hydrophilic), the two different thiols can be coadsorbed on the Au surface to form a well-ordered, mixed SAM with an intermediate surface property.

The stable, well-ordered structure of SAMs provides a reliable and flexible framework for surface chemistry studies. Alkanethiols and dialkyl disulfides with various tail groups (i.e., CH_3, CF_3, OH, COOH, C_6H_5) can be used to form SAMs with specific chemical and physical properties. Photochemically and electrochemically active terminal groups can also be introduced, and surface reactions such as ester and amide bond formations can be studied and used to introduce additional functionalities in situ. The chemical composition and physical structure of these SAMs can be altered to study the molecular origins of specific surface properties.

Monolayer Patterning

Besides altering the structure and properties of homogeneous SAMs, patterning—controlling the lateral placement of two or more chemically different SAMs—provides an additional method of synthetic control over surfaces. Patterns are useful in modeling biological interfaces such as cell surfaces, and are a prerequisite to the fabrication of magnetic, optical, or sensor devices.

A practical demonstration of patterning is shown in Figure 1.1, in which a SAM pattern is used to control the deposition of aniline, a conducting polymer. This system, described in Chapter Two, can be used to study mechanisms of polymer deposition and adhesion, and may have implications in device fabrication.

Monolayer patterns can be formed in one of several ways, as illustrated in Scheme 1.3. Perhaps the most basic way to localize monolayers to a specific region of the surface is to physically protect or "mask" the remaining regions with a protective layer. Patterns of photoresist are simply deposited on flat substrates to protect part of the surface from

Figure 1.1. A photograph of polyaniline selectively electrodeposited on a large Au-coated Si substrate. The polyaniline pattern (dark green) replicates the pattern initially generated on a photosensitive SAM.

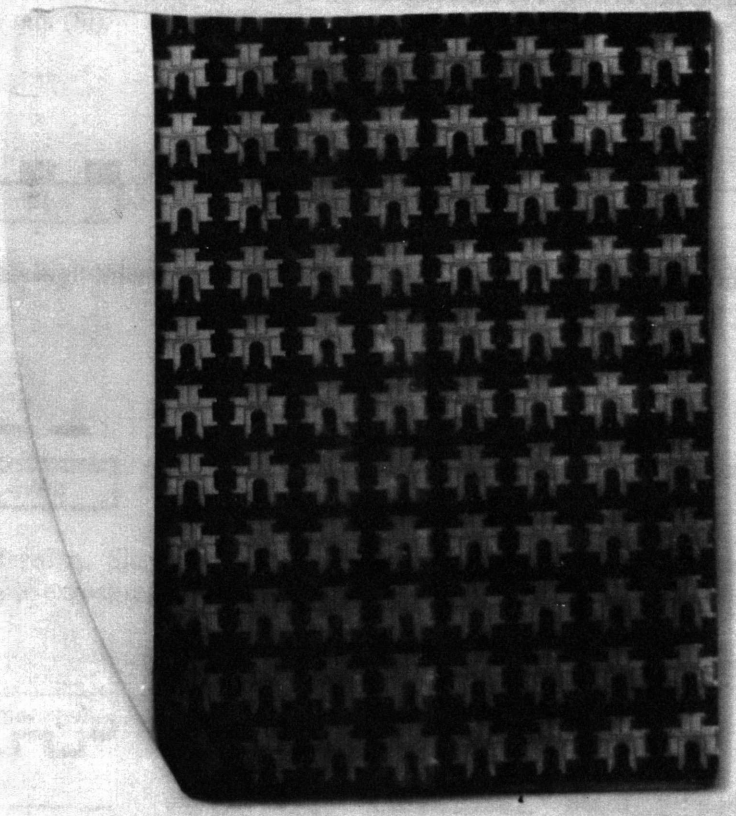

derivitization. A monolayer is then formed in the bare, unprotected regions of the surface. The original photoresist layer can then be removed. This method has been used with alkylsilanes to form surface patterns of CH_3 groups (a hydrophobic surface) on quartz (a hydrophilic surface) to control the behavior and orientation of cultured cells.[29]

Scheme 1.3. An illustration of several monolayer patterning methods. All methods can be used to fabricate patterns with lateral dimensions on the micron scale. Monolayers are ~30 Å in thickness; substrate thickness ranges from 100-1000 Å (Au supported on Si) to ~1 mm (Si).

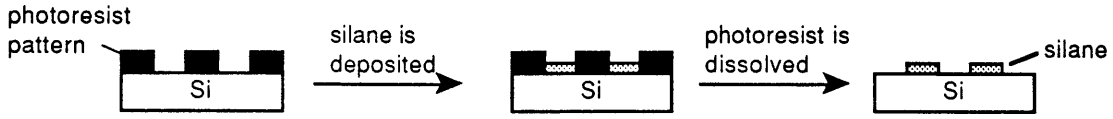

a. Substrate Masking. Silanes are patterned on Si or glass using photoresist to mask the surface.

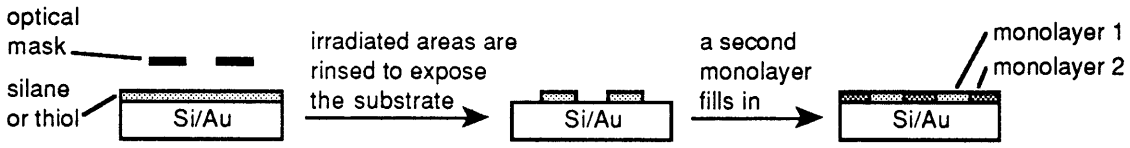

b. UV Photopatterning. Silane or thiol monolayers are destroyed by deep UV irradiation. They are rinsed away to expose regions of the substrate which can be coated with a second silane or thiol.

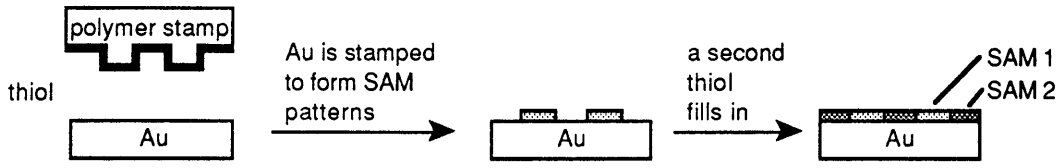

c. Microcontact printing. A polymer stamp is inked with an alkanethiol solution and applied to Au substrates to form rugged, defect-free, micron-scale SAM patterns. A second thiol can be used to functionalize remaining areas of the Au substrate.

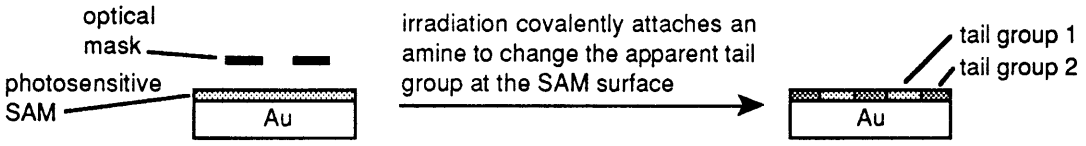

d. Aryl Azide Photopatterning. A SAM with a photosensitive aryl azide tail group is irradiated in the presence of a functionalized amine to introduce a second SAM tail group.

Though this method should be general for any type of surface (glass, Si, Au, etc.), it is not widely used, probably because of the incompatibility of the solvents used for photoresist stripping and monolayer formation, and fouling of the surface with photoresist before monolayer formation.

A more effective method of monolayer patterning is shown in Scheme 1.3b in which homogeneous SAMs are first formed and then selectively irradiated with UV light. In the case of silanes, the Si–C or C–C bond is broken and in an unknown mechanism, terminating the surface in OH;[30] in the case of alkanethiols, the corresponding sulfonate is formed.[31] In both cases, irradiated portions of the monolayer are rinsed away and a new, chemically different monolayer is formed in those regions. This approach is advantageous in that successive irradiations could conceivably be used to pattern multiple SAMs on the same surface, however complications are inherent. Assuming complete transformation of the irradiated region, incomplete desorption or dissolution of the irradiated monolayer, especially in areas of very small dimension, remains a distinct possibility. Complete formation of the second monolayer would then be questionable. Another practical limitation is the long irradiation time (~1 hr in some cases)[27a,b] necessary for monolayer photoreaction, important when considering the fabrication of multiple samples.

Monolayer patterns can be formed without physically blocking the sample or selectively desorbing homogeneous monolayers. Whitesides and coworkers have used a pen and alkanethiol "ink" to write SAMs on Au surfaces.[32] More recently, they have used stamps[33] instead of pens, a more effective method to repeatedly and selectively transfer alkanethiols to large surfaces (Scheme 1.3c). Stamps several centimeters in size can easily be formed using lithographic techniques. Photoresist is used to create a master pattern on a flat substrate—a mold—onto which polydimethylsiloxane is deposited, cured, and peeled away to yield a flexible, free-standing, polymeric stamp. This stamp, which contains the negative of the original photoresist image, is "inked" with an

alkanethiol solution, typically hexadecanethiol, using a lint-free cotton pad. The stamp is then applied to a bare Au surface by hand. A rugged, nearly defect-free SAM readily forms only in areas contacted by the stamp. Later, a second thiol can either be stamped in additional areas of the Au surface, or can be adsorbed from solution to fill in the remaining underivatized areas. Both simple and complex patterns can be formed on Au substrates with resolution well into the micron scale. This method is currently being used to form optical devices,[34] to study the chemistry of protein and cell adhesion,[35] and to form microstructures on various metal and semiconductor substrates.[36] Except for fabrication of the original master pattern, this process can be performed easily in a normal laboratory setting and appears to be the most effective, simple, and generally applicable method of SAM patterning to date.

The Use of Photosensitive Terminal Groups to Pattern SAMs

The fourth method of SAM patterning, illustrated in Scheme 1.3d, uses monolayers with photoactive terminal groups, and is the method used in experiments described throughout this thesis. This method differs from those described previously in that only the top portion of the SAM is altered; the originally formed Au–S bonds in the initially-deposited homogeneous SAM are retained. Since many studies and application of SAMs depend on the chemical and physical nature of the immediate surface (the top ~5 Å), this method of patterning is attractive because the internal structure of the SAM is not perturbed.

This method also demonstrates an elegant application of inorganic and organic photochemistry; we have used monolayers terminating in $(\eta^5\text{-}C_5H_5)Mn(CO)_3$ and aryl azide in our laboratory to form SAM patterns.[37] Irradiation of $(\eta^5\text{-}C_5H_5)Mn(CO)_3$ in the presence of a substituted phosphine results in exchange of CO by the phosphine. Selective irradiation of monolayers of 11-mercaptoundecylcyclopentadienylmanganese tricarbonyl, $HS(CH_2)_{11}(\eta^5\text{-}C_5H_4)\text{-}Mn(CO)_3$, on Au, and the corresponding silane on

silicon or glass, forms patterns on the surface. These photochemical transformations were first verified by IR and cyclic voltammetry.[38] Subsequently, SAM patterns have been characterized by secondary ion mass spectrometry. [39]

Photopatterning with Aryl Azide. The strategy of irradiating a photoreactive group in the presence of a trapping agent to form a patterned surface has been used successfully with a second system, one based on aryl azide. Monolayers terminating in the aryl azide moiety form readily on Au substrates from the corresponding disulfide, di-11-(4-azidobenzoate)-1-undecyl disulfide, **I**. As shown in Scheme 1.5, irradiation of Au-**I** SAMs in the presence of an amine results in the formation of two main photoproducts, each with the amine covalently attached to the surface.

The solution photochemistry of aryl azide derivatives has been investigated.[40] Both singlet and triplet nitrene species are formed from the photochemical loss of N_2. Subsequent reactions are illustrated in Scheme 1.4. In the presence of amines, the singlet phenyl nitrene undergoes ring expansion to form 2-amino-3H-azepine, **II**, via the 2-dehydroazepine adduct, or may be trapped directly to form phenyl hydrazine, **III**. Aniline is formed in the absence of amine reaction via the triplet state.

Scheme 1.4. Solution photochemistry of aryl azide in the presence of a secondary amine trapping agent. **II** and **III** are formed from the singlet; intersystem-crossing to the triplet yields the aniline adduct in the absence of amine.

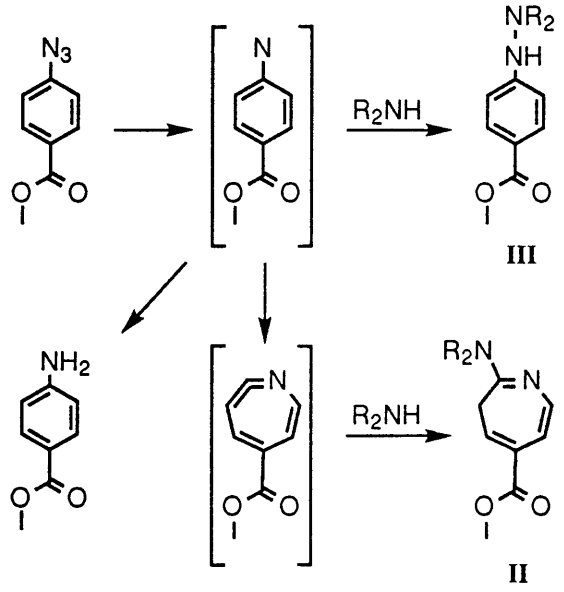

The product ratio of both solution and surface-confined species depends on additional ring substituents, irradiation power and duration, and the concentration of amine. For the covalent attachment of functionalized amines, SAM surfaces of **I** are irradiated in neat films[41] of an amine such as dibutylamine for 2 min at a wavelength of $\lambda > 260$ nm by a

medium-pressure Hg lamp (~10 mW/cm^2) resulting in a **II**:**III** ratio of 3:2 or greater. The total yield of covalent amine attachment approaches 100% (see sections on X-ray photoelectron spectroscopy and cyclic voltammetry below). Scheme **1.5** also shows several amines that have been photochemically attached to Au-**I** SAMs. Monolayer properties such as electron-transfer rate (degree of electrode passivation) and surface free

Scheme 1.5. Photochemistry of Au-I SAMs. Amines are chosen to alter SAM thickness and surface free energy. Ferrocene is used as a redox-active species.

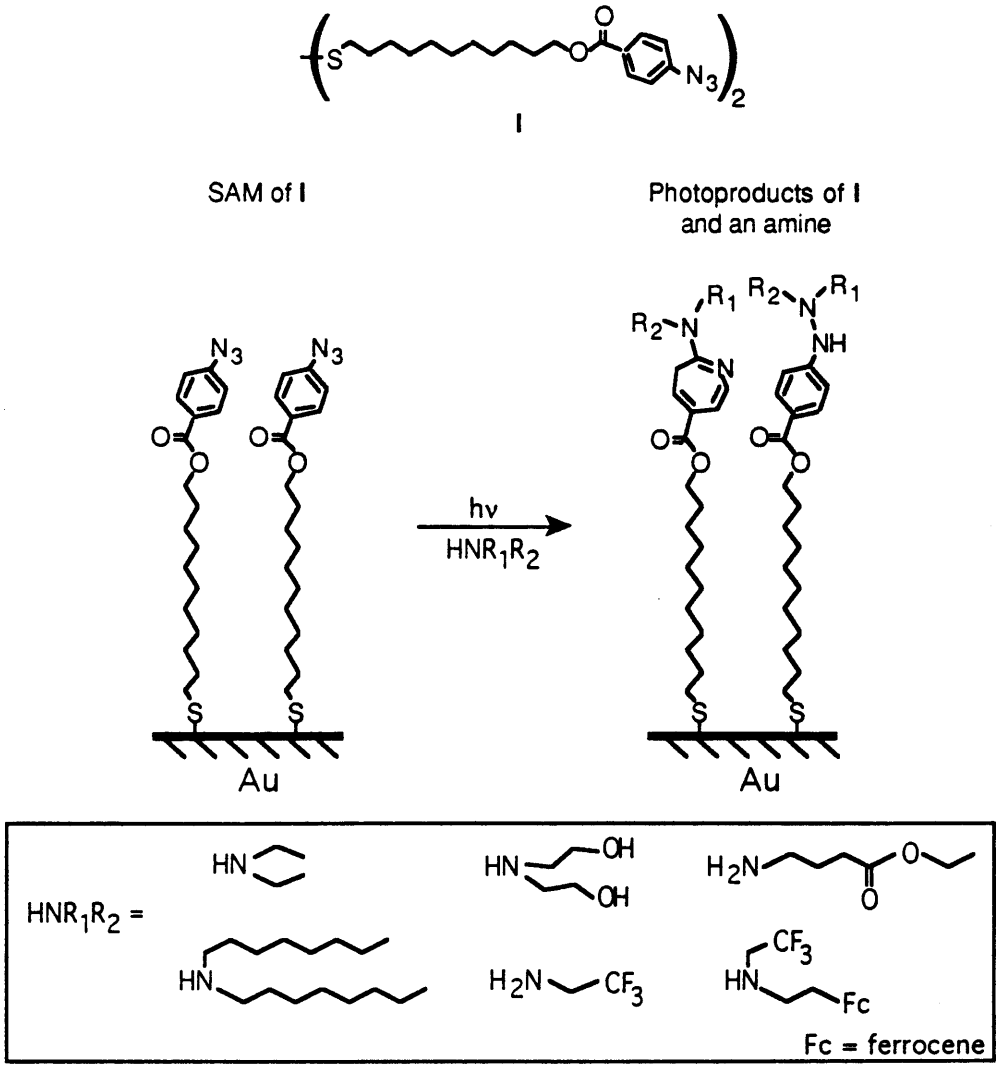

energy may be controlled by irradiating Au-**I** SAMs in the presence of various functionalized amines. Monolayers patterned with long-chain alkylamines, for instance, are used to alter electron transfer rates through the monolayers and to control the electrodeposition of conducting polymers as described in Chapter Two.

Characterization of SAMs on Gold

Many analytical techniques are used to characterize monolayers on electrode surfaces. Contact angle, ellipsometry, X-ray photoelectron spectroscopy, and cyclic voltammetry techniques have been used routinely to probe the surface free energy, physical structure, and chemical composition of SAMs on Au.

Ellipsometry. Ellipsometry is used to determine the structure and thickness of SAMs. When monochromatic, plane-polarized light is reflected from a SAM-coated Au surface, the components parallel and perpendicular to the surface are reflected differently resulting in a change in the overall polarization and amplitude of the light wave. Ellipsometry measures the ratio of the Fresnel reflection coefficients for the p and s polarizations. By comparing the phase shift (Δ) and the change in the ratio of the two amplitudes ($\tan\Psi$) between the parallel and perpendicular components of the reflected light, the thickness of the monolayer can be measured.[3] In principle, both the thickness and the refractive index of a film can be determined, but since SAMs are very thin (typically 20-30 Å) the refractive index must be estimated. Since SAMs are nearly crystalline alkane layers, the values of polyethylene or paraffin (1.45-1.5) are usually used.[3]

The width of the incident beam (~1 mm^2) means that ellipsometry measures SAM thickness on a macroscopic scale. Ellipsometry has been used to characterize alkanethiol SAMs, $Au–S(CH_2)_nCH_3$, as a function of n. These data verify that SAMs formed from short-chain thiols are more liquid-like (1.1 Å/CH_2) whereas SAMs of long-chain thiols are more crystalline (1.5 Å/CH_2), with extended chains tilted from the surface normal.

Bare Au, used as a comparison sample, is more susceptible to contamination than Au coated with a hydrophobic, methyl-terminated SAM. The interpretation of ellipsometric data, therefore, must take into account the presence of adventitious adsorbates on the bare, uncoated Au substrates. In Chapter Two, ellipsometry is used in conjunction with cyclic voltammetry to qualitatively probe the structure of irradiated and unirradiated Au-**I** SAMs.

Contact Angle. Contact angle measurements of liquids on solid surfaces are used to probe interfacial, or surface, free energy. When two immiscible liquids are in contact, the free energy change in expanding their contacting area by a unit area is called the interfacial energy, γ.[42] The contact angle is defined as the angle between the liquid-vapor and solid-vapor interfaces formed by a liquid drop on a solid, as shown in Scheme 1.6. Following application of a drop on the surface, the drop edge expands, increasing the area of the liquid-vapor interface (an energetically unfavorable process) and decreasing the area of the solid-vapor interface (an energetically favorable process). Under equilibrium conditions, the drop edge ceases to expand when the energies of these processes balance. For a water drop applied to a solid surface in air, this process usually results in a stable, measurable contact angle. Observations of contact angles, especially of water, surround us daily. A contact angle of nearly zero indicates a hydrophilic (water-loving), high-energy surface such as clean glass. High energy surfaces are usually reactive or prone to contamination by adsorption. A contact angle of 90° or more indicates a hydrophobic, low-energy surface such as Teflon. These surfaces are relatively passive and do not interact strongly with other materials.

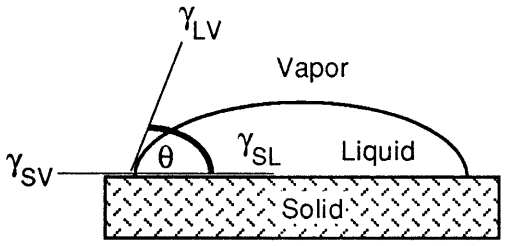

Scheme 1.6. A sessile drop in equilibrium on a solid surface forming a contact angle, θ.

Equation 1.3, Young's equation, relates the contact angle, θ, to the liquid-vapor, solid-

$$\gamma_{SV} = \gamma_{SL} + \gamma_{LV}\cos\theta \qquad (1.3)$$

vapor, and solid-liquid interfacial free energies. The Young equation assumes equilibrium conditions and an ideally smooth, homogeneous, unreactive surface. In the vast majority of case, however, the observed contact angle is not uniquely determined by γ_{SV} and γ_{SL}, and a range of stable contact angles is observable on the same surface. For example, a drop that is advancing (because, for example, the volume of the drop is increasing, or the sample is tilted) will have a larger contact angle than a drop that is receding on the same surface. This effect is called contact angle hysteresis and is indicative of non-equilibrium conditions. Detailed investigations of contact angle hysteresis[43] and quantitative interpretation of contact angles[44] have recently been reported.

The apparent complications of a contact angle behavior do not detract from its usefulness as a qualitative measurement. The interpretation of contact angles on SAM surfaces comprises a useful method in physical-organic surface chemistry to probe different aspects of surface free energy.[28a] In these studies the tail groups are systematically varied while leaving the rest of the surface—the underlying Au substrate, and the crystalline alkane region of the SAM—constant. By comparing the contact angles of water and hexadecane on various SAM surfaces, different chemical aspects of the solid-liquid interface can be probed.[45] For example, fluorinated alkanethiols such as $HS(CH_2)(CF_2)CF_3$ are more water- and oil-repellent than Teflon, with contact angles of 118° and 71° for water and hexadecane, respectively. A SAM terminating in Cl does not wet water (θ = 83°) but does wet hexadecane, and SAMs terminating in OH and COOH completely wet both water and oil, with contact angles of less than 10°. Other functionalities (such as $CH{=}CH_2$, Br, F, OCH_3, CO_2CH_3, CN, $CONH_2$)[45] and mixed monolayers of two different thiols result in surfaces with intermediate contact angles for both water and hexadecane. Additionally, water of varying pH can be used in contact angle titrations of acidic and basic terminal groups.[46] Contact angle measurements

provide a powerful way to measure surface properties in a qualitative manner and are a convenient tool in the physical-organic studies of SAM surfaces.

X-Ray Photoelectron Spectroscopy. The chemical composition of a surface can be characterized by X-ray photoelectron spectroscopy (XPS).[47] XPS is especially amenable to the study of SAMs because it is very surface-sensitive, probing only the top ~30Å of the surface.[48] Unlike most other surface analysis techniques used in our studies, XPS utilizes relatively expensive equipment and is conducted in ultrahigh vacuum (10^{-8}-10^{-10} Torr). Monochromatic X-rays, usually from either magnesium (Mg Kα = 1253.6 eV) or aluminum (Al Kα = 1486.6 eV) sources, irradiate the sample and ionize inner-shell electrons. The energy of these core electrons, E_k, is determined by the incoming photon energy, hν, and the binding energy, E_b, of the ionized electron.

$$E_k = h\nu - E_b - \phi_{sp} \tag{1.4}$$

The work function of the spectrometer, ϕ_{sp}, is included in eq 1.4 because the binding energies of solids are usually referenced to their Fermi level rather than the vacuum level. XPS spectra are usually reported in terms of the binding energy, E_k, of the detected electron. This binding energy, to a first approximation, is given by the Hartree-Fock eigenvalue of the core electron, E_{HF}, the difference in correlation energies between the unionized and single ionized atoms, ΔE_c, and the relaxation energy, E_r, that arises chiefly from screening of the core hole by the other electrons.

$$E_b = -E_{HF} + \Delta E_c - E_r \tag{1.5}$$

The local chemical environment of the irradiated atom shifts the binding energy of the ionized electron by several electron-volts. This chemical shift is what gives power and applicability to XPS as a tool for surface analysis. For example, the normal binding energy of carbon (CH_3) is 284.6 eV. The electron-withdrawing nature of fluorine shifts the binding energy of a perfluorinated carbon (CF_3) by more than 8 eV to ~293 eV.

Figure 1.2 shows the N 1s spectra of a native and irradiated SAM of **I**. The two N peaks in Figure 1.2a are characteristic of aryl azide in the unirradiated sample. The area

Figure 1.2. XPS spectra of the N 1s regions of (a) Au-**I** and (b) Au-**I** irradiated in the presence of $[CH_3(CH_2)_3]_2NH$. Complete loss of the high binding energy peak upon irradiation indicates complete loss of azide. The ratio of total peak area before and after irradiation can be used to estimate the yield of reaction, which is ~80% on this sample.

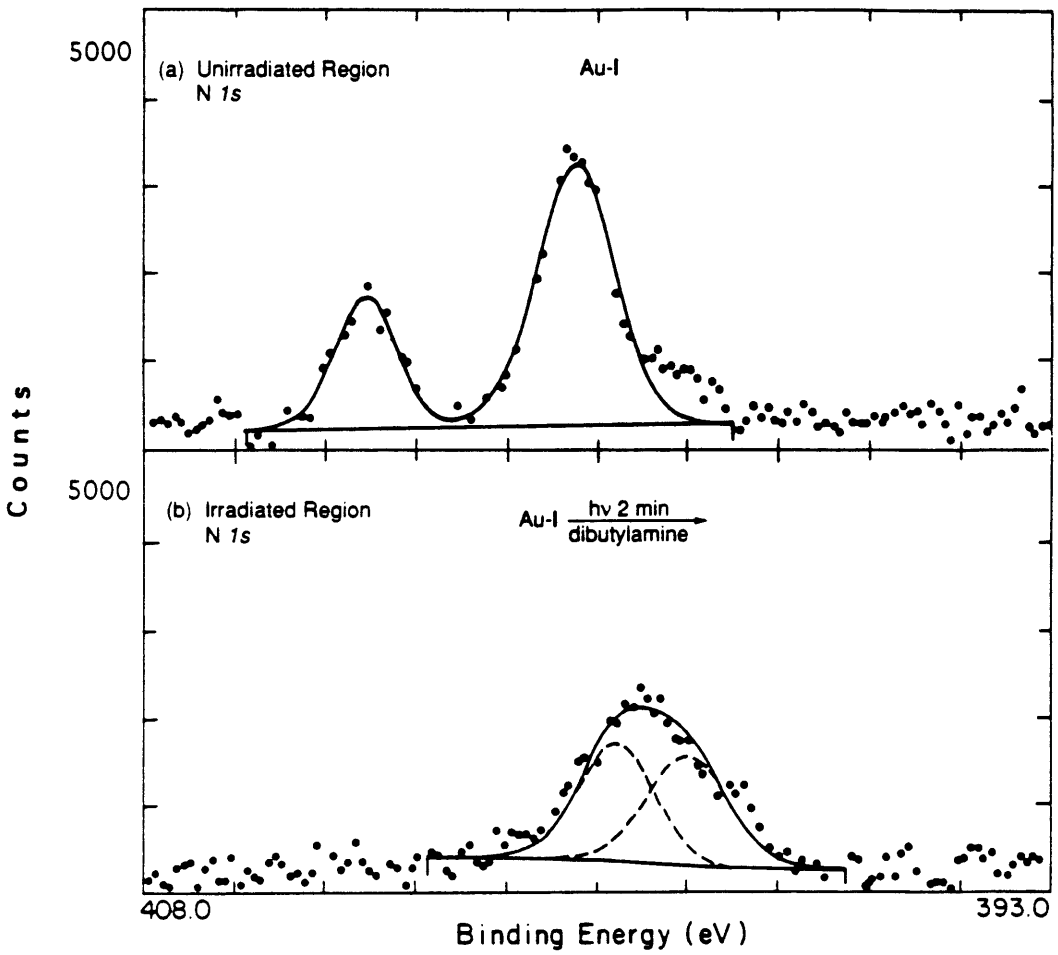
5000
(a) Unirradiated Region
N 1s
Au-I
5000
(b) Irradiated Region
N 1s
Au-I hν 2 min
dibutylamine
Counts
408.0
393.0
Binding Energy (eV)

ratio of these two peaks is 1:2. The smaller peak at 404.3 eV is shifted form the larger N 1s peak at 400.9 eV, and is assigned to the middle azide N atom which is positively charged in both reasonable Lewis structures for phenyl azide. Irradiation of a Au-**I** SAM (2 min, $\lambda > 260$ nm) in the presence of an amine such as dibutylamine results in loss of N_2 and covalent attachment of the amine. Figure 1.2b shows one broad peak (fitted as two) at 399.8 eV assigned to these N atoms.

If the yield of the photoreaction were 100%, the ratio of the total N peak areas of the native sample to that of the irradiated sample would be 3:2. In this case, the ratio is 3:1.81. Assuming that all azide lost N_2 upon irradiation, but only a fraction of amines were covalently attached, this ratio translates to a photoreaction yield of 81%. Thus, XPS can be used to characterize the chemistry and the yield of reactions on SAM surfaces.

Cyclic Voltammetry. Gold substrates may be used as working electrodes in electrochemical investigations of SAM surfaces. Cyclic voltammetry—the repeated oxidation and reduction of species in solution or confined to the surface—comprises the basic technique and is used to investigate the kinetics (the heterogeneous electron transfer rate) and the thermodynamics (the redox potential) of electrode reactions.

The reversible reduction and reoxidation of an electroactive group at a metal electrode can be written as

$$O + ne^- \underset{k_r}{\overset{k_f}{\rightleftharpoons}} R \qquad (1.6)$$

where O is the oxidized species, R the reduced species, and n electrons are exchanged at the forward, K_f, and backward, k_r, electron transfer rates. The total charge passed in the reaction of N moles is given by Faraday's Law,

$$Q = nFN \qquad (1.7)$$

where F = 96,486 C/mol.

The yield of a chemical reaction on a SAM surface can be monitored conveniently by cyclic voltammetry by using a reactive electroactive group. Ferrocene, $Fe(C_5H_5)_2$, has

Figure 1.3. An example of electrochemical SAM analysis. Cyclic voltammograms of a Au electrode coated with a SAM of **I** taken (a) before and (b) after irradiation in the presence of an amine attached to ferrocene are shown. Integration of the anodic wave yields a coverage of 3.3×10^{-10} mol/cm^2, roughly a monolayer of ferrocene groups, indicating almost 100% photoattachment of amine on this sample.

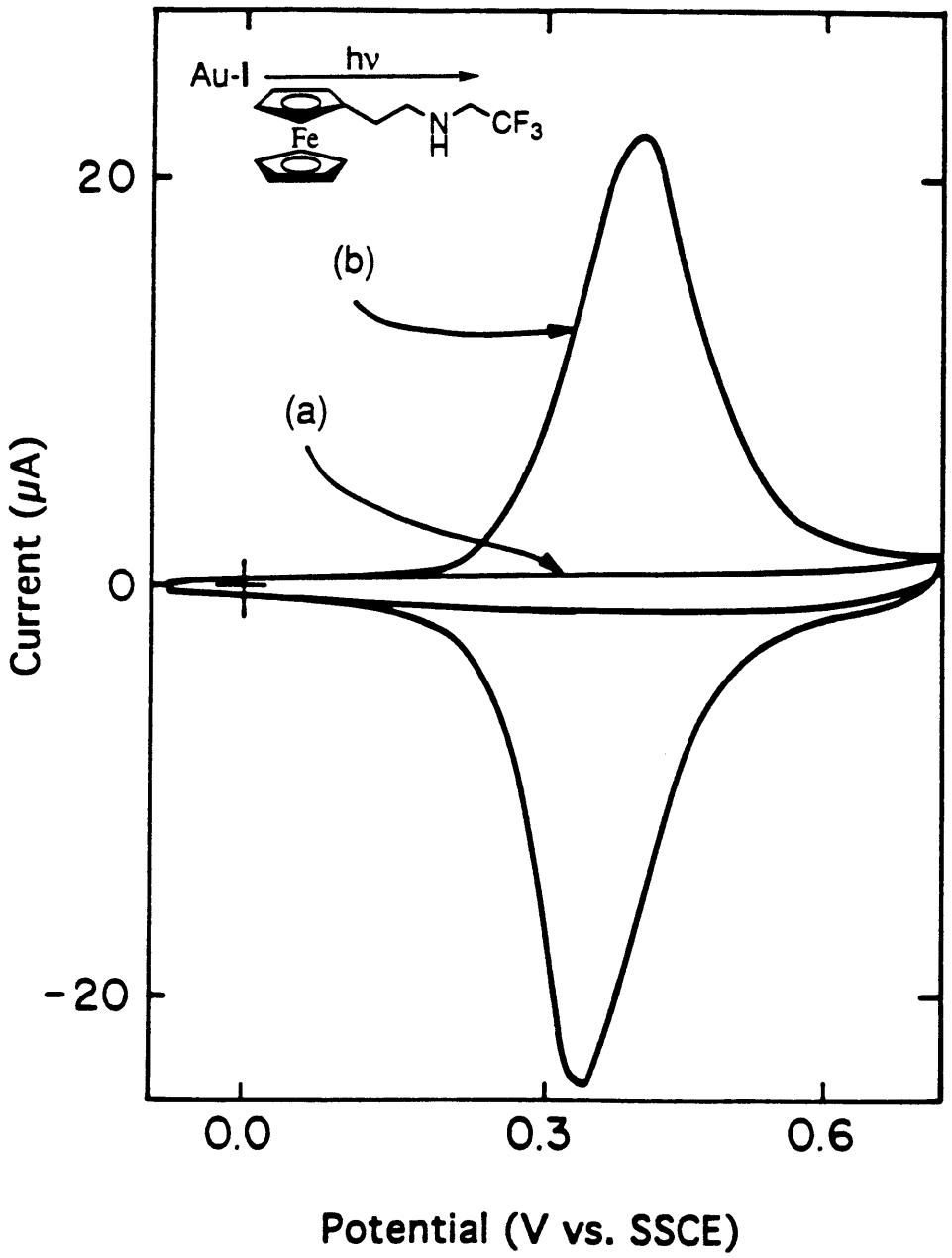
Au-I
hν
Fe
N
H
CF3
20
0
-20
(b)
(a)
Current (μA)
0.0
0.3
0.6
Potential (V vs. SSCE)

been used in our laboratories because it exhibits well-behaved, reversible redox behavior, and can be chemically modified; the photochemical reaction of aryl azide can also be studied by cyclic voltammetry using ferrocene.[49] A SAM of **I** on a Au electrode is irradiated in the presence of N-(2,2,2 trifluoroethyl)-N-(2-ferrocenylethyl)amine. A cyclic voltammogram of the modified electrode (Figure 1.3) verifies that the ferrocene group is confined to the SAM surface. The ferrocene coverage, Γ, can be measured by integrating either the cathodic or anodic wave:

$$\Gamma = \frac{N}{A} = \frac{Q}{nFA} \tag{1.7}$$

Integration of the anodic wave in Figure 1.3 yields a surface coverage of 3.3×10^{-10} mol/cm^2, which translates to roughly a full monolayer of ferrocene groups. The yield of this photochemical reaction is near unity, assuming that the SAM of **I** is close-packed with a full monolayer of aryl azide groups on the surface. As a point of reference, this surface coverage is within the range of coverages detected using disulfide SAMs already terminating in ferrocene ($3\text{-}4 \times 10^{-10}$ mol/cm^2).

Characterization of SAM Patterns.

Ellipsometry and XPS are used to analyze large areas (mm^2) of the surface. Cyclic voltammetry can be used to verify that electroactive species have been photoattached to Au-**I** SAMs, but how can micron-scale patterns be imaged? One way is by scanning electron microscopy (SEM).[50] Contrast in SEM images is sensitive to the composition of the SAMs and can be differentiate between several different SAMs on a given sample. Both homogeneous and patterned SAMs may be analyzed and imaged by secondary ion mass spectrometry (SIMS),[51] a semi-quantitative technique that can be used to identify chemical groups in the surface. The techniques of SIMS (especially with the new time-of-flight instruments[52]) and XPS are complimentary and have been used in our group to identify and map chemical species on many SAM surfaces.

Figure 1.4. An optical micrograph of a patterned Au-**I** substrate irradiated through a lithographic mask in the presence of $(HOCH_2CH_2)_2NH$. As the sample is cooled in a humid environment, water droplets spread and coalesce on irradiated, OH-terminated areas of the SAM pattern. Condensed water forms beads on the surrounding unirradiated, hydrophobic regions. The hydrophilic lines in the condensation image are 100 μm wide; the features in the middle of the image are 50 μm wide.

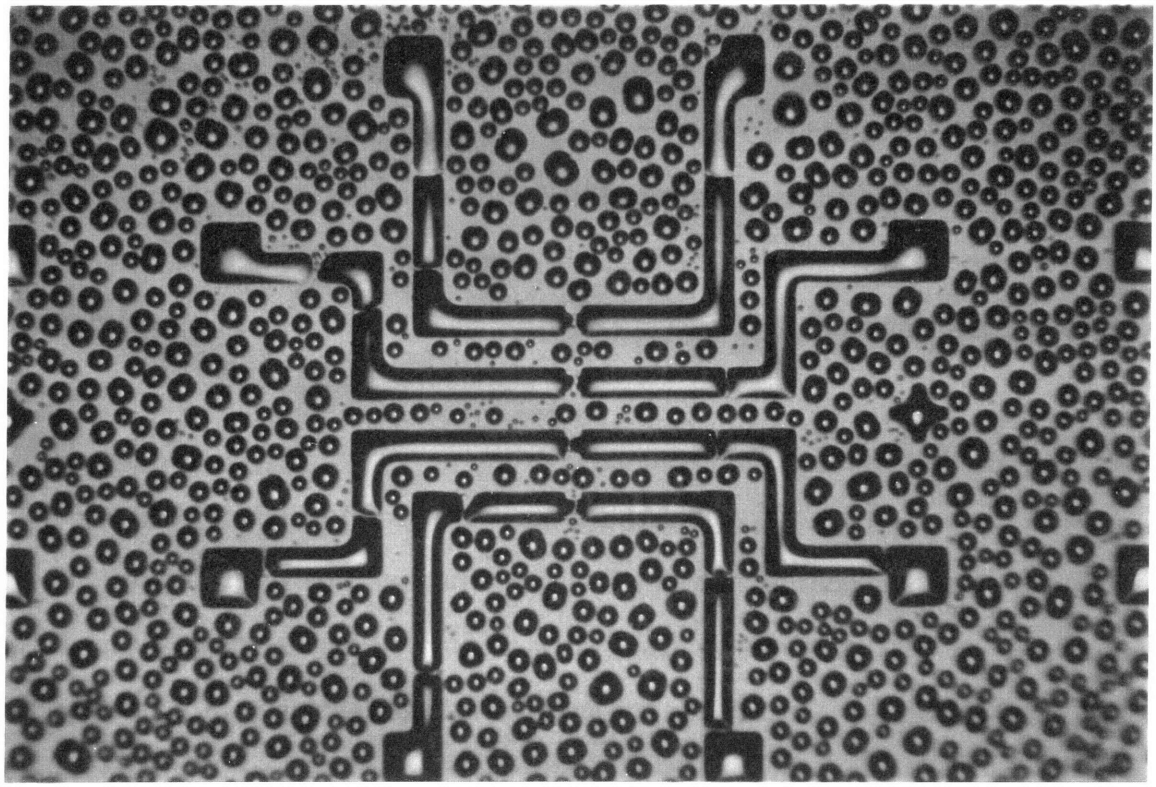

Photogenerated patterns on Au-**I** surfaces may be detected easily by using amines that alter the surface free energy of the surface. Au-**I** SAM surfaces irradiated in diethanolamine are very hydrophilic. Figure 1.4 shows a micrograph of a Au-**I** surface selectively irradiated in diethanolamine. Water has condensed on the cooled surface. Areas wet by water correspond to the hydrophilic, irradiated portions of the surface, and areas repellent to water are hydrophobic, still terminating in aryl azide. This method of using condensation figures[32] to visualize SAM patterns is an easy and convenient way to verify surface modification. In Chapters Five and Six, condensation figures are used to verify patterns of carboxylic acids on Au-**I** substrates used in chemical force microscopy experiments.

Practical and Fundamental Applications of SAMs

The ruggedness, stable structure, and ability to control the chemical properties of SAMs make them attractive models with which to study surface and interfacial phenomena. The techniques used to fabricate and analyze these surfaces are now being extended to fabricate more complex multilayer systems with high degrees on molecular order. These methods will improve future optical and electronic thin film devices, regardless of the type of thin organic film employed. The volume of reports in these areas of surface chemistry is high, and articles on these subjects can be found in several journals. Almost any current issue of *Langmuir*, for example, will contain several articles on topics involving SAMs.

Within the breadth of monolayer studies, a few examples of current work are worth mentioning. Control over SAM thickness and structure on metal electrodes allows the chemical effects of electron transfer to be investigated. Electron transfer between the electrode and a redox-active species in solution has been related to defects in monolayers, and capacitance measurements have been used to probe the permeability of monolayers to aqueous ions in terminally-substituted alkanethiols of the same length.[53] The kinetics of

electron transfer to thiols with pendant redox-active groups has also been studied as a function of chain length.[54] Research in this area is active since directional electron transfer reactions are the key to many biological processes and opto-electronic devices.

As the complexity and optimization of electronic and optical devices grows, molecular control in the fabrication process becomes increasingly important. An early effort to assemble multilayers used thiols as an adhesive layer for the deposition of silane multilayer structures.[55] More recent attempts at constructing multilayers on Au use inorganic salts to maintain a strong structural framework as successive layers are deposited. A thiol terminating in phosphonic acid provides a template for the repeated deposition of a divalent metal (Zn or Cu) and an alkanebisphosphonate.[56] Well-ordered films of up to 100 layers may be grown by alternately dipping the substrate into a solution of the metal and the alkanebisphosphonate at room temperature.

Monolayers can be selectively adsorbed on substrates containing Au and an insulator, as demonstrated previously by our research group.[57] In addition, thiols or disulfides on Au, and carboxylic acids on alumina,[58] isocyanides on Pt,[59] and carboxylic or phosphonic acids on ITO,[60] selectively and spontaneously adsorb to form SAMs from binary mixtures in solution. This method of "orthogonal self-assembly" introduces a new level of molecular control in monolayer systems, provides a promising method to connect and orient molecules between two different, closely-spaced, externally addressable electrode surfaces, and may be used in future efforts in device fabrication.

As stated above, SAM patterning is being used in both device applications and biological studies. Most recently, patterns prepared using polymeric stamps have been used to control the adhesion of proteins.[61] Extracellular matrix proteins can be patterned to define regions of the surface that support cell attachment. By varying the size and shape of the adhesive islands, cellular protein and DNA production rates can be modulated, demonstrating the importance of well-defined cell-surface interactions on cell

growth and behavior.[35] The possibility of using SAMs as biological recognition elements[62] in the development of biosensors[63] is currently being developed.

In conclusion, self-assembled monolayers are easy to use and constitute a stable, rugged framework for tail groups that support a wide degree of chemical manipulation. Monolayer chemistry has defined new questions in surface chemistry and has contributed to the sophistication and sensitivity of analytical techniques. The following chapters present some of our most recent applied and fundamental surface chemistry investigations using SAMs.

References

1. Several books on two-dimensional molecular films are available including (a) Ulman, A. *An Introduction to Ultrathin Organic Films from Langmuir-Blodgett to Self-Assembly*; Academic: San Diego, 1991, (b) Ulman, A. *Characterization of Organic Thin Films*; Butterworth-Heinemann: Boston, 1995, and (c) Roberts, G. *Langmuir-Blodgett Films*; Plenum: New York, 1990.
2. Sagiv, J. "Organized Monolayers by Adsorption. 1. Formation and Structure of Oleophobic Mixed Monolayers on Solid Surfaces" *J. Am. Chem. Soc.* **1980**, *102*, 92-98.
3. Wasserman, S. R.; Whitesides, G. M.; Tidswell, I. M.; Ocko, B. M.; Pershan, P. S.; Axe, J. D. "The Structure of Self-Assembled Monolayers of Alkylsiloxanes on Silicon: A Comparison of Results from Ellipsometry and Low-Angle X-Ray Reflectivity" *J. Am. Chem. Soc.* **1989**, *111*, 5852-5861.
4. (a) *Silanes, Surfaces, and Interfaces* Leyden, D. E., Ed.; Gordon and Breach: New York, 1986. (b) Haller, I. "Covalently Attached Organic Monolayers on Semiconductor Surfaces" *J. Am. Chem. Soc.* **1978**, *100*, 8050-8055.
5. Murray, R. W. "Chemically Modified Electrodes" *Acc. Chem. Res.* **1980**, *13*, 135-141 and references therein.
6. Balachander, N.; Sukenik, C. N. "Monolayer Transformation by Nucleophilic Substitution: Applications to the Creation of New Monolayer Assemblies" *Langmuir* **1990**, *6*, 1621-1627.
7. Parikh, A. N.; Allara, D. L.; Azouz, I. B.; Rondelez, F. "An Intrinsic Relationship between Molecular Structure in Self-Assembled *n*-Alkylsiloxane Monolayers and Deposition Temperature" *J. Phys. Chem.* **1994**, *98*, 7577-7590; (b) Ohtake, T.; Mino, N.; Ogawa, K. "Effect of Hydrocarbon Chain Length on Arrangement of Chemically Adsorbed Monolayers" *Langmuir* **1992**, *9*, 2081-2083.

8. Tillman, N.; Ulman, A.; Penner, T. L. "Formation of Multilayers by Self-Assembly" *Langmuir* **1989**, *5*, 101-111.

9. Swalen, J. D.; Allara, D. L.; Andrade, J. D.; Chandross, E. A.; Garoff, S.; Israelachvili, J.; McCarthy, T. J.; Murray, R.; Pease, R. F.; Rabolt, J. F.; Wynne, K. J.; Yu, H. "Molecular Monolayers and Films" *Langmuir* **1987**, *3*, 932-950.

10. Pease, A. C.; Solas, D.; Sullivan, E. J.; Cronin, M. T.; Holmes, C. P.; Fodor, S. P. A. "Light-Generated Oligonucleotide Arrays for Rapid DNA Sequence Analysis" *Proc. Natl. Acad. Sci. USA* **1994**, *91*, 5022-5026.

11. Fodor, S. P. A.; Read, J. L.; Pirrung, M. C.; Stryer, L.; Lu, A. T.; Solas, D. "Light-Directed, Spatially Addressable Parallel Chemical Synthesis" *Science* **1991**, *251*, 767-773.

12. Rozsnyai, L. F.; Benson, D. R.; Fodor, S. P. A.; Schultz, P. G. "Photolithographic Immobilization of Biopolymers on Solid Supports" *Angew. Chem. Int. Ed. Engl.* **1992**, *31*, 759-761.

13. Kurth, D. G.; Bein, T. "Surface Reactions on Thin Layers of Silane Coupling Agents" *Langmuir* **1993**, *9*, 2965-2973.

14. Brzoska, J. B.; Azouz, I. B.; Rondelez, F. "Silanization of Solid Substrates: A Step toward Reproducibility" *Langmuir* **1994**, *10*, 4367-4373.

15. Langmuir, I. "The Constitution and Fundamental Properties of Solids and Liquids. II. Liquids" *J. Am. Chem. Soc.* **1917**, *39*, 1848-1906.

16. For a detailed discussion of the energetics of solubility and monolayer formation, see Israelachvili, J. N. *Intermolecular and Surface Forces*; Academic: San Diego, 1992.

17. Pockels, A. in Letters to the Editor, "Surface Tension" *Nature* **1891**, *43*, 437-439.

18. (a) Blodgett, K. B. "Films Built by Successive Monomolecular Layers on a Solid Surface" *J. Am. Chem. Soc.* **1935**, *57*, 1007-1022. (b) Blodgett, K. B.; Langmuir, I.

"Built-Up Films of Barium Stearate and Their Optical Properties" *Phys. Rev.* **1937**, *51*, 964-982.

19. Zasadinski, J. A.; Viswanathan, R.; Madsen, L.; Garnaes, J.; Schwartz, D. K. "Langmuir-Blodgett Films" *Science* **1994**, *263*, 1726-1733.
20. Bain, C. D.; Troughton, E. B.; Tao, Y.-T.; Evall, J.; Whitesides, G. M.; Nuzzo, R. G. "Formation of Monolayer Films by the Spontaneous Assembly of Organic Thiols from Solution onto Gold" *J. Am. Chem. Soc.* **1989**, *111*, 321-335.
21. The dispersion interaction between alkanes is 1.4-1.8 kcal/mol per CH_2 group (see reference 1a, p. 89). See also reference 22.
22. Strong, L; Whitesides, G. M. "Structures of Self-Assembled Monolayer Films of Organosulfur Compounds Adsorbed on Gold Single Crystals: Electron Diffraction Studies" *Langmuir* **1988**, *4*, 546-558.
23. (a) Alves, C. A.; Smith, E. L.; Porter, M. D. "Atomic Scale Imaging of Alkanethiolate Monolayers at Gold Surfaces with Atomic Force Microscopy" *J. Am. Chem. Soc.* **1992**, *114*, 1222-1227. (b) Camillone, N.; Chidsey, C. E. D.; Liu, G.; Scoles, G. "Superlattice Structure at the Surface of a Monolayer of Octadecanethiol Self-Assembled on Au(111)" *J. Chem. Phys.* **1993**, *98*, 3503-3511.
24. Nuzzo, R. G.; Dubois, L. H.; Allara, D. L. "Fundamental Studies of Microscopic Wetting on Organic Surfaces. 1. "Formation and Structural Characterization of a Self-Consistent Series of Polyfunctional Organic Monolayers" *J. Am. Chem. Soc.* **1990**, *112*, 558-569.
25. Biebuyck, H. A.; Whitesides, G. M. "Interchange between Monolayers on Fold Formed from Unsymmetrical Disulfides and Solutions of Thiols: Evidence for Sulfur-Sulfur Bond Cleavage by Gold Metal" *Langmuir* **1993**, *9*, 1766-1770.

26. Biebuyck, H. A.; Bain, C. D. Whitesides, G. M. "Comparison of Organic Monolayers on Polycrystalline Gold Spontaneously Assembled from Solutions Containing Dialkyl Disulfides or Alkanethiols" *Langmuir* **1994**, *10*, 1825-1831.

27. Troughton, E. B.; Bain, C. D.; Whitesides, G. M.; Nuzzo, R. G.; Allara, D. L.; Porter, M. D. "Monolayer Films Prepared by the Spontaneous Self-Assembly of Symmetrical and Unsymmetrical Dialkyl Sulfides from Solution onto Gold Substrates: Structure, Properties, and Reactivity of Constituent Functional Groups" *Langmuir* **1988**, *4*, 365-385.

28. (a) Whitesides, G. M.; Laibinis, P. E. "Wet Chemical Approaches to the Characterization of Organic Surfaces: Self-Assembled Monolayers, Wetting, and the Physical-Organic Chemistry of the Solid-Liquid Interface" *Langmuir* **1990**, *6*, 87-96. (b) Bertilsson, L.; Liedberg, B. "Infrared Study of Thiol Monolayer Assemblies on Gold: Preparation, Characterization, and Functionalization of Mixed Monolayers" *Langmuir* **1993**, *9*, 141-149.

29. Clark, P.; Connolly, P.; Moores, G. R. "Cell Guidance by Micropatterned Adhesiveness In Vitro" *J. Cell Sci.* **1992**, *103*, 287-292.

30. (a) Dulcey, C. S.; Georger, J. H., Jr.; Krauthamer, V.; Stenger, D. A.; Fare, T. L.; Calvert, J. M. "Deep UV Photochemistry of Chemisorbed Monolayers: Patterned Coplanar Molecular Assemblies" *Science* **1991**, *252*, 551-554. (b) Bhatia, S. K.; Hickman, J. J.; Ligler, F. S. "New Approach To Producing Patterned Biomolecular Assemblies" *J. Am. Chem. Soc.* **1992**, *114*, 4432-4433. (c) Stenger, D. A.; Georger, J. H.; Dulcey, C. S.; Hickman, J. J.; Rudolph, A. S.; Nielsen, T. B.; McCort, S. M.; Calvert, J. M. "Coplanar Molecular Assemblies of Amino- and Perfluorinated Alkylsilanes: Characterization and Geometric Definition of Mammalian Cell Adhesion and Growth" *J. Am. Chem. Soc.* **1992**, *114*, 8435-8442.

31. (a) Tarlov, M. J.; Burgess, D. R. F. Jr.; Gillen, G. "UV Photopattering of Alkanethiolate Monolayers Self-Assembled on Gold and Silver" *J. Am. Chem. Soc.* **1993**, *115*, 5305-5306. (b) Huang, J.; Dahlgren, D. A.; Hemminger, J. C. "Photopatterning of Self-Assembled Alkanethiolate Monolayers on Gold: A Simple Monolayer Photoresist Utilizing Aqueous Chemistry" *Langmuir* **1994**, *10*, 626-628.

32. López, G. P.; Biebuyck, H. A.; Frisbie, C. D.; Whitesides, G. M. "Imaging of Features on Surfaces by Condensation Figures" *Science* **1993**, *260*, 647-649.

33. Kumar, A.; Whitesides, G. M. "Features of Gold Having Micrometer to Centimeter Dimensions can be Formed Through a Combination of Stamping with an Elastomeric Stamp and an Alkanethiol "ink" followed by Chemical Etching" *Appl. Phys. Lett.* **1993**, *63*, 2002-2004.

34. Kumar, A.; Whitesides, G. M. "Patterned Condensation Figures as Optical Diffraction Gratings" *Science* **1994**, *263*, 60-62.

35. Singhvi, R.; Kumar, A.; Lopez, G. P.; Stephanopoulos, G. N.; Wang, D. I. C.; Whitesides, G. M.; Ingber, D. E. "Engineering Cell Shape and Function" *Science* **1994**, *264*, 696-698.

36. Kumar, A.; Biebuyck, H. A.; Whitesides, G. M. "Patterning Self-Assembled Monolayers: Applications in Materials Science" *Langmuir* **1994**, *10*, 1498-1511.

37. Kang, D.; Wrighton, M. S. "Patterned Functionalization of Gold and Single Crystal Silicon via Photochemical Reaction of Surface-Confined Derivatives of $(\eta^5\text{-}C_5H_5)Mn(CO)_3$" *Langmuir* **1991**, *7*, 2169-2174.

38. Kang, D.; Wollman, E. W.; Wrighton, M. S. "Photochemical Reactions of Organometallic Molecules on Surfaces" in *Photosensitive Metal-Organic Systems*; Katul, C.; Serpone, N., Eds. Advances in Chemistry Series 238, ACS: Washington D. C., 1993, pp 45-65.

39. Wollman, E. W.; Kang, D.; Frisbie, C. D.; Lorkovic, I. M.; Wrighton, M. S. "Photosensitive Self-Assembled Monolayers on Gold: Photochemistry of Surface-Confined Aryl Azide and Cyclopentadienylmanganese Tricarbonyl" *J. Am. Chem. Soc.* **1994**, *116*, 4395-4404.

40. (a) Huisgen, R.; Vossius, D.; Appl, M. "Die Thermolyse des Phenylazids in primären Aminen; die Konstitution des Dibenzamils" *Chem. Ber.* **1958**, *91*, 1-12. (b) Huisgen, R.; Appl, M "Der Chemismus der Ringerweitung beim Zerfall des Phenylazids in Anilin" *Chem. Ber.* **1958**, *91*, 12-21. (c) Appl, M.; Huisgen, R. "Weiteres zur Thermolyse der Arylazide in Aminen" *Chem. Ber.* **1958**, *91*, 2961-2967. (d) Doering, W. von E.; Odum, R. A. "Ring Enlargement in the Photolysis of Phenyl Azide" *Tetrahedron* **1966**, *22*, 81-93.

41. Most amines used are clear, colorless liquids that can be spread between the substrate and the mask as a neat film, with slight heating if necessary. Solid amines may be disolved in a non-nucleophilic solvent such as tetrahydrofuran or N,N-dimethyl formamide; alcohols or water cannot be used as they will compete with the desired amine in the reaction with phenyl nitrene.

42. See reference 16, Chapter 15.

43. Chen, Y. L.; Helm, C. A.; Israelachvili, J. N. "Molecular Mechanisms Associated with Adhesion and Contact Angle Hysteresis of Monolayer Surfaces" *J. Phys, Chem.* **1991**, *95*, 10736-10747.

44. (a) Vogler, E. A. "Practical Use of Concentration-Dependent Contact Angles as a Measure of Solid-Liquid Adsorption. 1. Theoretical Aspects" *Langmuir* **1992**, *8*, 2005-2012. (b) Vogler, E. A. "Practical Use of Concentration-Dependent Contact Angles as a Measure of Solid-Liquid Adsorption. 2. Experimental Aspects" *Langmuir* **1992**, *8*, 2013-2020.

45. Bain, C. D.; Whitesides, G. M. "Modeling Organic Surfaces with Self-Assembled Monolayers" *Angew. Chem. Int. Ed. Engl.* **1989**, *28*, 506-512.

46. (a) Wamser, C. C.; Gilbert, M. I. "Detection of Surface Functional Group Asymmetry in Interfacially-Polymerized Films by Contact Angle Titrations" *Langmuir* **1992**, *8*, 1608-1614. (b) Lee, T. R.; Carey, R. I.; Biebuyck, H. A.; Whitesides, G. M. "The Wetting of Monolayer Films Exposing Ionizable Acids and Bases" *Langmuir* **1994**, *10*, 741-749. (c) Creager, S. E.; Clarke, J. "Contact-Angle Titrations of Mixed ω-Mercaptoalkanoic Acid/Alkanethiol Monolayers on Gold. Reactive vs. Nonreactive Spreading, and Chain Length Effects on Surface pK_a Values" *Langmuir* **1994**, *10*, 3675-3683.

47. *Practical Surface Analysis by Auger and X-ray Photoelectron Spectroscopy*; Briggs, D., Seah, M. P., Eds.; Wiley: New York, 1983.

48. Laibinis, P. E.; Bain, C. D.; Whitesides, G. M. "Attenuation of Photoelectrons in Monolayers of *n*-Alkanethiols Adsorbed on Copper, Silver, and Gold" *J. Phys. Chem.* **1991**, *95*, 7017-7021.

49. Wollman, E. W. Ph. D. Thesis, Massachusetts Institute of Technology, 1993.

50. López, G. P.; Biebuyck, H. A.; Whitesides, G. M. "Scanning Electron Microscopy Can Form Images of Patterns in Self-Assembled Monolayers" *Langmuir* **1993**, *9*, 1513-1516. (b) Wollman, E. W.; Frisbie, C. D.; Wrighton, M. S. "Scanning Electron Microscopy for Imaging Photopatterned Self-Assembled Monolayers on Gold" *Langmuir* **1993**, *9*, 1517-1520.

51. (a) Frisbie, C. D.; Martin, J. R.; Duff, R. R. Jr.; Wrighton, M. S. "Use of High Lateral Resolution Secondary Ion Mass Spectrometry to Characterize Self-Assembled Monolayers on Microfabricated Structures" *J. Am. Chem. Soc.* **1992**, *114*, 7142-7145. (b) Frisbie, C. D.; Wollman, E. W.; Martin, J. R.; Wrighton, M. S. "Secondary Ion Mass Spectrometry for Characterizing Photopatterned, Self-

Assembled Monolayers on Gold" *J. Vac. Sci. Tech. A* **1993**, *11*, 2368-2372. (c) Frisbie, C. D.; Wollman, E. W.; Wrighton, M. S. "High Lateral Resolution Secondary Ion Mass Spectrometry of Photopatterned Self-Assembled Monolayers Containing Aryl Azide" submitted for publication in *Langmuir*.

52. Benninghoven, A. "Chemical Analysis of Inorganic and Organic Surfaces and Thin Films by Static Time-of-Flight Secondary Ion Mass Spectrometry (TOF-SIMS)" *Angew. Chem. Int. Ed. Engl.* **1994**, *33*, 1023-1043.

53. Chidesy, C. E. D.; Loiacono, D. N. "Chemical Functionality in Self-Assembled Monolayers: Structural and Electrochemical Properties" *Langmuir* **1990**, *6*, 682-691.

54. See, for example, (a) Finklea, H. O.; Hanshew, D. D. "Electron-Transfer Kinetics in Organized Thiol Monolayers with Attached Pentaammine(pyridine)ruthenium Redox Centers" *J. Am. Chem. Soc.* **1992**, *114*, 3173-3181, (b) Chidsey, C. E. D. "Free Energy and Temperature Dependence of Electron Transfer at the Metal-Electrolyte Interface" *Science* **1991**, *251*, 919-922.

55. Ulman, A.; Tillman, N. "Self-Assembling Double Layers on Gold Surfaces: The Merging of Two Chemistries" *Langmuir* **1989**, *5*, 1418-1420.

56. Yang, H. C.; Aoki, K.; Hong, H.-G.; Sackett, D. D.; Arendt, M. F.; Yau, S.-L.; Bell, C. M.; Mallouk, T. E. "Growth and Characterization of Metal(II) Alkanebisphosphonate Multilayer Thin Films on Gold Surfaces" *J. Am. Chem. Soc.* **1993**, *115*, 11855-11862.

57. Hickman, J. J.; Ofer, D.; Zou, C.; Wrighton, M. S.; Laibinis, P. E.; Whitesides, G. M. "Selective Functionalization of Gold Microstructures with Ferrocenyl Derivatives via Reaction with Thiols or Disulfides: Characterization by Electrochemistry and Auger Electron Spectroscopy" *J. Am. Chem. Soc.* **1991**, *113*, 1128-1132.

58. Laibinis, P. E.; Hickman, J. J.; Wrighton, M. S.; Whitesides, G. M. "Orthogonal Self-Assembled Monolayers: Alkanethiols on Gold and Alkane Carboxylic Acids on Alumina" *Science* **1989**, *245*, 845-847.

59. Hickman, J. J.; Laibinis, P. E.; Auerbach, D. I.; Zou, C.; Gardner, T. J.; Whitesides, G. M.; Wrighton, M. S. "Toward Orthogonal Self-Assembly of Redox Active Molecules on Pt and Au: Slective Reaction of Disulfide with Au and Isocyanide with Pt" *Langmuir* **1992**, *8*, 357-359.

60. Gardner, T. J.; Frisbie, C. D.; Wrighton, M. S. "Systems for Orthogonal Self-Assembly of Electroactive Monolayers on Au and ITO: An Approach to Molecular Electronics" *J. Am. Chem. Soc.*, in press.

61. López, G. P.; Biebuyck, H. A.; Härter, R.; Kumar, A.; Whitesides, G. M. "Fabrication and Imaging of Two-Dimensional Patterns of Proteins Adsorbed on Self-Assembled Monolayers by Scanning Electron Microscopy" *J. Am. Chem. Soc.* **1993**, *115*, 10774-10781.

62. (a) Spinke, J.; Liley, M.; Guder, H.-J.; Angermaier, L.; Knoll, W. "Molecular Recognition at Self-Assembled Monolayers: The Construction of Multicomponent Multilayers" *Langmuir* **1993**, *9*, 1821-1825. (b) Spinke, J.; Liley, M.; Schmitt, F.-J.; Guder, H.-J.; Angermaier, L.; Knoll, W. "Molecular Recognition at Self-Assembled Monolayers: Optimization of Surface Functionalization" *J. Chem. Phys.* **1993**, *99*, 7012-7019.

63. Mrksich, M.; Whitesides, G. M. "Patterning Self-Assembled Monolayers Using Microcontact Printing: A New Technology for Biosensors?" submitted for publication in *Tends in Biotechnology*.

CHAPER TWO

SELECTIVE DEPOSITION OF CONDUCTING POLYMERS VIA MONOLAYER PHOTOPATTERNING

Introduction

Conducting polymers may be selectively electrodeposited on Au surfaces using photochemically patterned disulfide SAMs. Patterns of electropolymerized aniline, 3-methyl-thiophene, and pyrrole replicate the pattern formed by selective irradiation of SAMs of di-11-(4-azidobenzoate)-1-undecyl disulfide, **I**. As described in Chapter One, irradiation of Au-**I** SAMs in the presence of various primary or secondary amines results in the attachment of the amine in very high yields. Patterned SAM substrates are fabricated by irradiating Au-**I** surfaces through a mask in the presence of a functionalized amine, as depicted in Scheme 2.1. The non-irradiated regions terminate in aryl azide,

Scheme 2.1. Irradiation of Au-**I** SAMs through a mask in the presence of functionalized amines produces a patterned SAM.

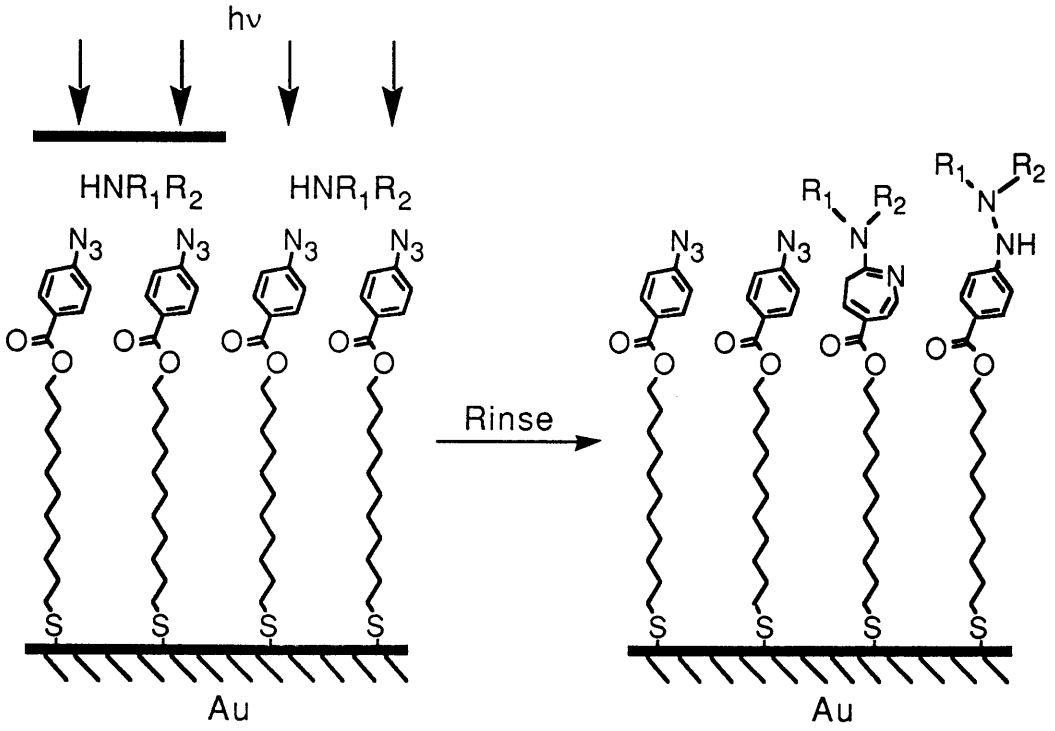

and the irradiated regions terminate in the functionality of the chosen amine. The initial motivation of this study was to determine whether SAM patterns could be used to effect the deposition of a bulk material. As described in Chapter One, an obvious way to pattern SAMs is in surface free energy, or wettability. Selective irradiation of Au-**I** SAMs in the presence of $(HOCH_2CH_2)_2NH$ produces hydrophilic surfaces that are easy to distinguish from the remaining unirradiated, hydrophobic SAM regions which terminate in aryl azide. The first experiment in controlling the deposition of a bulk material in this fashion achieved contrast in Pt electroplating.[1] The surface was prepared by selectively irradiating a SAM of **I** in $(HOCH_2CH_2)_2NH$. Subsequent electrodeposition of Pt resulted in deposition of polycrystalline Pt only on the hydrophilic regions of the surface. This result was first explained by thermodynamic differences in Pt nucleation between hydrophlic and hydrophobic regions, but the issue was never resolved.

Polyaniline is the second material that was selectively deposited onto Au-**I** samples.[2] To use metal and conducting polymer films as active elements in, for example, circuits, LEDs, and detectors, it will be necessary to control the lateral formation or deposition of these materials. Methods to pattern polypyrrole, polythiophene, and polyaniline derivatives by selective oxidation of the corresponding monomer have recently been reported,[3,4] including other reports of selective polymer deposition by use of a chemically patterned surface.[5] In the selective deposition of polyaniline it was the difference in electron transfer rate, not surface free energy, that resulted in deposition contrast. The same control of polymer deposition was additionally possible with poly(3-methylthiophene) and polypyrrole. As with polyaniline, near-micron resolution patterns of these polymers were obtained easily.[6]

This chapter describes the selective electrodeposition of three important classes of conducting polymers—polyaniline, poly(3-methylthiophene), and polypyrrole—from either aqueous or organic solution. Research in the Wrighton Group has focused heavily on the chemical, electronic, and electrochemical properties of several conducting

polymers including polyaniline, polythiophene, and polypyrrole.[7] The polymer patterns are characterized by optical microscopy, X-ray photoelectron spectroscopy (XPS), stylus profilometry, and cyclic voltammetry. Electrochemical studies of the monomers and two reversible redox couples, $Fe(CN)_6^{3-/4-}$ and N,N,N',N'-tetramethyl-1,4-phenylene-diamine$^{2+/+/0}$ (TMPD), through different homogeneous SAMs used as components in the SAM patterns confirm our preliminary finding[2] that differences in electron transfer rate through the different SAMs primarily account for the polymer patterns. We therefore expect this method to be one generally applicable to the selective electrodeposition of a wide variety of organic materials on appropriately patterned SAM substrates.

Experimental Section

Materials. All solvents (HPLC grade) and chemicals (highest purity available) were purchased from commercial sources and used as received unless otherwise stated. The synthesis of di-11-(4-azidobenzoate)-1-undecyl disulfide, **I**, has been reported.[8] All amines (Aldrich) were distilled from KOH under reduced pressure and stored under Ar. Aniline and pyrrole (Aldrich) were distilled under reduced pressure and kept in the dark (pyrrole was refrigerated) until used. TMPD (Aldrich) was purified by sublimation.

Polycrystalline Au substrates were prepared by thermal evaporation (Edwards Auto 306 Cryo evaporator) of a 20 Å Cr adhesion layer followed by 1000 Å of Au on 2.5 cm x 1.2 cm pieces of Si (100) wafers (Silicon Sense: Nashua, NH; test grade, 500 μm thick). Before evaporation, the Au (99.99% wire) was cleaned in aqua regia, rinsed with Millipore H_2O, EtOH, and oven dried.

Mask Fabrication. The Cr-on-glass mask was fabricated at MIT and was originally designed for use in the fabrication of microelectrodes by standard lithographic techniques. The feature sizes on the mask range from 2-100 μm.

Formation of SAMs. Monolayers of **I** were formed by immersion of the Au substrates in 2-3 mM methylcyclohexane solutions for at least 12 h. Monolayers of dodecanethiol were formed for at least 2 h from 2-3 mM EtOH solutions. In all cases, SAMs were formed on Au-coated Si substrates immediately after evaporation. Before use or characterization, all SAM substrates were rinsed in EtOH (SAM substrates of **I** were first rinsed with methylcyclohexane, then EtOH) and dried with a stream of dry Ar.

Photopatterning of Au-I SAMs. A drop of the desired amine was placed on freshly rinsed and dried Au-**I** substrates. For fabrication of micron-sized features, the mask was then placed on top of the substrates, Cr-side down, forcing the amine to spread evenly across the samples. The assembly was irradiated through the mask by a 200 W Hg short-arc lamp through a filter (10 cm path length, quartz walls filled with 1:1:1 H_2O: EtOAc: EtOH; $\lambda > 260$ nm) for 2 min. For fabrication of large simple patterns, a quartz plate was

used instead of the mask. A small piece of Si was fixed to the plate to mask one section of the samples from irradiation. After irradiation, the samples were carefully removed from the mask, rinsed with copious amounts of EtOH, and dried with Ar.

Polymerization. Aniline: Substrates were immersed in an aqueous 0.11 M solution (0.85 M H_2SO_4, 0.25 M $NaHSO_4$) of aniline. Using a potentiostat (RDE4: Pine Instruments) the substrate was repeatedly cycled at 200 mV/sec between 0.0 V and a maximum positive potential between 0.85 V and 1.20 V vs. SCE. In most cases described in this report, the substrate was cycled between 0.0 V and 1.2 V for 4-6 scans, then between 0.0 V and 0.8 V until the pattern was clearly visible (~10 cycles). The substrates were then rinsed with H_2O and dried with Ar.

3-methylthiophene and pyrrole: Substrates were immersed in a 0.10 M or 0.14 M solution (of 3-methylthiophene or pyrrole, respectively) of 0.1 M [*n*-Bu_4N]PF_6 in CH_3CN. Samples were scanned from 0.0 V to ~1.7 V or ~1.05 V vs. Ag wire, for 3-methylthiophene and pyrrole, respectively, until the polymer was sufficiently thick (~10 s) as judged by eye. The substrates were then rinsed with CH_3CN and dried with Ar.

Stylus Profilometry. A Dektak 3 (Veeco/Sloan Technology: Santa Barbara, CA) was used with a 12.5 μm radius tip (0.1 μm horizontal resolution), and 37 s scan rate.

X-ray Photoelectron Spectroscopy. The XPS data were acquired on an SSX-100 spectrometer (Surface Science Instruments) equipped with an Al Kα source, quartz monochromator, concentric hemispherical analyzer, and multichannel detector. Spectra were aquired at an incident angle of 55° (with respect to normal) at a 100 eV pass energy, 600 μm spot size, and 100 W electron beam power. Binding energies were referenced to the Au $4f_{7/2}$ peak at 84.0 eV.

Cyclic Voltammetry. Cyclic voltammograms were measured using a Pine Instruments RDE4 potentiostat and recorded with a Kipp and Zonen BD90 XY chart recorder. An O-ring cell was used to maintain a constant surface area (0.71 cm^2) from sample to sample. Measurements of 1.0 mM $K_4Fe(CN)_6$ and TMPD were made from the

aqueous and CH_3CN electrolyte solutions described above, respectively. All measurements in aqueous solution are referenced to SCE, those in CH_3CN to Ag wire. The Ag wire was measured to be 0.22 V positive of SCE. The two redox couples were observed to be unstable over the period of several hours in the solutions used. The measurements were made in air and saturating the solutions with Ar had little effect. Therefore, both $K_4Fe(CN)_6$ and TMPD solutions were freshly prepared immediately before each measurement from stable stock solutions. After the brief set-up and measurement (~3 min) the solution was removed and the equipment was thoroughly rinsed with the appropriate solvent. This method provided consistent results for these series of measurements.

Ellipsometry. Monolayer thickness was measured on a Gaertner L116A Ellipsometer using a wavelength of 6328 Å and an incident angle of 70°. Readings were first taken from freshly evaporated Au substrates to establish optical constants, then on the same samples after monolayer formation. Thickness of the bare Au samples was assumed to be zero. The average value of three measurements taken on each of three points across the substrate, and an assumed index of refraction of 1.46, were used to calculate SAM thickness using the software supplied with the instrument. Scatter in the data was small, typically ±1 Å.

Results and Discussion

Films of polyaniline, poly(3-methylthiophene), and polypyrrole can be selectively deposited electrochemically on Au substrates containing photopatterned SAMs. The patterned substrates were formed by irradiating SAMs of di-11-(4-azidobenzoate)-1-undecyl disulfide, **I**, on Au through a mask in the presence of various primary or secondary amines, as described above. The patterned substrates were rinsed, dried, and placed in a 0.1 M monomer (aniline, 3-methylthiophene, or pyrrole) solution containing electrolyte. Using a potentiostat, the substrates were brought to a potential at which the monomer was oxidized, thus initiating polymerization. Regardless of the amine used in photochemical patterning (typically either $[CH_3(CH_2)_3]_2NH$ or $[CH_3(CH_2)_7]_2NH$), distinct polymer patterns replicating the mask pattern formed within less than a minute. The samples were then removed from solution, rinsed, dried, and stored in air. The patterns of conducting polymers formed by this technique are easily seen by visual inspection.

Demonstration of Selective Polymer Deposition. Selectively deposited films of polyaniline, poly(3-methylthiophene), and polypyrrole are clearly seen on the underlying Au substrate. Figure 2.1 shows millimeter and micron resolution optical micrographs of these three polymer patterns. These patterns exactly match that of the mask used during the selective irradiation of Au-**I** in the presence of $[CH_3(CH_2)_7]_2NH$. The dark regions correspond to polymer films 0.02 to 0.2 μm thick (see discussion of stylus profilometry below) covering the non-irradiated regions of the monolayer. The light regions contain little or no polymer and are composed of irradiated SAMs of **I**, and the underlying Au substrate.

The thickness of the selectively deposited films is more precisely and most easily determined by stylus profilometry. Figure 2.2 shows line profiles of the three polymer patterns, each on two different regions of the pattern. The thickness of each of the polymer films in the large features ranges from 0.1 μm to 0.2 μm, although films as thick

Figure 2.1. Optical micrographs of polyaniline, poly(3-methylthiophene) and polypyrrole patterns formed by oxidizing the monomers on patterned SAM substrates, as described in the text. The dark regions correspond to polymer deposited on non-irradiated SAMs of **I**. The light regions contain little or no polymer and correspond to Au-**I** SAMs irradiated in the presence of $[CH_3(CH_2)_7]_2NH$. The microstructures in the bottom micrographs are 4 μm center-to-center.

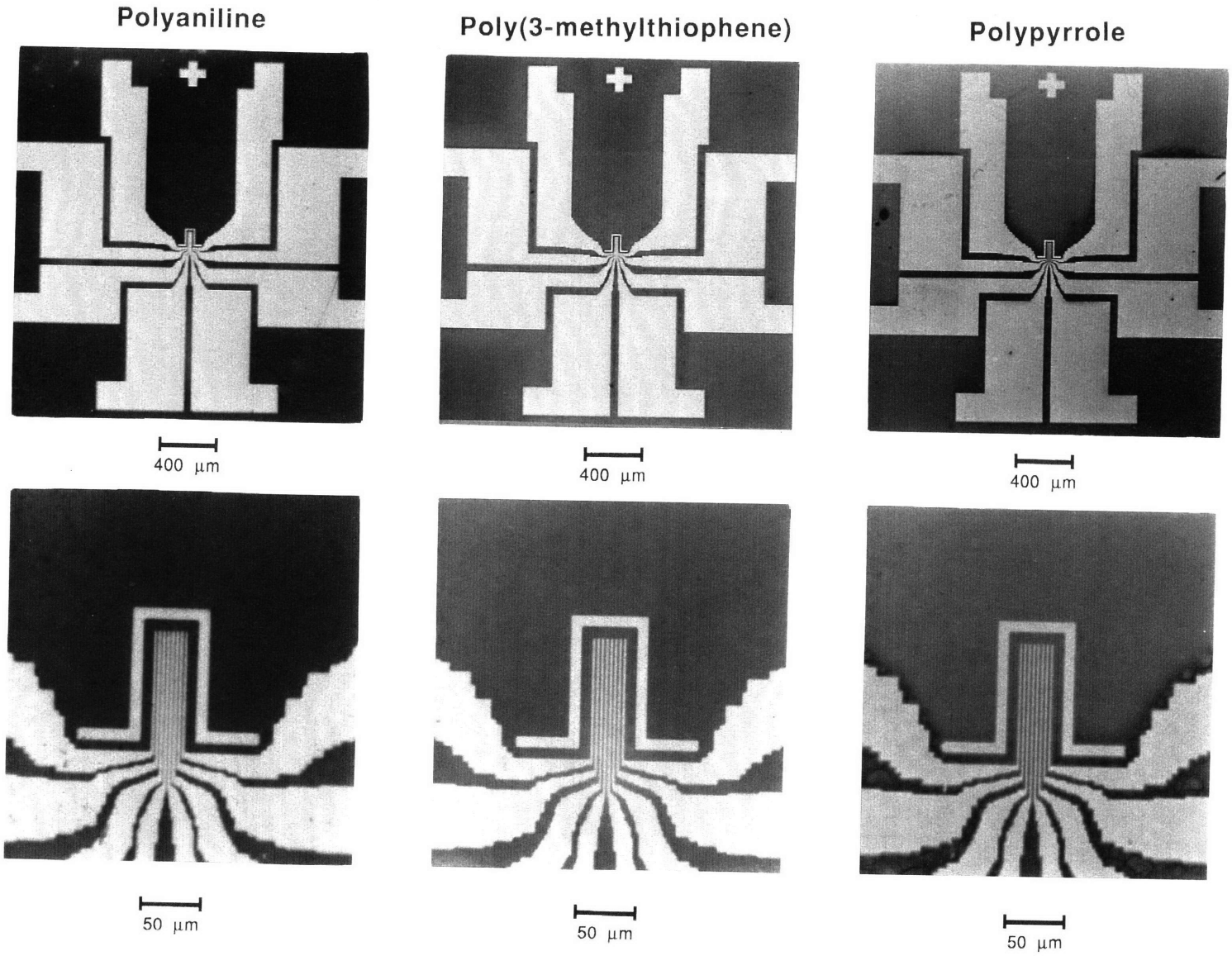
Polyaniline
Poly(3-methylthiophene)
Polypyrrole
400 μm
400 μm
400 μm
50 μm
50 μm
50 μm

Figure 2.2. Stylus profilometry traces of (three upper traces) the low resolution and (three lower traces) high resolution microline features. The line profiles are taken from the same samples shown in Figure 2.1.

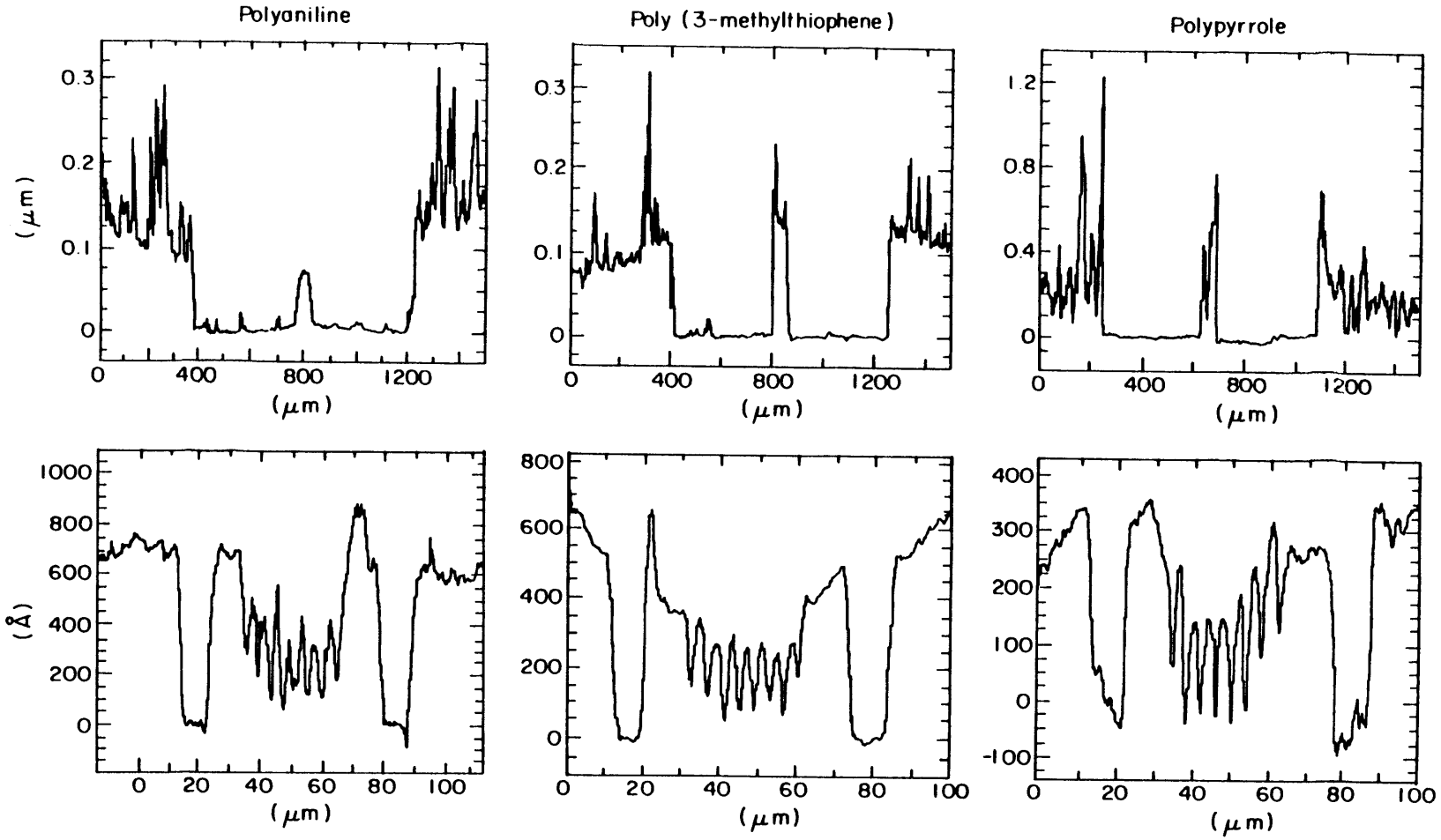
Polyaniline
Poly (3-methylthiophene)
Polypyrrole
(μm)
(μm)
(Å)
(μm)

as 0.5 μm have been measured on some samples. The films in the micro-patterned regions appears to be thinner, about 300-600 Å (see below), and measurement of the highest resolution features (the 7 polymer microlines are 4 μm center-to-center) appears to approach the lateral resolution limit of the profilometer for this type of sample. The difference in roughness between the coated and uncoated regions of the patterns, most evident in the large pattern features, is another indication of the deposition selectivity. Contrast between the rough polymer regions and the relatively smooth Au regions hints that there is little or no polymer on the irradiated regions of the SAM-coated surface.

A more rigorous characterization of the selectively deposited polymer films is provided by X-ray photoelectron spectroscopy (XPS) and cyclic voltammetry. For these analyses, larger-scale patterns were fabricated using nearly identical methods used to prepare the samples shown in Figure 2.1. Polymer was deposited on centimeter-sized photopatterned Au-**I** substrates by irradiating half of each substrate in the presence of $[CH_3(CH_2)_7]_2NH$ or $[CH_3(CH_2)_3]_2NH$. By profilometry, selectively deposited polymer films ranged from 0.15 to 0.5 μm in thickness. Figure 2.3 shows N 1s and Au 4f XPS spectra of a sample with selectively deposited polyaniline. In Figure 2.3a the analysis area is a non-irradiated region of **I** that was anodically cycled in the aniline polymerization solution (i.e., dark regions in Figure 2.1). The single N peak at a binding energy of 399.2 eV is attributed to the N in polyaniline. The azide N peak (404.1 eV), and the Au peaks, not shown, have been completely attenuated by the selectively deposited polymer. Figures 2.3b and 2.3c show spectra of an adjacent area irradiated in $[CH_3(CH_2)_3]_2NH$ that had also been subjected to polymerization conditions (i.e., light regions in Figure 2.1). Here, the N (399.2 and 400.6 eV) and Au peaks (84.0 and 87.6 eV) are essentially the same as those of a native SAM of **I** irradiated in $[CH_3(CH_2)_3]_2NH$. Little or no polyaniline is detected by XPS in this region of the surface.

Figure 2.3. A comparison of N 1s and Au 4f XPS spectra of a polyaniline pattern: (a) a polyaniline-coated region showing one N peak and strongly attenuated Au peaks; (b), (c) a region without polyaniline showing N and Au peaks, consistent with a monolayer of irradiated aryl azide, respectively. The Au 4f peak of the polyaniline region is completely attenuated and is not shown.

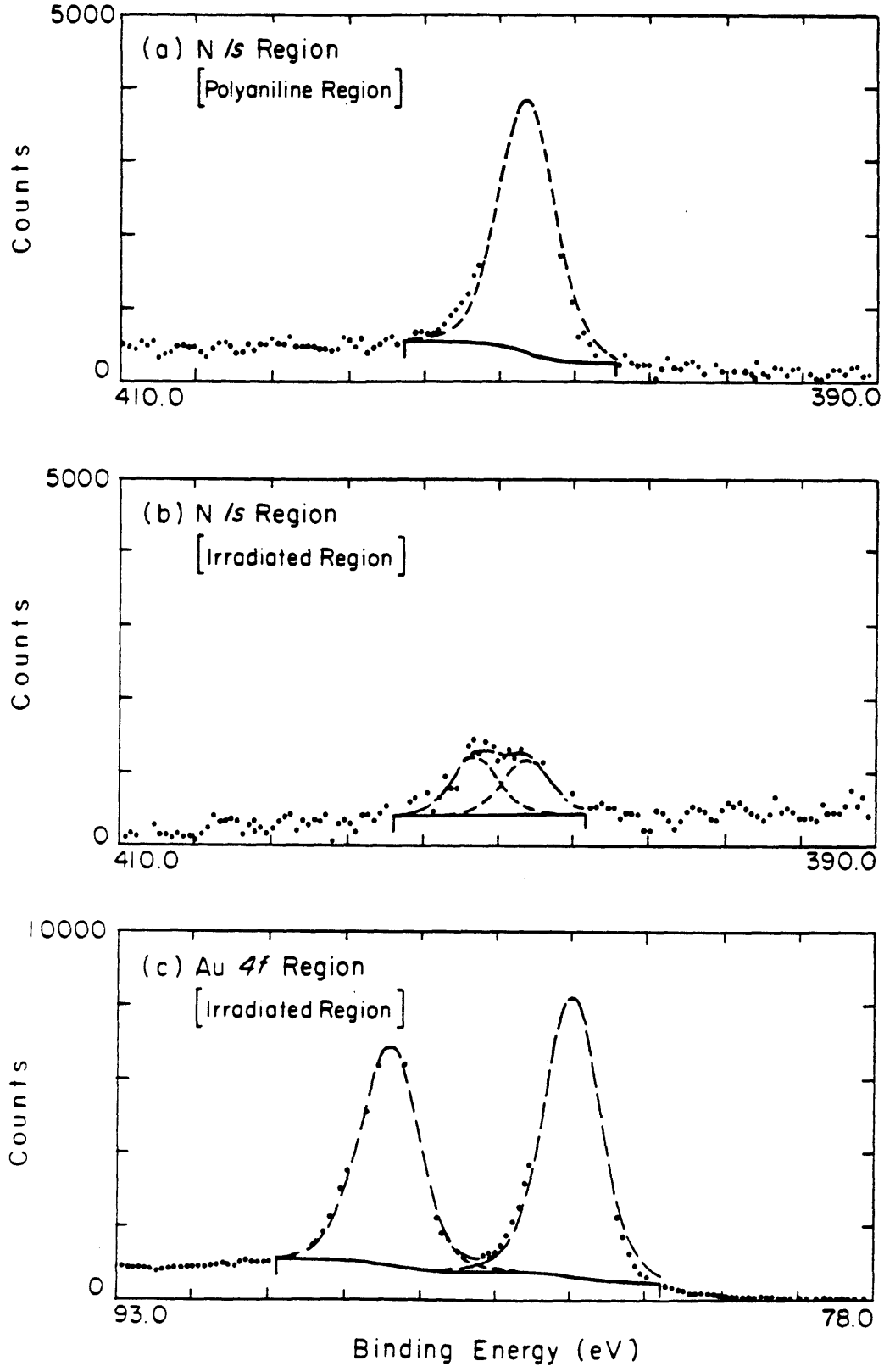
5000
(a) N 1s Region
[Polyaniline Region]
Counts
0
410.0
390.0
5000
(b) N 1s Region
[Irradiated Region]
Counts
0
410.0
390.0
10000
(c) Au 4f Region
[Irradiated Region]
Counts
0
93.0
78.0
Binding Energy (eV)

Selectively deposited films of poly(3-methylthiophene) and polypyrrole were similarly analyzed. The S 2p peak (163.9 eV) was used to detect polymer in the case of poly(3-methylthiophene). Spectra of selectively deposited poly(3-methylthiophene) and poly-pyrrole films, not shown, are in qualitative agreement with those shown in Figure 2.3 of polyaniline. Data for all three polymer systems, in addition to those of native SAMs of **I** and **I** irradiated in the presence of $[CH_3(CH_2)_3]_2NH$, are presented in Table 2.1. Each SAM region of **I** shows a large N or S peak attributed to the heteroatom in the polymer, and significantly or completely attenuated Au peaks. Regions of irradiated **I** show N and Au peaks which resemble those of native SAMs both in binding energy and in counts. In the case of pyrrole, the relatively strong N peak may be attributed to a small

Table 2.1. XPS analysis of the two polymer pattern regions

		Counts[a] (x 1000)		
SAM	Treatment	Au 4f	N 1s	S 2p
I	none	220	20	
Irradiated **I**	none	150	10	
I	aniline	0	40	
Irradiated **I**	aniline	170	10	
I	3-methylthiophene	2	0	30
Irradiated **I**	3-methylthiophene	170	10	0
I	pyrrole	0	80	
Irradiated **I**	pyrrole	170	30	

[a] Counts are taken from all peaks corresponding to the appropriate atom. Peak binding energies are as follows: Au 4f, 84.0 and 87.6 eV; N 1s, 399.2 and 400.6 eV; S 2p, 163.9 eV.

amount of polymer, however the strong Au signal indicates the amount of polymer must indeed be minute. (Due to the high surface sensitivity of XPS, an extremely small amount of polypyrrole in this region could significantly increase the N 1s signal intensity.) Taken as a whole, the data for the three polymer systems are consistent and offer the same conclusions: polymer selectively grows only on SAMs of **I**—non-irradiated regions of the substrate—and little or no polymer forms on irradiated regions.

The final method used to establish selectivity in polymer deposition is cyclic voltammetry, which provides an electrochemical method of polymer detection. Figure 2.4 shows representative cyclic voltammograms of three simple patterned samples prepared identically to those used in the XPS analysis. The non-irradiated regions clearly show reversible or quasi-reversible oxidation peaks of the polymer (solid curves) and are consistent with voltammograms reported in the literature.[7c,9] In all three cases the irradiated regions of the sample show only small capacitative currents (dashed curves) and no peaks that can be ascribed to polymer. Cyclic voltammetry is very sensitive to the presence of redox-active species, and current from electropolymerized material can easily be detected at μC levels. The data in Figure 2.4 show that polymer contrast is very high; the ratio of polymer on non-irradiated Au-**I** regions to irradiated Au-**I** regions is greater than 1000:1. Polymer is selectively deposited on non-irradiated SAMs of Au-**I** and no polymer is present on the irradiated regions of the sample.

Factors Influencing Selective Polymer Deposition. Patterns of all three polymers are formed easily. Variation of amine used in the irradiation and the maximum potential used during electropolymerization have slight effects (see below) but in all cases polymer initially deposits on non-irradiated regions of the sample. The exact degree of contrast, ultimate resolution, thickness, uniformity, and other physical characteristics of the polymers depends on subtle electropolymerization conditions. Many patterned samples have been prepared and examined under a microscope at various stages of polymerization. In the case of polyaniline, selective deposition in the highest resolution

Figure 2.4. Cyclic voltammetric plots of (a) polyaniline, (b) poly(3-methylthiophene), and (c) polypyrrole patterns. Solid lines (—) are voltammograms from regions of Au-**I** SAMs; dashed lines (- -) are voltammograms from regions of Au-**I** SAMs irradiated in the presence of $[CH_3(CH_2)_7]_2NH$.

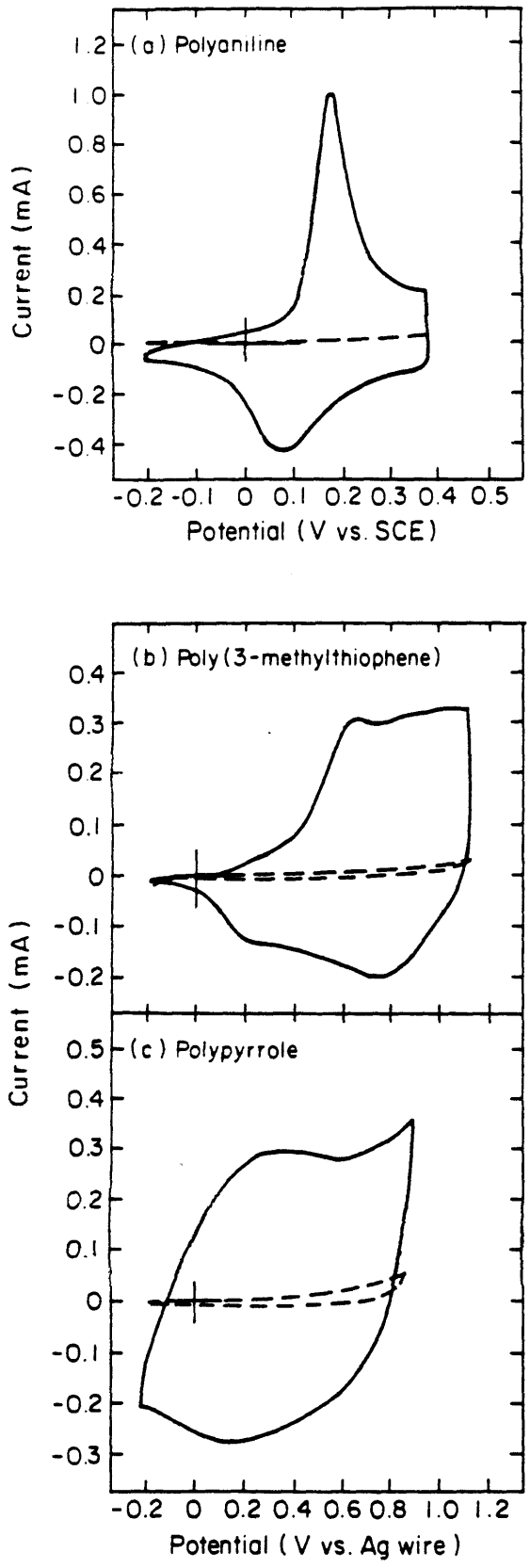
(a) Polyaniline
(b) Poly(3-methylthiophene)
(c) Polypyrrole
Current (mA)
Potential (V vs. SCE)
Potential (V vs. Ag wire)

areas of the sample occurred only after polymer had first selectively deposited on the larger lateral features of the SAM pattern. Evidence of this behavior is shown in Figure 2.2; the larger lateral features seem to be thicker than the high resolution features. The reason for slow polymer growth on the higher resolution features is not yet known but does not preclude the formation of micron-sized features after additional electropolymerization. This behavior was not observed with poly(3-methylthiophene) or polypyrrole; the high and low resolution regions of these patterns were equally visible at all polymer thicknesses.

As discussed in the next section, it is our hypothesis that electron transfer rate differences between the two regions of the patterned SAM is chiefly responsible for selective polymer deposition. The two regions of the SAM pattern also differ chemically, however. While the exposed regions of the irradiated SAMs consist of alkane chains, the non-irradiated regions terminate in a potentially reactive aryl azide group. The possibility of azide reaction with monomer can be ruled out by preparing SAM patterns with no terminal azide groups. After the initial irradiation of Au-**I** SAMs, a second irradiation results in a monolayer pattern terminating in two different amines.[10] The aryl azide groups have been completely reacted in these SAMs. Electropolymerization on these SAM patterns also results in polymer patterns, with polymer first depositing on the thinner SAM regions. Contrast in these patterns is low due to the relatively small difference in electron transfer rate between the different irradiated Au-**I** SAMs. This result is consistent with our hypothesis however, and indicates that the chemical nature of the terminal SAM groups is not of principal importance.

Selective Polymer Deposition and Differences in Electron Transfer Rate through Different Regions in Patterned SAMs. In this study, the most important difference between irradiated and non-irradiated SAMs in the monolayer pattern is attenuation of electron transfer. Figure 2.5 shows plots of current density vs. potential for the oxidation of aniline in aqueous solution on various homogeneous SAM surfaces. Similar plots for

3-methylthiophene and pyrrole in CH_3CN are shown in Figures 2.6 and 2.7, respectively. The curves can be thought of as the first sweeps in cyclic voltammograms of the respective monomers and are consistent with the patterning results. Compared to bare Au, Au modified with **I** shows less current for monomer oxidation. Most important, photochemically functionalized SAMs of **I** yield even less oxidation current. The current density values on homogeneous samples of dodecanethiol are shown as a comparison.

Useful information about electropolymerization is contained in these qualitative results. The data presented in Figures 2.5-2.7 suggest that patterns can be formed by oxidizing the monomer at potentials that are different for two regions of the SAM pattern, and that the highest contrast patterns can be fabricated at potentials of the largest current difference. Several electropolymerization trials have supported this notion. Though patterns of polyaniline can be formed by repeatedly cycling between 0.0 V and a maximum potential as low as 0.8 V, the best patterns are made by first cycling between 0.0 V and 1.2 V. To maximize contrast, after a small amount of conducting material has deposited on non-irradiated regions (after 4-5 scans), the maximum potential is reduced to 0.8 V. The large overpotential is avoided so that aniline continues to polymerize on the newly deposited polymer surface and not on the passivated monolayer surface. Similar control over the polymerization of 3-methylthiophene and pyrrole is more difficult since a maximum potential is held constant until polymer pattern has formed completely—only then is the potential returned to 0.0 V.

Qualitative differences in electron transfer rate between different SAMs can be additionally probed by cyclic voltammetry of reversible one-electron redox couples. A comparison of cyclic voltammograms of $Fe(CN)_6^{3-/4-}$ in the aqueous polymerization solution on several homogeneous SAMs is presented in Figure 2.8. The two upper sets of curves show the diminution of electron transfer of SAMs of **I** and dodecanethiol compared to that of bare Au. The current at $E_{1/2}$ on a Au-**I** SAM is reduced by a factor of 10^3 from that on bare Au. The lower voltammograms compare current on SAMs of

Figure 2.5. Current vs. potential curves for aniline (0.11 M in aqueous 0.85 M H_2SO_4, 0.25 M $NaHSO_4$). Each point (taken from a linear sweep voltammogram at 200 mv/s, 0.0-1.2 V vs. SCE) is the average of at least four measurements from freshly prepared samples. Curves are meant to guide the eye only.

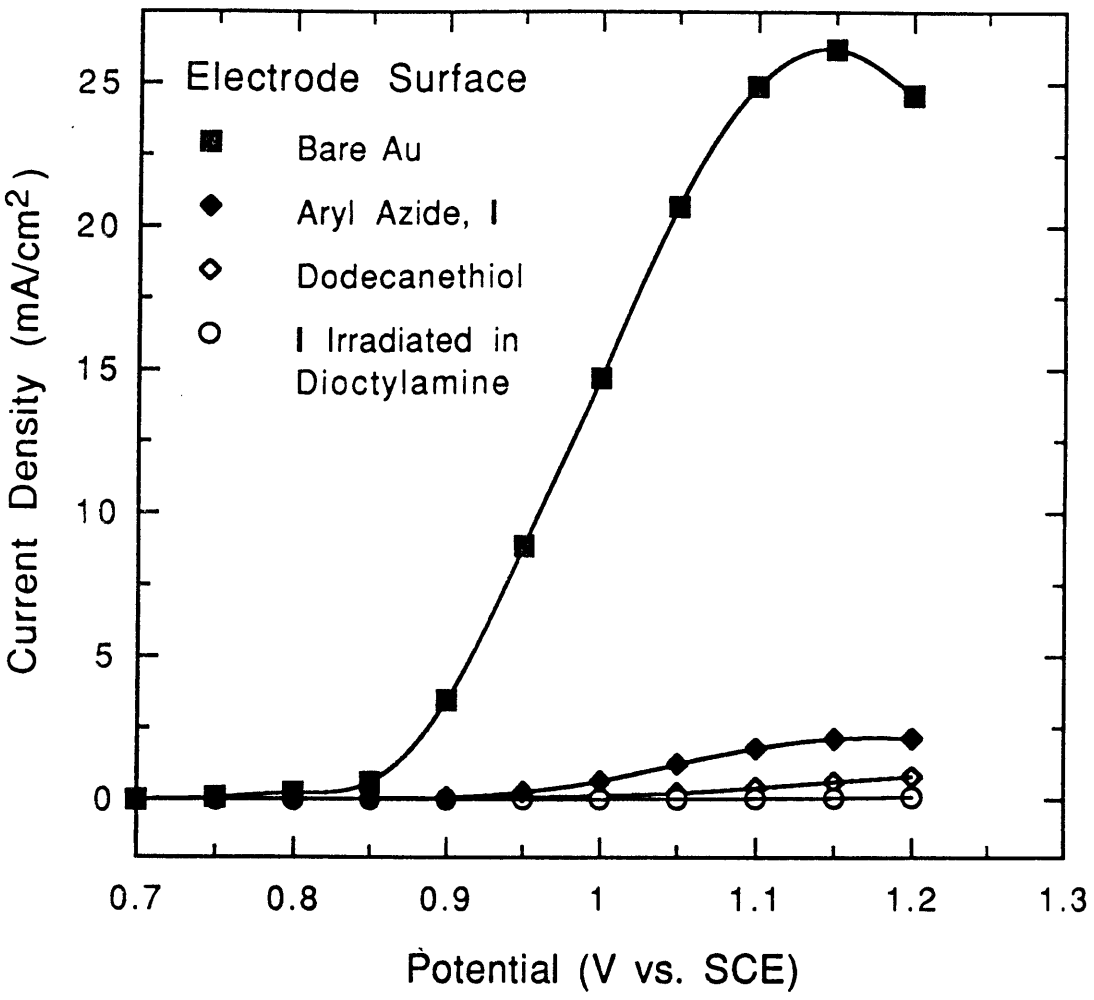
Electrode Surface
Bare Au
Aryl Azide, I
Dodecanethiol
I Irradiated in Dioctylamine
Current Density (mA/cm2)
25
20
15
10
5
0
0.7
0.8
0.9
1
1.1
1.2
1.3
Potential (V vs. SCE)

Figure 2.6. Current vs. potential curves for 3-methylthiophene (0.10 M in CH_3CN, 0.1 M [*n*-Bu_4N]PF_6). Each point (taken from a linear sweep voltammogram at 200 mv/s, 0.0-1.7 V vs. Ag wire) is the average of at least two measurements from freshly prepared samples. Curves are meant to guide the eye only.

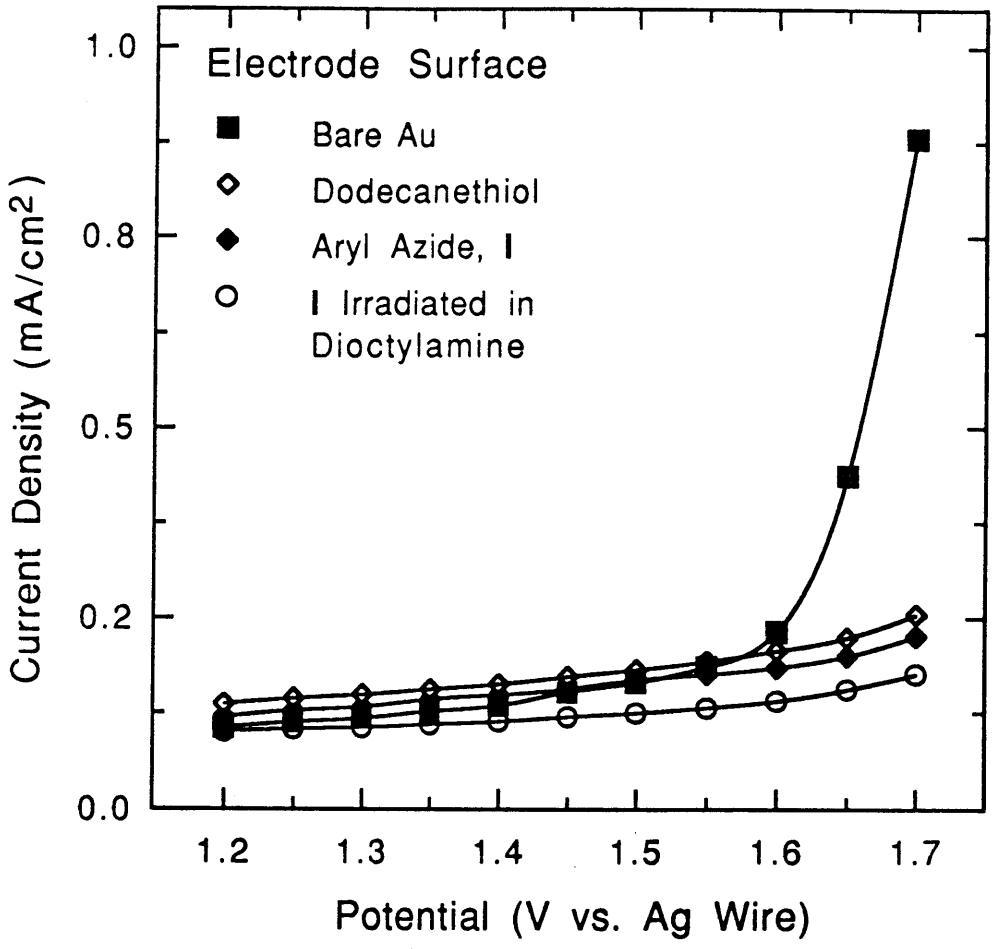
Electrode Surface
Bare Au
Dodecanethiol
Aryl Azide, I
I Irradiated in Dioctylamine
Current Density (mA/cm2)
1.0
0.8
0.5
0.2
0.0
1.2
1.3
1.4
1.5
1.6
1.7
Potential (V vs. Ag Wire)

Figure 2.7. Current vs. potential curves for pyrrole (0.14 M in CH_3CN, 0.1 M [*n*-$Bu_4N]PF_6$). Each point (taken from a linear sweep voltammogram at 200 mv/s, 0.0-1.2 V vs. Ag wire) is the average of at least two measurements from freshly prepared samples. Curves are meant to guide the eye only.

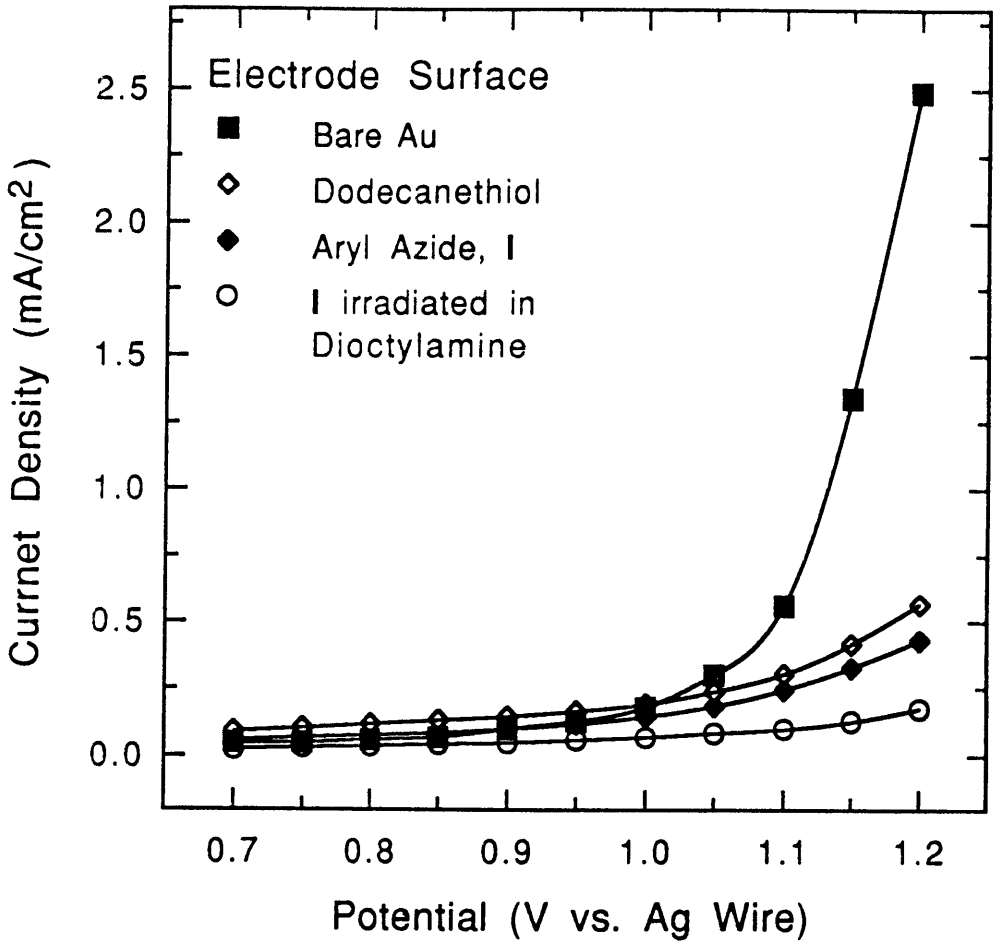
Electrode Surface
Bare Au
Dodecanethiol
Aryl Azide, I
I irradiated in Dioctylamine
Currnet Density (mA/cm2)
2.5
2.0
1.5
1.0
0.5
0.0
0.7
0.8
0.9
1.0
1.1
1.2
Potential (V vs. Ag Wire)

Figure 2.8. Current vs. potential plots for $Fe(CN)_6^{3-/4-}$ (1.0 mM in aqueous polymerization solution, 200 mV/s) on bare Au and various homogeneous SAM surfaces.

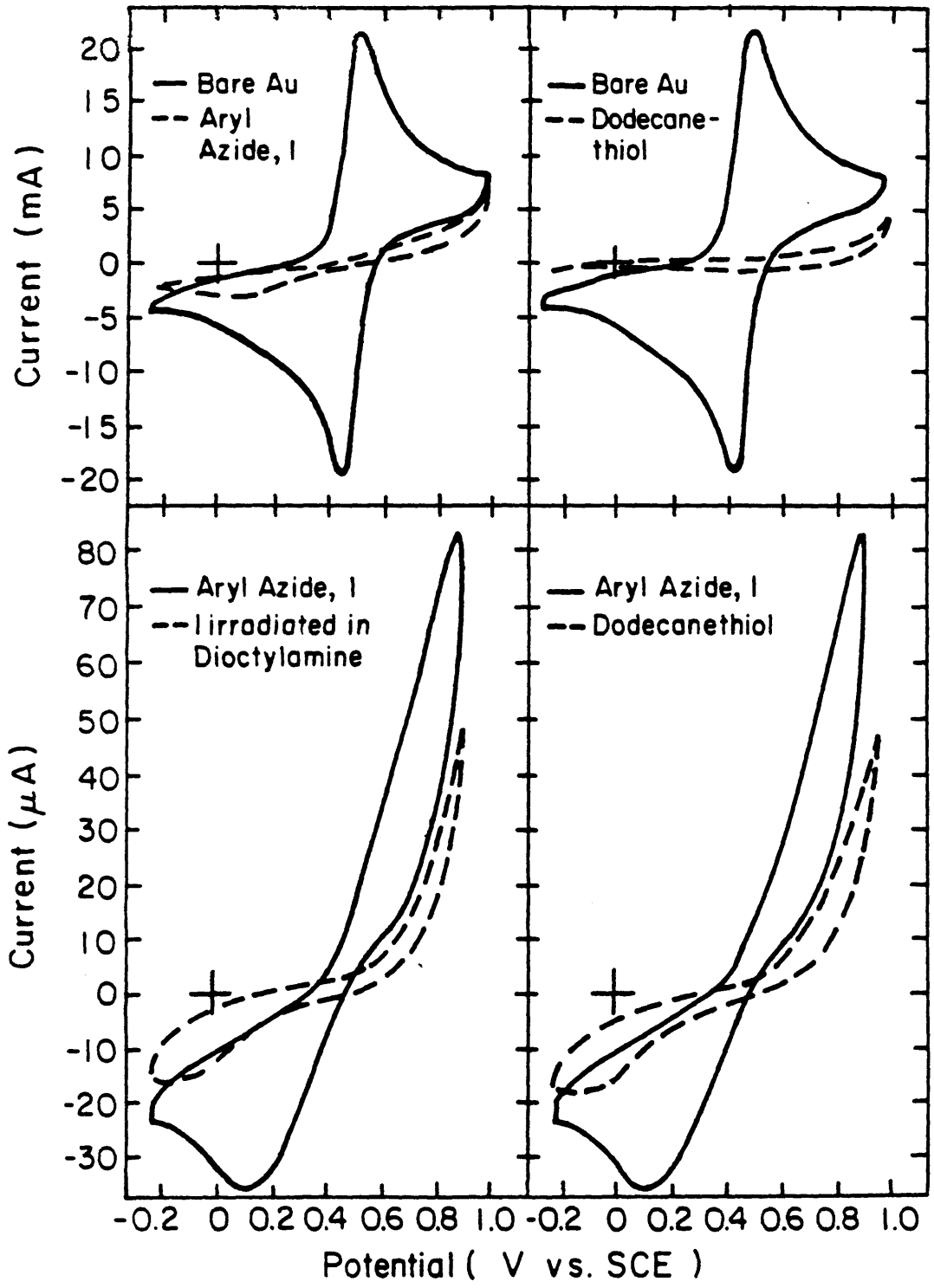
Bare Au
Aryl Azide, I
Bare Au
Dodecane-thiol
Aryl Azide, I
I irradiated in Dioctylamine
Aryl Azide, I
Dodecanethiol
Current (mA)
Current (μA)
Potential (V vs. SCE)

Figure 2.9. Current vs. potential plots for $TMPD^{2+/+/0}$ (1.0 mM in CH_3CN polymerization solution, 200 mV/s) on bare Au and various homogeneous SAM surfaces.

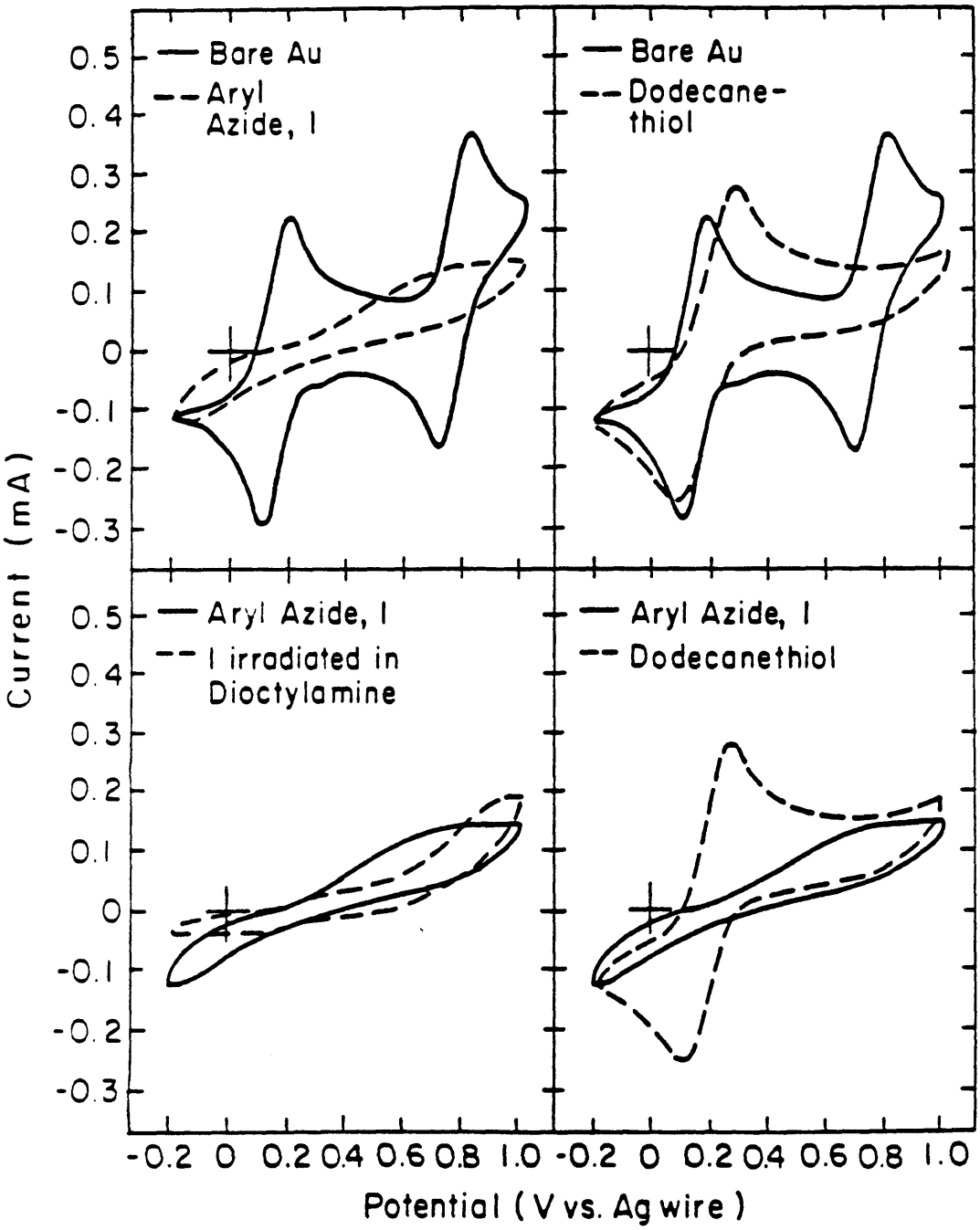
Bare Au
Aryl Azide, I
Bare Au
Dodecane-thiol
Aryl Azide, I
I irradiated in Dioctylamine
Aryl Azide, I
Dodecanethiol
Current (mA)
0.5
0.4
0.3
0.2
0.1
0
-0.1
-0.2
-0.3
-0.2 0 0.2 0.4 0.6 0.8 1.0
Potential (V vs. Ag wire)

irradiated **I** and dodecanethiol to SAMs of **I**. The current at $E_{1/2}$ on SAMs of both irradiated **I** and dodecanethiol are reduced by an additional order of magnitude from that on Au-**I**. Differences in electron transfer rate to this reversible one-electron couple are in general agreement with those during the irreversible oxidation of aniline (Figure 2.5). For aniline, current density at E_p (~1.15 V vs. SCE) is highest on bare Au, and reduced by a factor of 10 on a SAM of Au-**I**. Monolayers of dodecanethiol attenuate electron transfer to a greater extent, followed by SAMs of irradiated **I**. Figures 2.6 and 2.7 show that current densities for the oxidation of 3-methylthiophene and pyrrole, respectively, are attenuated to a *greater* extent on SAMs of **I** than SAMs of dodecanethiol, and are consistently attenuated the most on monolayers of irradiated **I**. As in the case of aqueous solution, a reversible redox couple was used to model qualitative electron transfer rate differences in CH_3CN. Cyclic voltammograms of $TMPD^{2+/+/0}$ (Figure 2.9) on these homogeneous SAM surfaces show the same trend as those of $Fe(CN)_6^{3-/4-}$, specifically that electron transfer rate is the greatest on bare Au, followed by SAMs of **I**, dodecanethiol, and irradiated **I**. (The cyclic voltammogram of TMPD on dodecanethiol, shown in Figure 2.9, is unusual. The first redox couple is accessible, but the second one is not. This behavior is unlike that on **I** or irradiated **I** and we do not currently have a satisfactory model to explain this behavior.) All electrochemical measurements in this study reveal that the trends in electron transfer attenuation through various homogeneous SAMs are in qualitative agreement. With the two reversible redox couples and the three monomers, aniline, 3-methylthiophene, and pyrrole, electron transfer rates decrease as follows:

$$\text{bare Au} >> \mathbf{I} \geq \text{dodecanethiol} > \text{irradiated } \mathbf{I}.$$

Trends in relative oxidation rates of the monomers on different regions of the substrate can be explained by a simple model of SAM structure and thickness. Ellipsometry shows that SAMs of **I**, which can be described as undecanethiol with an ester-linked phenyl azide terminal group, are thicker than SAMs of dodecanethiol, which

have only a methyl terminal group. The thickness of SAMs of **I**, **I** irradiated in $[CH_3(CH_2)_7]_2NH$ or $[CH_3(CH_2)_3]_2NH$, and dodecanethiol was measured to be 22, 25-28, and 14 Å, respectively, assuming a constant index of refraction for all measured SAMs.[11] From cyclic voltammetry and ellipsometry, we propose a simple, qualitative structural model of the SAMs used in this study to account for selective electrodeposition of conducting polymers, illustrated in Scheme 2.2. Electron transfer is obviously fastest on clean, bare Au. SAMs of simple alkanethiols, such as dodecanethiol are well known to form closely packed monolayers[12] and to attenuate electron transfer.[13] Moreover, electron transfer is known, and has been measured in the case of monolayers with pendant redox centers,[14] to decrease exponentially with increasing distance, according to eq 2.1, where k is the apparent rate constant at zero overpotential, and β is the tunneling parameter. In this study, a similar analysis is complicated by using SAMs with

$$k = k^\circ \exp(-\beta d) \qquad (2.1)$$

different terminal substituents, not simple alkanethiols of varying length. Although structural order is maintained in SAMs with small terminal groups,[15] the ideal structure may be perturbed in several ways by the introduction of bulky terminal functionalities such as phenyl azide. Steric crowding may effect the monolayer tilt angle and density, and may thus increase the number of pinhole sites in the monolayer. We hypothesize these defects to be present to some extent in Au-**I** SAMs. Our observation of increased electrode passivation with SAMs of dodecanethiol compared with SAMs of **I**, even though ellipsometry shows that SAMs of **I** are thicker, supports this notion. Figures 2.5-2.8 show that electron transfer to aniline, 3-methylthiophene, pyrrole, and the reversible couple $Fe(CN)_6^{3-/4-}$, is faster through SAMs of **I** than through SAMs of dodecanethiol. To the extent that ellipsometry measurements are accurate for these three monolayer types, irradiation of Au-**I** SAMs in the presence of alkylamines increases monolayer thickness slightly. However, changes in the electron transfer behavior are substantial. Figure 2.10 shows increasing electron transfer rate attenuation for aniline

Scheme 2.2. A structural model of various electrode surfaces.

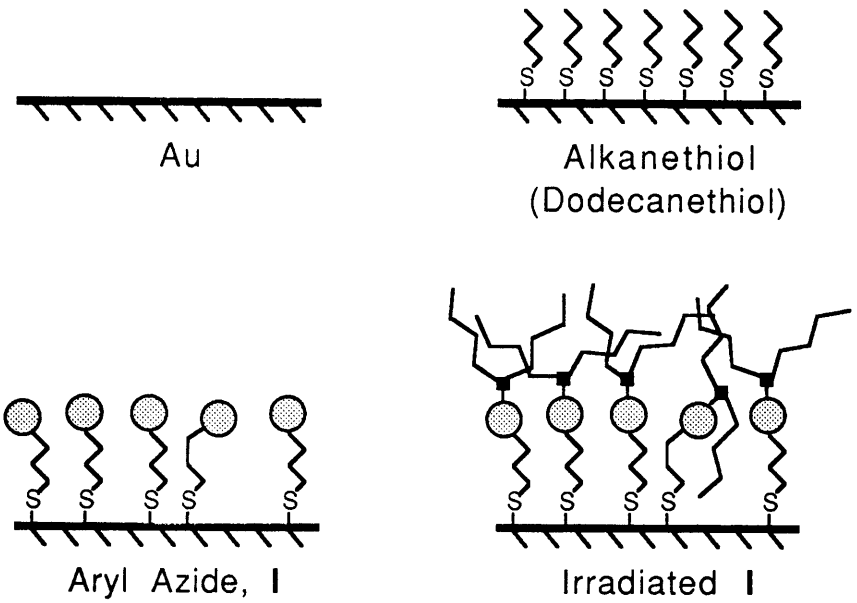

oxidation through successively longer photoattached alkylamines on SAMs of Au-**I**. Again, Scheme 2.2 illustrates our explanation. Irradiation terminates the monolayer in alkyl chains which further block the electrode. These alkyl chains are likely to be structurally disordered, and may even bend downward towards the substrate at pinhole sites. The lack of correlation of SAM thickness with alkyl chain length in photoattached amines is consistent with this model. Electron transfer may occur via electron tunneling through the monolayer, or by diffusion of the redox species to bare Au at pinhole sites in the SAM.[13,15] Additional electrochemical and spectroscopic analysis may help to develop the structural model further, and to determine the mechanism of electron transfer through the various SAMs used in this study. At the present time, our results confirm our hypothesis: in all cases, SAMs of **I** irradiated in $[CH_3(CH_2)_3]_2NH$ or $[CH_3(CH_2)_7]_2NH$ block electron transfer to a greater extent than non-irradiated Au-**I** SAMs, and agree with the observations that polymer is selectively electrodeposited on non-irradiated portions of Au-**I** SAMs.

Figure 2.10. Current vs. potential curves for aniline (0.11 M in aqueous 0.85 M H_2SO_4, 0.25 M $NaHSO_4$) on various SAM surfaces. Each point (taken from a linear sweep voltammogram at 200 mv/s, 0.0-1.2 V vs. SCE) is the average of at least four measurements from freshly prepared samples. Curves are meant to guide the eye only.

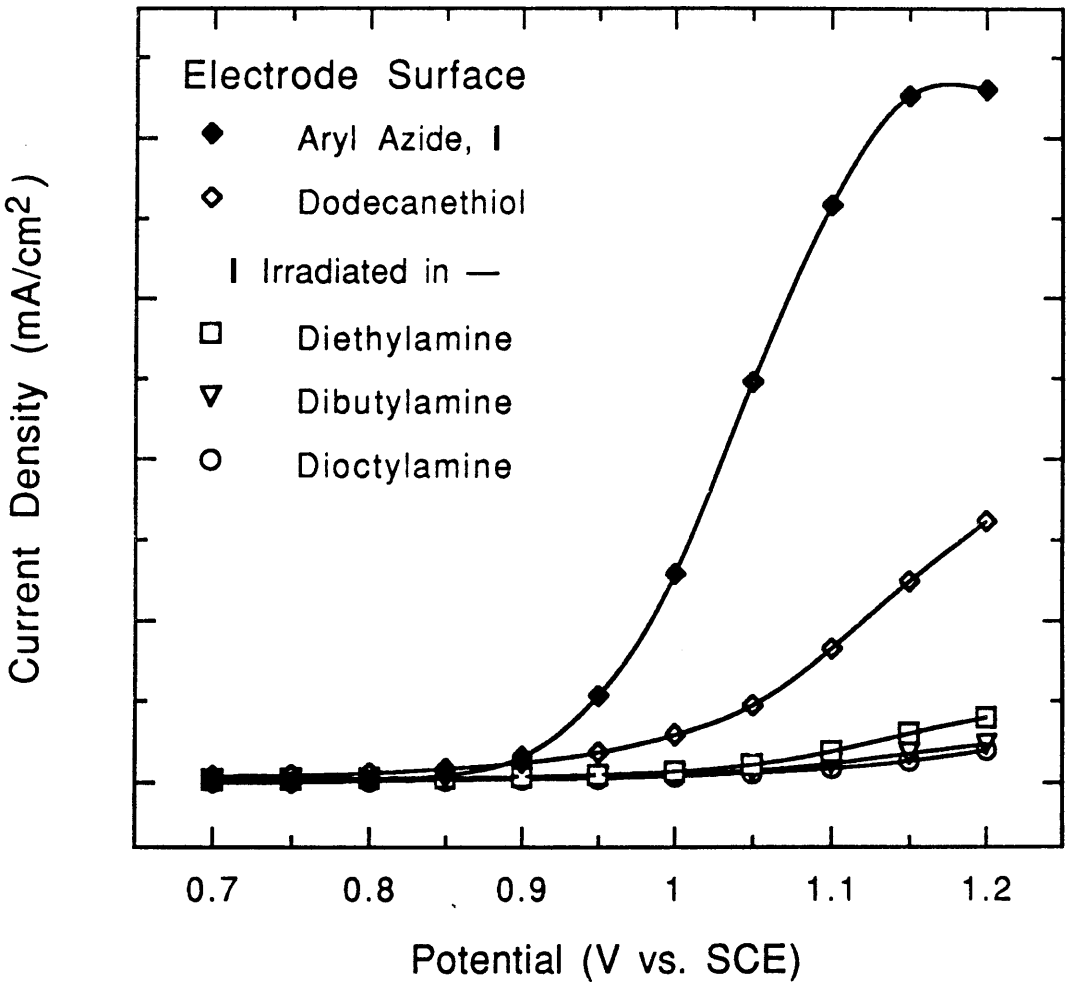
Electrode Surface
Aryl Azide, I
Dodecanethiol
I Irradiated in —
Diethylamine
Dibutylamine
Dioctylamine
Current Density (mA/cm2)
0.7
0.8
0.9
1
1.1
1.2
Potential (V vs. SCE)

Conclusions

Selective irradiation of Au surfaces modified with SAMs of **I** in the presence of secondary amines results in photoattachment of the amine only in irradiated portions of the surface. Electropolymerization of aniline from aqueous solution, and 3-methylthiophene and pyrrole from CH_3CN, produces polymer film patterns that replicate the lithographic patterns. The patterns can be readily visualized and characterized by stylus profilometry, XPS, and cyclic voltammetry. Voltammetric studies of the three monomers as well as two reversible redox couples, $Fe(CN)_6^{3-/4-}$ and $TMPD^{2+/+/0}$ show that differences in electron transfer rates through the different components of the SAM pattern is the principal reason for selective polymerization. Since patterning occurs readily in both aqueous or organic solutions with three redox-active species, we expect this technique to be applicable to the selective electrodeposition of a variety of other compounds on appropriately patterned SAM substrates.

References

1. Wollman, E. W. Ph.D. Thesis, Department of Chemistry, Massachusetts Institute of Technology, 1993.
2. Rozsnyai, L. F.; Wrighton, M. S. *J. Am. Chem. Soc.* **1994**, *116*, 5993-5994.
3. (a) Yoneyama, H.; Kitayama, M. *Chem. Lett.* **1986**, 657. (b) Okano, M.; Itoh, K.; Fujishima, A. *J. Electrochem. Soc.* **1987**, *134*, 837. (c) Okano, M.; Kikuchi, E.; Itoh, K.; Fujishima, A. *J. Electrochem. Soc.* **1988**, *135*, 1641. (d) Segawa, H.; Shimidzu, T.; Honda, K. *J. Chem. Soc., Chem. Commun.* **1989**, 132. (e) Kern, J.-M.; Sauvage, J.-P. *J. Chem. Soc., Chem. Commun.* **1989**, 657. (f) Bargon, J.; Behnck, W.; Weidenbrück, T.; Ueno, T. *Synth. Met.* **1991**, *43*, 1111. (g) Abdou, M. S. A.; Xie, Z. W.; Leung, A. M.; Holdcroft, S. *Synth. Met.* **1992**, *52*, 159.
4. (a) Wuu, Y.-M.; Fan, F.-R. F.; Bard, A. J. *J. Electrochem. Soc.* **1989**, *136*, 885. (b) Sasano, K.; Nakamura, K.; Kaneto, K. *Jpn. J. Appl. Phys.* **1993**, *32*, L863.
5. (a) Nishizawa, M.; Shibuya, M.; Sawaguchi, T.; Matsue, T.; Uchida, I. *J. Phys. Chem.* **1991**, *95*, 9042. (b) Nishizawa, M.; Miwa, Y.; Matsue, T.; Uchida, I. *J. Electrochem. Soc.* **1993**, *140*, 1650.
6. Rozsnyai, L. F.; Wrighton, M. S. *Langmuir*, in press.
7. For an extensive account, see McCoy, C. H. Ph.D. Thesis, Department of Chemistry, Massachusetts Institute of Technology, June 1995. See also (a) McCoy, C. H.; Wrighton, M. S. *Chem. Mater.* **1993**, *5*, 914, (b) Leventis, N.; Schloh, M. O.; Natan, M. J.; Kickman, J. J.; Wrighton, M. S. *Chem. Mater.* **1990**, *2*, 568, (c) Ofer, D.; Crooks, R. M.; Wrighton, M. S. *J. Am. Chem. Soc.* **1990**, *112*, 7869, and references therein.
8. Wollman, E. W.; Kang, D.; Frisbie, C. D.; Lorkovic, I. M.; Wrighton, M. S. *J. Am. Chem. Soc.* **1994**, *116*, 4395.

9. Skotheim, T. A., Ed., *Handbook of Conducting Polymers*; Marcel Dekker: New York, 1986; Vol. 1.

10. Substrates of Au-**I** were first irradiated through a mask in the presence of dioctylamine. After rinsing and drying, the entire substrate was irradiated in the presence of diethylamine. Samples prepared in this manner are composed of patterns of the two amines, as discussed in reference 14b.

11. Ellipsometry can only give accurate measures of SAM thickness if the indices of refraction of each individual SAM are known. For all the SAMs, we have used an index of refraction of 1.46, however differences in monolayer packing density and chemical composition may alter the refraction index to give incorrect thickness values. For example, although the thickness of SAMs of irradiated **I** was greater than that of the non-irradiated monolayer in all cases, the thickness did not correlate with alkylamine chain length. Though the value of 1.46 may be high for disordered films, a decrease by as much as 0.1 would result in a thickness increase of only ~1.5 Å (See Wasserman, S. R.; Whitesides, G. M.; Tidswell, I. M.; Ocko, B. M.; Pershan, P. S.; Axe, J. D. *J. Am. Chem. Soc.* **1989**, *111*, 5852 and references therein for a more detailed discussion). We therefore feel that ellipsometry measurements in conjunction with electrochemical data yield an accurate, if only qualitative, model of SAM thickness in this study.

12. (a) Nuzzo, R. G.; Fusco, D. L.; Allara, D. L. *J. Am. Chem. Soc.* **1987**, *109*, 2358. (b) Bain, C. D.; Troughton, E. B.; Tao, Y.-T.; Evall, J.; Whitesides, G. M.; Nuzzo, R. G. *J. Am. Chem. Soc.* **1989**, *111*, 321. (c) Bain, C. D.; Evall, J.; Whitesides, G. M. *J. Am. Chem. Soc.* **1989**, *111*, 7155. (d) Bain, C. D.; Whitesides, G. M. *J. Am. Chem. Soc.* **1989**, *111*, 7164.

13. Porter, M. D.; Bright, T. B.; Allara, D. L.; Chidsey, C. E. D. *J. Am. Chem. Soc.* **1987**, *109*, 3559.

14. (a) Li, T. T.-T.; Weaver, M. J. *J. Am. Chem. Soc.* **1984**, *106*, 6107. (b) Finklea, H. O.; Hanshew, D. D. *J. Am. Chem. Soc.* **1992**, *114*, 3173.

15. Nuzzo, R. G.; Dubois, L. H.; Allara, D. L. *J. Am. Chem. Soc.* **1990**. *112*, 558.

CHAPTER THREE

CONTROLLING THE ADHESION OF CONDUCTING POLYMER FILMS WITH PATTERNED SELF-ASSEMBLED MONOLAYERS

Introduction

The fabrication of polymer-based devices and composite materials often involves depositing a polymer on a metal surface. The polymer may be deposited chemically, electrochemically, or cast from solution; the surface may be insulating or conducting, organic or inorganic. Adhesion of the polymer to the surface, and the physics and chemistry of the interface, are critical to the overall function of the device or material. Current research in this area relies heavily on physical characterization of the interface, and many chemical aspects of the polymer/metal interface are poorly understood.[1] An early study of evaporated metals (Cu, Ni, and Cr) on various insulating polymers used X-ray photoelectron spectroscopy (XPS) to link the presence of metal-oxygen complexes to high interface adhesion.[2] Additional studies using XPS and other spectroscopic techniques begin to elucidate atomic structure, but do not provide a clear chemical model of the interface.[3]

The chemical nature of both insulating and conducting surfaces can be controlled conveniently with monolayers.[4] In our research group, we have been using self-assembled monolayers (SAMs) of alkane thiols and disulfides on Au. Long-chain alkane thiols and disulfides are well-known to form stable, rugged, and ordered two-dimensional assemblies on Au surfaces.[1a,5] Photosensitive terminal groups can be used to form two-dimensional patterns on the surface,[6] and SAMs of di-11-(4-azidobenzoate)-1-undecyl disulfide, **I**, can be used to control the electrodeposition of conducting polymers.[7] Aniline, 3-methylthiophene, and pyrrole can be selectively electropolymerized on SAM surfaces in arbitrary patterns with near-micron resolution with a contrast of nearly 1000:1.[8] In this chapter, we describe how SAMs can be used to alter the adhesion of polyaniline and poly(3-methylthiophene) films to the surface, and how SAM patterns allow these films to be selectively removed and transferred to adhesive tape—a flexible, insulating support.

Experimental Section

Materials. All solvents (HPLC grade) and chemicals (highest purity available) were purchased from commercial sources and used as received unless otherwise stated. The synthesis[6] and use of di-11-(4-azidobenzoate)-1-undecyl disulfide, **I**, in controlling polymer deposition[7,8] has been reported. All amines (Aldrich) were distilled from KOH under reduced pressure and stored under Ar except 2,2,2-trifluoroethylamine (Aldrich), which was used as received. Dodecanethiol (Aldrich) was used as received. A sample of $HS(CH_2)_{11}(CF_2)_4CF_3$ was kindly provided by G. M. Whitesides at Harvard University, and 11-mercaptoundecanoic acid was synthesized according to a published procedure.[9] Aniline (Aldrich) was distilled under reduced pressure and kept in the dark until used.

Polycrystalline Au substrates were prepared by thermal evaporation (Edwards Auto 306 Cryo evaporator) of a 20 Å Cr adhesion layer followed by 1000 Å of Au on 2.5 cm x 1.2 cm pieces of Si (100) wafers (Silicon Sense: Nashua, NH; test grade, 500 μm thick). Before evaporation, the Au (99.99% wire) was cleaned in aqua regia, rinsed with Millipore H_2O, EtOH, and oven dried.

Formation of SAMs. Monolayers of **I** were formed by immersion of the Au substrates in 2-3 mM methylcyclohexane solutions for at least 12 h. Monolayers of all other alkanethiols were formed for at least 2 h from 2-3 mM EtOH solutions. In all cases, SAMs were formed on Au-coated Si substrates immediately after evaporation. Before use or characterization, all SAM substrates were rinsed in EtOH (SAM substrates of **I** were first rinsed with methylcyclohexane, then EtOH) and dried with a stream of dry Ar.

Photopatterning of Au-I SAMs. A drop of the desired amine was placed on freshly rinsed and dried Au-**I** substrates. For fabrication of micron-sized features, a mask (chrome on quartz) was placed on top of the substrates, Cr-side down, forcing the amine to spread evenly across the samples. The assembly was irradiated through the mask by a 200 W Hg short-arc lamp through a filter (10 cm path length, quartz walls filled with 1:1:1 H_2O: EtOAc: EtOH; $\lambda > 260$ nm) for 2 min. After irradiation, the samples were

carefully removed from the mask, rinsed with copious amounts of EtOH, and dried with a stream of Ar.

Polymer Deposition and Tape Transfer. Substrates were immersed in an aqueous solution (0.85 M H_2SO_4, 0.25 M $NaHSO_4$) of aniline, or a 0.1 M [*n*-Bu_4N]PF_6/CH_3CN solution of 3-methylthiophene. The polymer was ~1.0 M in all cases. Using a potentiostat (RDE4: Pine Instruments) the Au substrate was repeatedly cycled at 200 mV/sec between 0.0 V and ~1.0 V (aniline) or between 0.0 V and ~1.7 V (3-methylthiophene) past the point of pattern formation, until polymer coated the entire substrate and were 0.1-0.2 μm thick. The substrates were then rinsed (H_2O for polyaniline, CH_3CN for poly(3-methylthiophene) and dried with a stream of Ar. Scotch tape (3M) was applied to the dried polymer samples by pressing the tape with a soft cotton swab. The tape was removed by carefully peeling from a corner or side of the sample by hand.

Results and Discussion

Primary or secondary amines covalently attach to monolayers of **I** upon irradiation to form two stable photoproducts.[6] Monolayers of **I** have been used to form patterns on Au substrates with a variety of functionalized amines. The photochemical transformations have been characterized by cyclic voltammetry, reflection absorption IR, and X-ray photoelectron spectroscopy (XPS),[6] while patterns have been visualized by scanning electron microscopy[10], secondary ion mass spectrometry,[6,11] condensation figures,[6] and chemical force microscopy.[12] During electropolymerization, electrons must be transferred between the monomer species and the electrode. Aniline, 3-methylthiophene, and pyrrole deposit selectively and replicate the pattern of irradiated Au-**I** electrodes because of differences in electron transfer through the different SAM regions.[7,8] Polymer films preferentially deposit on unirradiated SAM regions—regions of higher electron transfer rate. Polymer films do not form initially on irradiated regions, however.

Prolonged oxidation of the corresponding monomer eventually results in polyaniline or poly(3-methylthiophene) film deposition on the entire patterned substrate. Importantly, the interface between the polymer film and irradiated SAMs of **I** differs fundamentally from that with native, unirradiated SAMs. Patterns in surface free energy can be formed by using the appropriate amine during substrate irradiation and pattern formation. For example, diethanolamine is used to fabricate very hydrophilic surface regions. Polymer films adhere more strongly to these hydrophilic, OH-terminated SAM regions than to unirradiated portions of the surface that terminate in aryl azide. Adhesive tape can be used to selectively remove the polymer film from the surface. This method of selectively removing polymer films from patterned Au-**I** substrates is illustrated in Scheme 3.1.

To investigate polymer adhesion to different SAM terminal groups, homogeneous SAMs were used. Peel tests were used to qualitatively probe the adhesion of poly(3-methylthiophene) on bare Au and three SAM terminal groups: COOH, CH_3, and CF_3.

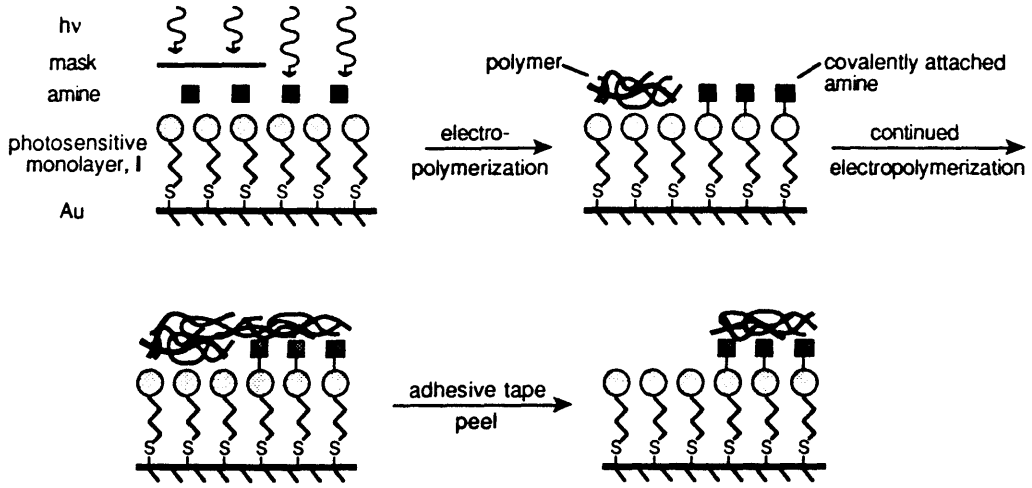

Scheme 3.1. Photosensitive SAMs of **I** on a flat Au surface are irradiated through a mask in the presence of a functionalized amine. Electrochemical oxidation of aniline or 3-methylthiophene results in selective polymer deposition on unirradiated portion of the sample. The entire substrate is coated with a thin polymer film (0.1-0.2 μm) after additional electropolymerization. Adhesive tape is applied to the sample and peeled away to selectively remove the polymer film. The original pattern is transferred to the tape while the inverse remains on the sample.

Adhesion was quite low on the bare Au surface and most of the polymer peeled off easily. This low adhesion exemplifies the weak polymer/metal interface that is often encountered in devices. Polymer adhesion was highest on the COOH-terminated surface. A comparatively large force was needed to pull the tape from this sample compared to that on bare Au, and very little of the film was romoved as seen by eye. Polymer adhesion to SAMs with CH_3 and CF_3 terminal groups was lower than on bare Au. Films were removed very easily from the CF_3 surface and completely transferred to the adhesive tape. Notably, this surface could be used for up to three subsequent polymer deposition/peel experiments with apparently no polymer left on the sample. Nearly complete transfer suggests that the monolayer in this case remains intact after polymer removal.[13]

This adhesion trend follows our expectations on the basis of surface free energy. High energy, hydrophilic surfaces promote adhesion and adsorption, while low energy,

hydrophobic surfaces are passive in most physical and chemical processes.[14] Water was used to measure the contact angle on the four surfaces. The trend in contact angle on each surface follows the trend in adhesion (contact angle:surface): 5-10°:COOH; 60°:bare Au;[15] ~100°:CH_3; ~120°:CF_3.

The qualitative measurements of polymer adhesion on homogeneous SAM surfaces were used to control adhesion laterally. That is, the appropriate choice of functionalized amine in the irradiation of Au-**I** surfaces allowed us to use patterned SAM surfaces as templates for selective polymer film removal. Native, unirradiated Au-**I** surfaces are hydrophobic ($\theta \approx 80°$) and polymer adhesion to these regions were expected to be low. Adhesion to hydrophilic regions, such as SAM regions terminating in OH or COOH, was expected to be high.

Figure 3.1 shows micrographs of a patterned sample of polyaniline before and after adhesive tape application. The surface consists of a Au-**I** SAM irradiated through a mask in the presence of $(HOCH_2CH_2)_2NH$. Regions coated with polymer are unirradiated and terminate in aryl azide. The gold-colored squares (10 x 10 μm) correspond to irradiated, OH-terminated surface areas. As seen in the micrograph, polymer growth on the irradiated areas of this sample has already begun, and the edges of the irradiated squares are round. Additional electropolymerization results in polymer deposition on the entire substrate. Adhesive tape applied to the sample and peeled away removes polymer from the unirradiated, hydrophobic surface regions. A polymer film is left behind preferentially on the each irradiated, OH-terminated portion of the surface, as shown in the second micrograph.

The process of selectively removing polymer film from patterned Au-**I** samples was successful for the two polymers we deposited. A photograph of polyaniline and poly(3-methylthiophene) samples is shown in Figure 3.2. The Au sample on the left shows aniline that has been electropolymerized past the point of pattern formation to cover both the unirradiated and irradiated portions of the sample. The tape used to selectively

remove the polymer from the bottom half of the sample has been placed on a glass slide and is shown below the Au substrate. The sample on the left of Figure 3.2 shows a sample of poly(3-methylthiophene) treated similarly. It is clear from Figure 3.2 that polymer has selectively been removed from the Au sample and transferred to the adhesive tape. On both adhesive tape samples, optical microscopy shows high-resolution (~2 μm) features corresponding to features on the mask and Au-**I** samples.

Figure 3.1. Micrographs of polyaniline on patterned Au electrodes. Patterns were made by irradiating a Au-**I** SAM in the presence of $(HOCH_2CH_2)_2NH$ for two minutes. The square-shaped features are 10 x 10 μm^2 and terminate in OH. The sample to the left shows polymer selectively depositing on the unirradiated regions of the sample, and beginning to deposit on the irradiated regions. Continued electropolymerization results in complete polymer coverage of these areas. Adhesive tape is applied to the sample to selectively remove polymer from the unirradiated regions, as shown in the sample at the right.

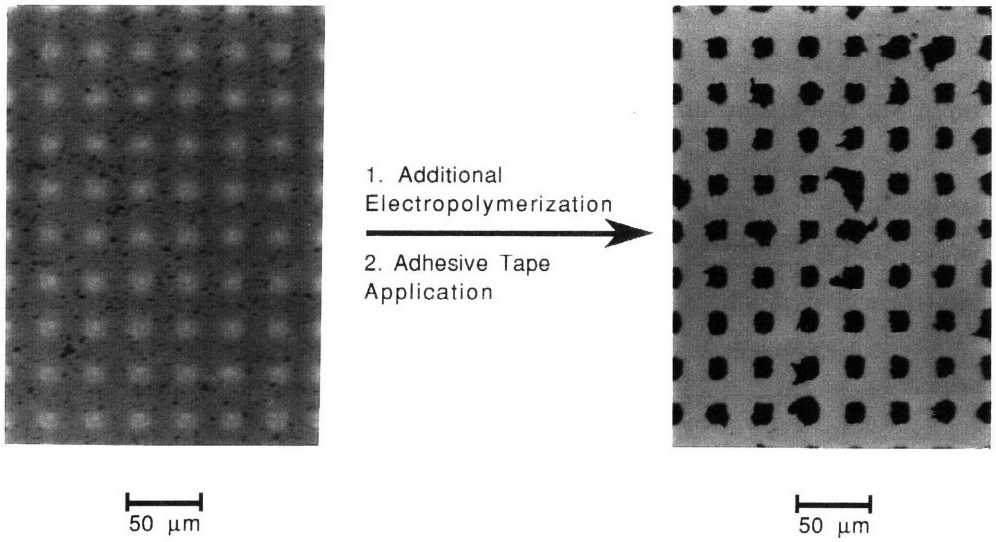
1. Additional
Electropolymerization
2. Adhesive Tape
Application
50 μm
50 μm

Figure 3.2. Patterned Au and adhesive tape samples containing (left) patterned polyaniline and (right) poly(3-methylthiophene) films. The SAM patterns were made using $(HOCH_2CH_2)_2NH$ (see text). The mask used in fabrication of the sample was originally designed for use in the fabrication of microelectrodes; the small features range in size from 2-100 μm. The SAMs in these areas terminate in OH and are hydrophilic. Transfer of polymer film from hydrophobic regions of the Au sample to the adhesive tape is successful for both polymers. Optical microscopy has identified features replicating those of the mask of near-micron resolution (~2 μm) on both adhesive tape samples.

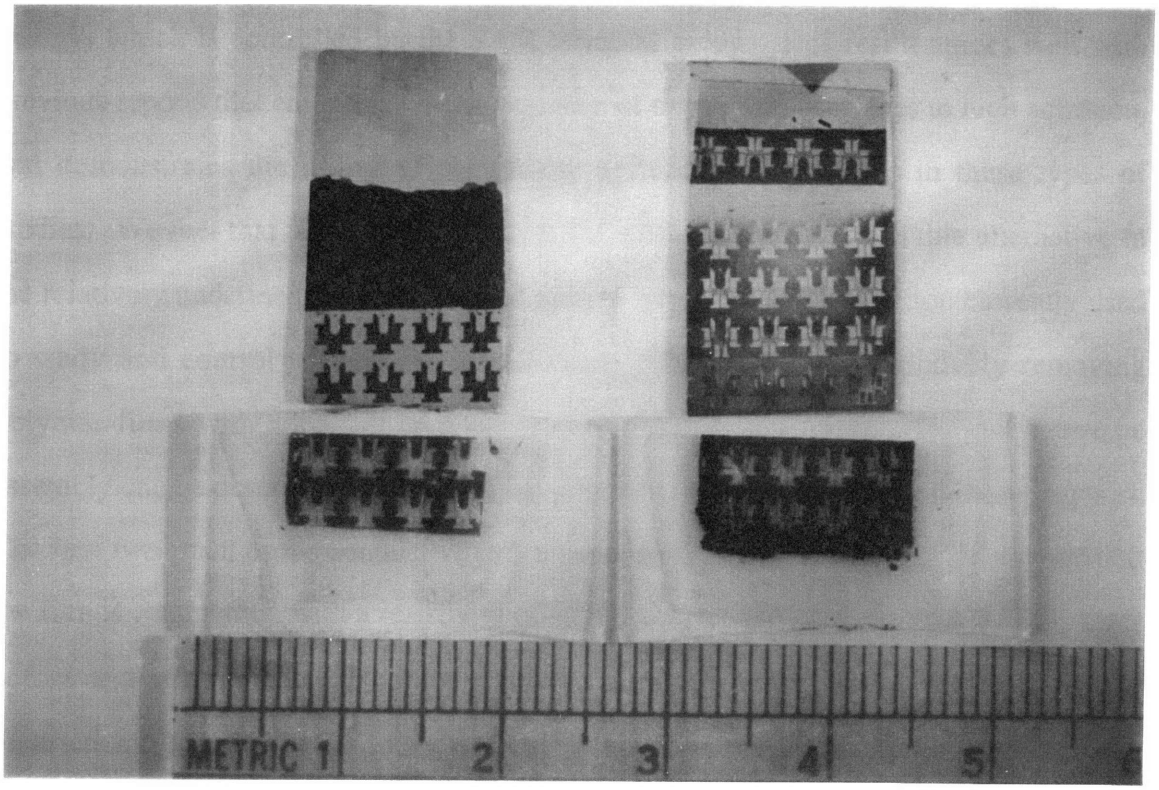
METRIC 1
2
3
4
5

Conclusions

This chapter shows that SAMs can be used to control the adhesion of polyaniline and poly(3-methylthiophene) films to a metal electrode, and that arbitrary, high-resolution polymer patterns can be transferred to adhesive tape. Fundamentally, this study probes the chemical nature of the polymer/metal interface: adhesion increases with surface free energy, which is controlled by the SAM terminal group. This result agrees well with previous reports that emphasize the importance of oxygen-rich surfaces to high adhesion, and demonstrates the utility of chemically defined SAM surfaces in these types of studies. We feel that well-characterized SAM surfaces represent a viable alternative to the relatively undefined methods such as plasma treatment and irradiation currently used to study and control polymer/metal adhesion. The method of selectively removing polymer films with adhesive tape also has practical implications. The polymer/tape assembly can be described as a conducting polymer film on a flexible, insulating support. The first two-point probe conductivity measurement on a polyaniline sample showed that the film is conducting, with a resistivity of ~1500 Ω/cm. The nature of the SAM surfaces before and after adhesive tape application is currently being investigated and will be reported shortly, along with a detailed characterization of the transferred polymer film. We expect that the integrity of transferred films will depend greatly on the tensile strength of the polymer. This critical property may be controlled by altering electro-polymerization conditions, or by utilizing appropriate polymer blends. The method described in this chapter demonstrates that the chemical nature of a surface can be defined by SAMs, and that these surfaces can be used to increase understanding and control of materials properties. The possibility of using these techniques in device and materials fabrication are currently being explored.

References

1. See for example (a) *Polymer-Solid Interfaces*; Pireaux, J. J.; Bertrand, P.; Brédas, J. L., Eds.; IOP: London, 1992, (b) *Physics of Polymer Surfaces and Interfaces*; Sanchez, I. C., Ed.; Butterworth-Heinemann: Boston, 1992, (c) *Interfaces in New Materials*; Grange, P.; Delmon, B., Eds.; Elsevier: New York, 1991, and references therein.
2. Burkstrand, J. M. *J. Appl. Phys.* **1981**, *52*, 4795.
3. For a recent review, see Pireaux, J. J. *Synth. Met.* **1994**, *67*, 39.
4. (a) Ulman, A. *An Introduction to Ultrathin Organic Films from Langmuir-Blodgett to Self-Assembly*; Academic: San Diego, 1991. (b) Roberts, G. *Langmuir-Blodgett Films*; Plenum: New York, 1990. (c) *Silanes, Surfaces, and Interfaces*; Leyden, D. E., Ed.; Gordon and Breach: New York, 1986.
5. Ulman, A. *Characterization of Organic Thin Films*; Butterworth-Heinemann: Boston, 1995.
6. Wollman, E. W.; Kang, D.; Frisbie, C. D.; Lorkovic, I. M.; Wrighton, M. S. *J. Am. Chem. Soc.* **1994**, *116*, 4395.
7. Rozsnyai, L. F.; Wrighton, M. S. *J. Am. Chem. Soc.* **1994**, *116*, 5993.
8. Rozsnyai, L. F.; Wrighton, M. S. *Langmuir*, in press.
9. Bain, C. D.; Troughton, E. B.; Tao, Y.-T.; Evall, J.; Whitesides, G. M.; Nuzzo, R. G. *J. Am. Chem. Soc.* **1989**, *111*, 321.
10. Wollman, E. W.; Frisbie, C. D.; Wrighton, M. S. *Langmuir* **1993**, *9*, 1517.
11. (a) Frisbie, C. D.; Wollman. E. W.; Martin, J. R.; Wrighton, M. S. *J. Vac. Sci. Technol A* **1993**, *11*, 2368. (b) Frisbie, C. D.; Wollman. E. W.; Wrighton, M. S. submitted for publication in *Langmuir*.

12. (a) Frisbie, C. D.; Rozsnyai, L. F.; Noy, A.; Wrighton, M. S.; Lieber, C. M. *Science* **1994**, *265*, 2071. (b) Noy, A; Frisbie, C. D.; Rozsnyai, L. F.; Wrighton, M. S.; Lieber, C. M. *J. Am. Chem. Soc.*, in press.

13. This assumption will be tested in the near future by XPS analysis of the surface.

14. (a) Israelachvili, J. *Intermolecular & Surface Forces*; Academic: San Diego, 1992. (b) Adamson, A. W. *Physical Chemistry of Surfaces*; Wiley: New York, 1990.

15. Au is very susceptible to contamination. The Au surface in this experiment had been exposed to air for 2 days and was not cleaned. Freshly evaporated or cleaned Au should have a low contact angle; adhesion on a clean sample should be higher than on an uncleaned sample.

PART TWO

FUNDAMENTAL STUDIES OF SELF-ASSEMBLED MONOLAYERS: MEASURING ADHESION AND FRICTION AT THE MOLECULAR SCALE

CHAPTER FOUR

AN INTRODUCTION TO
CHEMICAL FORCE MICROSCOPY

The manifestation and consequences of adhesion and friction are central to studies in surface science. The ability to control these properties is an important factor in improving machines and tools, from ball-bearings and high-speed turbine blades, to ship hulls and ski bases, to artificial tissue and prostheses. In aerospace, high-temperature, and computer applications especially, the use of liquid lubricants is not practical and the intrinsic properties of dry, unlubricated surfaces become increasingly important.

Specific chemical changes at surfaces can be used to alter adhesion and friction. Chapter One described how otherwise identical gold surfaces treated with different self-assembled monolayers (SAMs) can either sustain or repel drops of water or other liquids. Precise chemical control of a surface can be used in further tribological studies. With the advent of techniques such as atomic force microscopy (AFM) to probe forces at a very local scale, physical-organic studies of the microscopic causes of adhesion and friction become possible, and we can begin to relate microscopic behavior to macroscopic phenomena.

Adhesion and Friction

Adhesion and friction are understood well on the macroscopic scale. The earliest theories of friction were simple, showing us that the force needed to drag a weight or load L up an inclined plane is simply

$$F = L \tan\theta \tag{4.1}$$

A friction coefficient, μ, can then be defined:

$$\mu = dF/dL = \tan\theta \tag{4.2}$$

This simple model accounts for most of our observations: From eq 4.1, it is apparent that on the macroscopic scale, friction is independent of contact area for most types of hard solid surfaces. (Surfaces that deform elastically or plastically, such as rubber, behave differently.) At first, this rule seems counterintuitive, but it agrees qualitatively with

observation. Friction between two surfaces is determined by *microscopic* contact points. As the macroscopic contact area between two point increases, the load per unit area (pressure) decreases, decreasing the density of contact points. The opposite is also true of course. Since the contact area and number of contact points are inversely proportional, friction is independent of contact area. Friction and the friction coefficient are independent of contact area and sliding velocity. From eq 4.1, we also realize that friction is related to load and that fiction and adhesion are related. Even in the absence of an applied load or weight, two surfaces that adhere to each other will experience a finite friction force when sliding past each other.

The Hertz and JKR Theories of Adhesion. On the microscopic scale, two surfaces contact through a single point, and eq 4.1 does not hold. In the late 1800's, Hertz developed a theory to explain the contact area and deformation of two smooth elastic spheres as they are brought into contact with each other and then pulled apart.[1] For two spheres of R_1 and R_2 pressed together with a load P_0, the radius a_0 of the circles of contact is given by eq 4.3, where k_i is the elastic constant of the corresponding material, determined by the Poisson ratio ν, and the Young's modulus, E.

$$a_0^3 = \frac{3}{4}\pi(k_1 + k_2)\frac{R_1R_2}{R_1 + R_2}P_0 \quad \text{or} \quad a_0^3 = \frac{RP_0}{K} \tag{4.3}$$

$$k_i = \frac{1 - \nu_i^2}{\pi E_i}; \quad R = \frac{R_1R_2}{R_1 + R_2}; \quad K = \frac{4}{3\pi(k_1 + k_2)}$$

As the two spheres are pressed together, two given distant points in them will approach each other by a distance δ, called the elastic displacement, resulting from local compression near the contact region.

$$\delta^3 = \frac{9}{16}\pi^2(k_1 + k_2)^2 RP_0^2 \tag{4.4}$$

This theory was satisfactory until the 1960's, when some experimental contradictions were reported: the contact areas observed between spheres of rubber or glass at low and

even negative loads were finite, while Hertz theory predicted a contact area of zero at pull-off ($P_0 = 0$, see eq 4.3). These observations indicated that some additional attractive force between the two bodies was operative—a force not considered by Hertz. It wasn't until the last few decades that Johnson, Kendall, and Roberts[2] showed that an additional term γ accounts for the actual load P_1 between the two spheres, which is always larger that the applied load, P_0.

$$P_1 = P_0 + 3\gamma\pi R + \sqrt{6\pi\gamma R P_0 + (3\gamma\pi R)^2} \tag{4.5}$$

Here, γ is the work of adhesion per unit contact area. On separating two media 1 and 2 in a surrounding medium 3, the work of adhesion is given by the Dupré equation: $\gamma = \gamma_{13} + \gamma_{23} - \gamma_{12}$. Note that in eq 4.5, $P_1 = P_0$ in the absence of any surface free energy. That is, for two hypothetically non-reactive spheres, JKR theory simplifies to Hertz theory.

The contact area radius according to JKR theory, a_1, is just as it is according to Hertz theory, only P_1 instead of P_0.

$$a_1^3 = \frac{R}{K}\left(P_0 + 3\gamma\pi R + \sqrt{6\pi\gamma R P_0 + (3\gamma\pi R)^2}\right) \quad \text{or} \quad a_1^3 = \frac{RP_1}{K} \tag{4.6}$$

At an applied load of zero ($P_0 = 0$), the contact area radius is finite:

$$a_1^3 = \frac{6\gamma\pi R^2}{K} \tag{4.7}$$

When the applied load is negative, the contact area decreases until the two bodies separate. This negative load, which is the force at separation, is also referred to as the force of adhesion, F_{ad}. In order to obtain a real solution for eq 4.6,

$$6\pi\gamma R P_0 \leq (3\gamma\pi R)^2 \quad \text{or} \quad P_0 \geq \frac{3}{2}\gamma\pi R \tag{4.8}$$

The spheres will separate, therefore, when

$$P_0 = -F_{ad} = -\frac{3}{2}\gamma\pi R \tag{4.9}$$

Note that this value is independent of the elastic constant K of the material, but depends simply on the work of adhesion, γ, and a geometric factor R. (Later in Chapter Six, the

work of adhesion will be symbolized by W_{st}.) By substituting eq 4.9 into eq 4.6, the contact area radius between the two spheres at the point of separation, a_s, can be determined.

$$a_s^3 = \frac{3}{2}\frac{\gamma\pi R^2}{K} \tag{4.10}$$

In order to make detailed local measurements of adhesion and friction between two surfaces, sophisticated equipment is needed. Fortunately, in the past 15 years, a new type of surface analysis tool has been developed so that classical, macroscopic behavior can be studied at the molecular scale.

Atomic Force Microscopy[3]

In 1986, Gerd Binnig and Heinrich Rohrer shared the Nobel Prize in Physics for their invention of the scanning tunneling microscope (STM).[4] The STM was the first instrument able to measure interactions directly between individual atoms, and to generate images of surfaces with atomic resolution. The technique took advantage of new developments in piezoelectric crystals, and involved scanning a small sharp tip back and forth across a sample while monitoring a small electrical tunneling current between a metallic tip, and a conducting sample separated by only a few angstroms. Since the invention of the STM, the concept of scanning a small tip over a sample to detect a tunneling current has been generalized to detect other interactions, including magnetic and electrostatic forces, and electrochemical and optical signals. Inorganic, organic, and biological samples have been studied with several types of scanning probe microscopes[5]

The most widely used scanning probe instrument derived from the STM is the atomic force microscope.[6] (AFM: This abbreviation, and abbreviations for other techniques are used for both the instruments as well as the techniques.) Several defining components of the AFM can be identified:

1. A sharp, micron-sized tip fixed at the end of a long, flexible cantilever.
2. A method of sensing cantilever deflection.
3. A feedback system to monitor force and control tip deflection.
4. A system, usually made from piezoelectric crystals, to scan either the tip or the sample back and forth laterally, and to control precisely the separation between them.
5. A computer interface to relate tip movement to sample features, and a display system to convert the measured data from a scan into a three-dimensional image.

Scanning probe instruments have been custom-built, and in the past several years excellent microscopes have become available from commercial sources. In our experiments, we use a Nanoscope III built by Digital Instruments, Inc.

Figure 4.1 limns the basic AFM design. The sample rests on top of a piezoelectric scanner and the tip rests at the end of a flexible cantilever. The tip and sample are brought into contact or "engaged" by extending the sample toward the tip until a certain force is detected, situating the tip within nanometers of the surface. As the sample is scanned back and forth, the tip moves up and down in response to surface forces such as electrostatic, capillary, and/or van der Waals forces. These interactions can be either attractive or repulsive and are measured by monitoring the tip deflection. Light from a small diode laser is reflected from the backside of the cantilever and directed into a position sensitive photodiode. Tip deflections on the order of 0.1 Å can be measured. The scan size can be varied from 10 x 10 nm^2 to 150 x 150 μm^2 by using the appropriate piezoelectric scanner. The resulting image is displayed as an image of surface force and is usually interpreted as a height or "topographic" map of the scanned area.

The force between the tip and the surface can be controlled precisely. While the spring constants of atoms are on the order of 10 N/m,[7] the spring constants of cantilevers range from 0.05-50 N/m. AFM can therefore be used as a non-destructive imaging technique, and in the case of soft samples, as a micromachining tool.[8]

Figure 4.1. A schematic illustration of an AFM. The sample rests on a piezoelectric crystal which is used to control the separation between the sample and the tip, and to scan the sample laterally. The tip rests at the end of a long, flexible cantilever. Normal forces (height) and lateral forces (friction) are detected by monitoring the deflection of a light beam that is reflected from the backside of the cantilever into a position-sensitive photodiode.

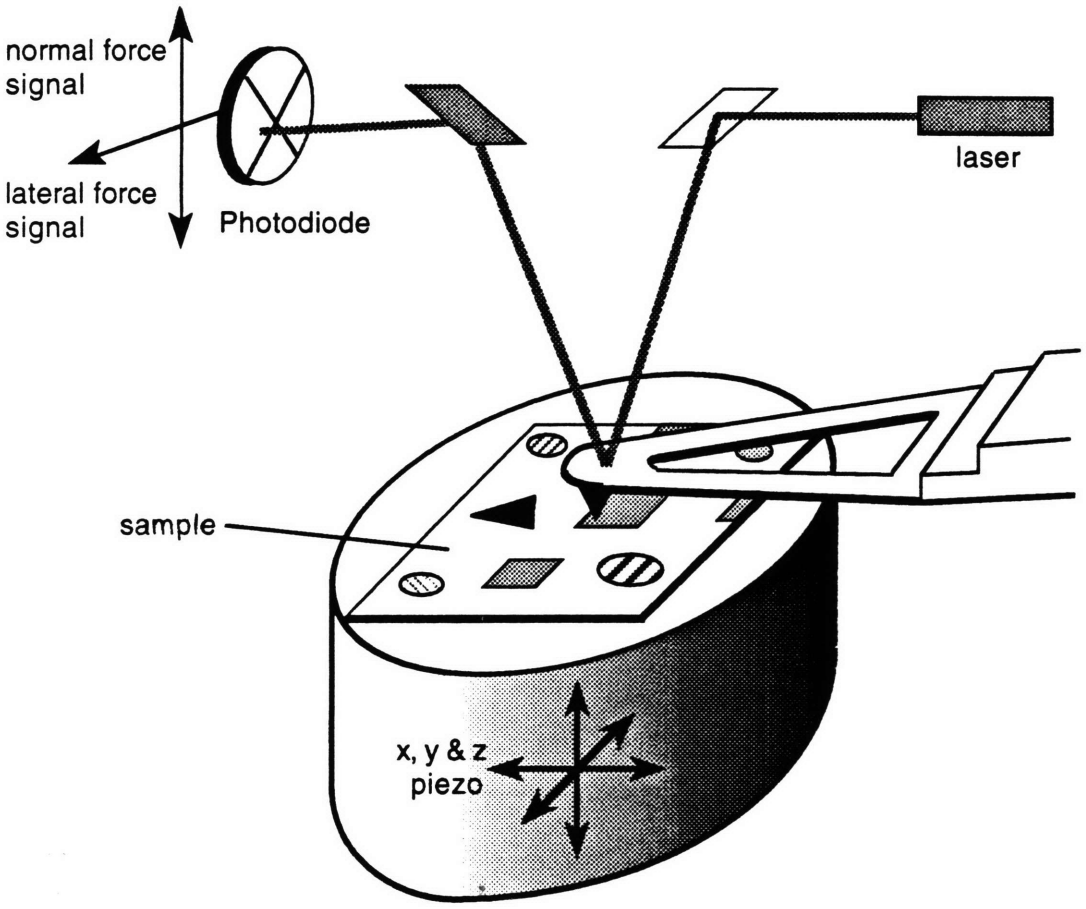
normal force
signal
lateral force
signal
Photodiode
laser
sample
x, y & z
piezo

Adhesion and Friction Force Measurements. The adhesion force is the force required to separate the tip from contact with the sample and is measured by recording tip deflection (force) as a function of distance. The acquisition of a force-distance curve, during which the sample is fixed in the lateral dimensions, is illustrated in Scheme 4.1. The piezoelectric tube is extended until the sample comes into contact with the tip (position 2). As the piezo extends further (position 3), the tip is deflected upwards. A reverse in bias causes the piezo to reverse direction and retract the sample from the tip. However, after the sample is brought back to its original contacting position (position 4), the tip continues to adhere to the sample (position 5). When a large enough negative load is applied (see eq 4.9), the tip finally springs out of contact and returns to its normal resting state. The difference in force between the point of highest applied negative load (position 5) and the resting state of the tip (position 6) is the adhesion force.

Scheme 4.1. An illustration of a force-distance measurement. The piezoelectric tube extends and the sample makes contact with the tip (2). As it extends further, the tip bends upward (3). The piezo then retracts and the tip continues to adhere to the sample (5) past the point of original contact (4). When the cantilever deflection exceeds the adhesion force, the tip jumps back to its resting position (6).

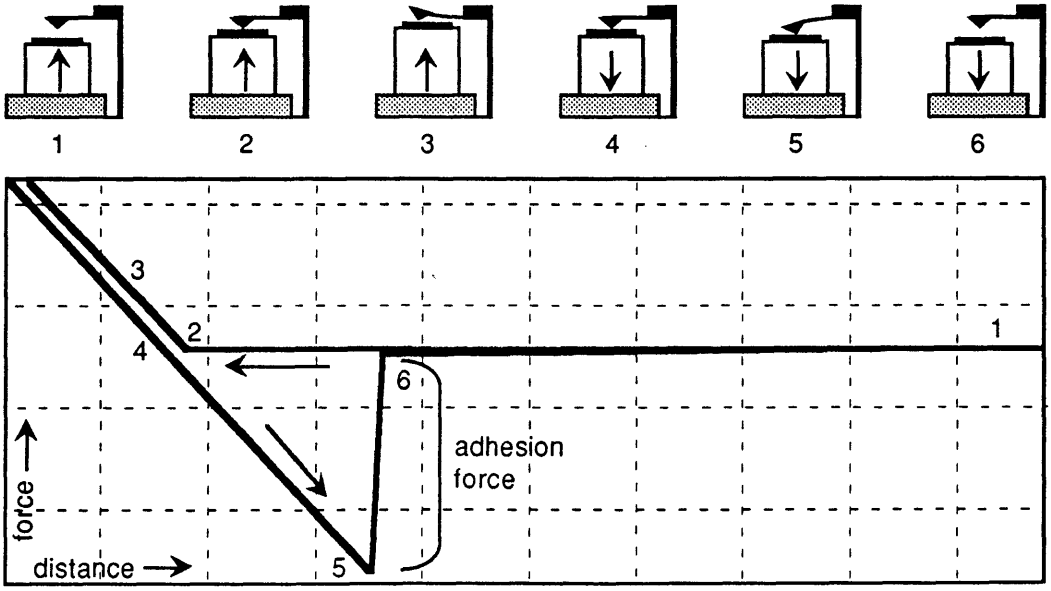

Adapted from Nanoscope III User's Manual, Digital Instruments

Friction is measured by lateral deflection, or torsion, of the tip. When AFM is used to measure friction, it is sometimes referred to as friction force microscopy (FFM) or lateral force microscopy (LFM). As the sample is scanned laterally, a friction-force image of the sample is generated. Since the tip and sample are in contact at a single point[9] and since contact area increases with applied load (eq 4.6), the friction force is expected to be proportional to the adhesion force. Friction is affected by topographic features on the sample; nanometer-sized bumps and depressions deflect the tip both vertically and laterally. Importantly, friction features can also be detected on nominally flat samples—surfaces that have featureless AFM images. In this regard, LFM is useful in probing surface features that are distinct (but not necessarily unrelated) from those measured by AFM, and is quickly becoming a valuable surface science tool.

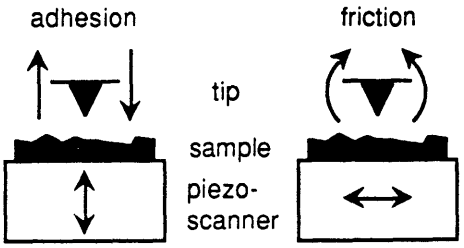

Scheme 4.2. Adhesion is measured by deflection as the sample is retracted from the tip; friction is measured by torsion as the sample is scanned under the tip.

The AFM and LFM measure physical interactions between the tip and the surface. The type and source of this force, however, are difficult to control and are often unknown. In very hard contact, the force between the tip and sample is ultimately due to electrostatic repulsion. Additional forces arise from several other interactions[10] and become dominant at the working forces of AFM. Van der Waals interactions are strong at nanometer separations, and a thin layer of water on the tip and sample leads to capillary forces even in "dry" air.[11] Capillary forces can be elliminated by immersing the tip and sample in a liquid, but then hydrophobic forces may dominate. More importantly, the chemical nature of the surface, and especially the tip, is usually not well defined and may change during image acquisition. Although AFM can be used to study surfaces at a local scale, the exact type of tip-surface interaction often cannot be controlled and has only recently been investigated in detail.[12]

Chemical Force Microscopy

If local interactions can be measured and understood, how can the type and strength of interactions between the tip and surface be controlled in a chemically specific manner? In developing chemical force microscopy (CFM), it was our goal to define the chemical nature of the tip and sample surface. The concept of CFM in its most basic form is captured in Scheme 4.3. Both the tip and the surface are modified with chemical groups X and Y that are expressed on their outer surfaces. A specific and predictable interaction will dominate the measured force between the tip and surface for a given molecular tip/surface pair. Different interaction types and strengths can be studied by changing the chemical groups X and Y. The potential for CFM to elucidate the chemical basis of adhesion and friction, and the microscopic relationship between them, motivated our initial investigations.

Scheme 4.3. A conceptual illustration of chemical force microscopy. Molecules on the probe tip, X, are used to sense specific interactions with chemical groups, Y, on the surface.

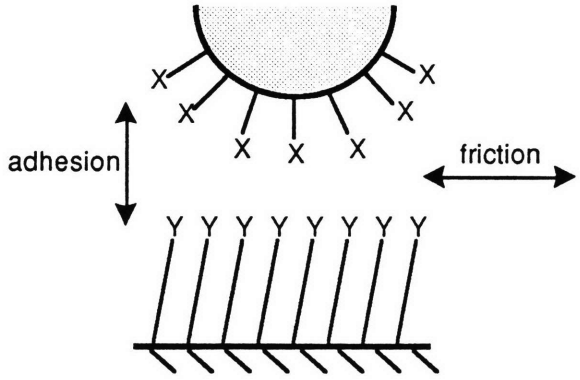

X	Y	Interaction
$-CH_3$	$-CH_3$	van der Waals
-COOH	-COOH	hydrogen bond
-COOH	$-NH_2$	acid-base
$-COO^-$	$-NR_3^+$	electrostatic

Previous chemical studies of adhesion and friction have been performed with a surface force apparatus (SFA).[13] The SFA is composed of two smooth surfaces immersed in a liquid that can be brought towards and slid past each other in a highly controlled manner. Lipid monolayers and bilayers can also be deposited on the two surfaces. Fundamental interactions between surfaces including van der Waals, electrostatic, solvation, and hydrophobic forces have been investigated using SFA. As shown in the following two chapters, the results agree qualitatively with those of CFM.

Chemical force microscopy allows chemical interactions to be probed on a more local scale than SFA. Using eqs 4.9 and 4.10, the pull-off force and contact area between the tip and sample can be calculated (see Chapters Five and Six). As measured, tips range in radius from R = 60-150 nm. If X and Y are both methyl groups[14] and the surrounding solvent is ethanol, the work of adhesion, γ, is estimated to be 5 mN/m. These values yield an adhesion force between F_{ad} = 1.4-3.5 nN. It is shown in Chapters Five and Six that these calculated values are in good agreement with our measured values. The elastic constant of the tip and surface (in our experiments they are both coated with Au, K = 6.4 x 10^{10} N/m^2) can be used in eq 4.10 to estimate the contact radius at pull-off, giving a contact area of ~4-14 nm^2. In the case of sharp tips, (R = 60 nm, a_s = 1.1 nm, contact area = 3.8 nm^2) this means that only about 15-20 functional group pairs are in contact.[15] Chemical force microscopy probes interactions on the local scale indeed!

A distinct advantage of CFM is its ability to image samples. The sharp, chemically-defined probe tips are used to probe local chemical features on an otherwise featureless surface. Several investigations between known molecular tip/surface combinations X and Y could conceivably be used to construct a database of interaction forces. These data could be used later to obtain maps of surfaces with unknown chemical features. Some of these possibilities and current effort in this direction are discussed in future chapters.

It must be stressed that CFM cannot always eliminate the different forces (van der Waals, electrostatic, capillary, etc.) between the tip and sample, but in certain cases (choosing the appropriate functional groups in the appropriate solvent) the overriding interaction can be attributed to a chemical interaction between functional groups on the tip and sample. To be sure, CFM is an extension of AFM.[16] However, "chemical force microscopy" transforms AFM from an instrument detecting physical forces to a new, chemically-specific measurement and imaging tool. The evolution is simple and powerful, demonstrating three important and new features in scanning probe microscopy:

1. Tip/surface interactions arise from known chemical forces.
2. The type and strength of interaction can be knowingly altered.
3. High-resolution images—"chemical maps"—can be obtained on chemically heterogeneous, topographically flat, featureless surfaces.

As a final note, the attachment of functional groups on the tip demonstrates the ability to control chemistry at a very local or "nanoscopic" scale—an ability important in the current efforts in molecular-scale materials fabrication. In developing CFM we hope that it will be useful as an analytical tool in chemical investigations of a variety of surface and interfacial phenomena.

References

1. (a) Hertz, H. J. Reine, *Angew. Math.* **1881**, *92*, 156-171. (b) Hertz, H. in *Miscellaneous Papers*; Macmillan: London, 1896, p 146.
2. Johnson, K. L.; Kendall, K.; Roberts, A. D. "Surface Energy and the Contact of Elastic Solids" *Proc. R. Soc. Lond. A.* **1971**, *324*, 301-313.
3. Among many books and review articles, see (a) *STM and SFM in Biology* Marti, O.; Amrein, M. Eds. Academic Press: San Diego, 1993. (b) Rugar, D.; Hansma, P. "Atomic Force Microscopy" *Phys. Today* **1990**, *43(10)*, 23-30. (c) Frommer, J. "Scanning Tunneling Microscopy and Atomic Force Microscopy in Organic Chemistry" *Angew. Che. Int. Ed. Engl.* **1992**, *31*, 1298-1328.
4. Binnig, G.; Rohrer, H. "Scanning Tunneling Microscopy—from Birth to Adolescence (Nobel Lecture)" *Angew. Chem. Int. Ed. Engl.* **1987**, *26*, 606-614 and references therein.
5. For reviews of scanning probe microscope instrumentation and studies, see Chapter 1 in reference 3a, reference 3c, and references therein.
6. Binnig, G.; Quate, C. F.; Gerber, Ch. "Atomic Force Microscope" *Phys. Rev. Lett* **1986**, *56*, 930-933.
7. The vibrational frequencies ω of atoms in solids is ~10^{13} Hz. The mass m is on the order of 10^{-25} kg. The spring constant $k = m\omega^2$ and is therefore ~10 N/m. (Taken from reference 3b.)
8. See, for example, Liu, G.; Salmeron, M. B. "Reversible Displacement of Chemisorbed *n*-Alkanethiol Molecules on Au(111) Surfaces: An Atomic Force Microscopy Study" *Langmuir* **1994**, *10*, 367-370.
9. Microscopic irregularities in tip shape and substrate roughness may result in more than a single tip-substrate contacts, however, in the correlation between friction and adhesion still holds.

10. In principle, all intermolecular forces can be figured from classical electrostatics, but additional classification and alternate calculation is more efficient and practical.

11. Our results from CFM experiments conducted in a dry N_2 atmosphere (a drybox) were qualitatively similar to those gathered from experiments conducted in air with no humidity control.

12. For several recent reports on investigating the role of van der Waals and hydrophobic forces on adhesion in AFM see (a) Ducker, W. A.; Sneden, T. J.; Pashley, R. M. "Direct Measurement of Colloidal Forces Using an Atomic Force Microscope" *Nature* **1991**, *353*, 239-241, (b) Tsao, Y.-H.; Evans, D. F.; Wennerstöm, H. "Long-Range Attractive Force Between Hydrophobic Surfaces Observed by Atomic Force Microscopy" *Science* **1993**, *262*, 547-550, (c) Li, Y. Q.; Tao, N. J.; Pan, J.; Garcia, A. A.; Lindsay, S. M. "Direct Measurements of Interaction Forces between Colloidal Particles Using the Scanning Force Microscope" *Langmuir* **1993**, *9*, 637-641, and references in Chapters Five, Six, and Seven of this thesis.

13. See (a) Israelachvili, J. N. *Intermolecular and Surface Forces*; Academic: San Diego, 1992; pp 169-172, (b) Yoshizawa, H.; Chen, Y.-L.; Israelachvili, J. "Fundamental Mechanisms of Interfacial Friction. 1. Techniques for Direct Measurements of Forces between Surfaces in Liquids at the Atomic Scale" *Chemtracts—Anal. Phys. Chem.* **1989**, *1*, 1-12, (c) Israelachvili, J. N. "Relation between Adhesion and Friction" *J. Phys. Chem.* **1993**, *97*, 4128-4140, and references therein.

14 A similar calculation for other molecular groups (i.e., X = Y = COOH) is complicated by the additional chemical interaction (i.e., hydrogen bond) in the estimation of the work of adhesion.

15. Electron diffraction (Strong, L.; Whitesides, G. M. *Langmuir* **1988**, *4*, 546) was used to show that dodecanethiol chains in a close-packed SAM on Au occupy 21.4 $Å^2$/chain.

16. The introduction and use of the term "chemical force microscopy" has been criticized as premature and misleading because at present, CFM cannot unambiguously identify chemical unknowns. We do not mean to imply this ability, however, and as discussed in the text, feel that the term "chemical force microscopy" is appropriate, descriptive, and useful. See Frommer, J. in Letters to the Editor, "Chemical Force Microscopy" *Chem. Eng. News* **1994**, *72(51—December 19)*, 74-77 and the pursuing response. See also Baum, R. in News of the Week, "Chemical Force Microscopy Method Maps Functional Groups on Surfaces" *Chem. Eng. News* **1994**, *72(40—October 3)*, 6.

CHAPTER FIVE

FUNCTIONAL GROUP IMAGING BY CHEMICAL FORCE MICROSCOPY

Introduction

This chapter describes the first experiments in chemical force microscopy in a collaborative project between our research group and the group of Professor Lieber at Harvard University.[1] In these experiments, the interaction between two known molecular groups are measured near the molecular scale. Lubrication in mechanical devices and recognition in biological systems are examples of two important scientific problems in which the spatial arrangement and interactions between chemical functional groups play an essential role.[2] Techniques that directly probe the interactions between molecules and/or molecular assemblies with high spatial resolution could thus provide a means for significantly enhancing the molecular level understanding of these areas. Several methods are now available to measure forces between macromolecules and molecular assemblies, including the surface forces apparatus (SFA),[2-4] optical tweezers,[5] and atomic force microscopy (AFM).[6-11] The SFA has been used to measure adhesive and frictional forces between macroscopic assemblies of molecules,[4] while optical tweezers have been used to probe interactions between individual macromolecules;[5] neither technique can, however, be used to map the spatial arrangement of functional groups that give rise to the observed interactions. AFM could in principle be used to measure interactions between different functional groups and map their spatial arrangement, although recent AFM studies have focused only on measuring the forces between ligand-receptor pairs attached to the tip and sample surface.[12,13]

In this chapter, AFM studies that address both the interaction and the spatial mapping of chemically distinct functional groups are presented. These investigations focus on adhesive and friction force measurements of organic monolayers which have been lithographically patterned to produce a two-dimensional geometrical distribution of distinct functional groups. Using probe tips that have been functionalized with either hydrophobic or hydrophilic molecules, the adhesive interactions between simple hydrophobic-hydrophobic, hydrophobic-hydrophilic and hydrophilic-hydrophilic molecules can be

measured reproducibly. Importantly, the differences in these adhesive interactions correlate directly with the friction images of the patterned sample surface, demonstrating that the spatial distribution of hydrophilic (COOH) and hydrophobic (CH_3) functional groups can be predictably mapped using functionalized tips. Potential applications and limitations of this new approach, chemical force microscopy, are discussed.

Conventional repulsive mode AFM images are obtained by recording the vertical deflection of a cantilever/probe tip assembly (often Si_3N_4) while rastering a sample in contact with the tip. Images of organic and biological materials produced by this means reflect the topography of these materials,[10] but do not provide information about the chemical nature of different groups at these surfaces. It is also possible, by monitoring the lateral forces on the cantilever, to record an image of the friction forces between the tip and sample.[8] Recent experiments involving the friction mapping of organic mono- and multilayer films have shown that friction differences are observed between distinct regions in these samples,[14,15] although the mechanism of contrast in these images may not be directly related to a chemical interaction between the tip and sample.[14] We believe that the chemical sensitivity of AFM can be rationally enhanced by modifying the probe tip with specific functional groups. In conjunction with this idea, we hypothesized that the magnitude of the friction force on the probe tip is directly correlated with the magnitude of the adhesive force between the tip and the sample. On the molecular level the fundamental relationship between adhesion and friction is unclear, although a recent report has addressed this issue experimentally.[4] Our premise nevertheless provides a simple approach to implementing chemically sensitive mapping by AFM; that is, by modifying probe tips with complimentary/noncomplimentary functional groups it should be possible to predict the friction contrast in images of surfaces patterned with different functional groups.

Results and Discussion

We have used AFM to investigate systems consisting of cantilever-tip assemblies that have been covalently modified with self-assembled monolayers (SAMs) terminating in specific functional groups, and organic SAM surfaces that contain a lithographically defined arrangement of two different functional groups (Figure 5.1). Self-assembly is an attractive method for modifying the probe tips[16] and sample surfaces since it yields robust (i.e., covalent) monolayer coatings.[17] In the experiments described below, we focus on surfaces that have been patterned with both CH_3 (hydrophobic) and COOH (hydrophilic) groups and probe tips that have been functionalized with either CH_3 or COOH terminated molecules. We expect that this approach can be readily generalized to study other interactions including those between charged and/or chemically reactive groups, and the specific binding between substrates and enzymes or nucleic acid oligomers.

Figure 5.2 shows force versus cantilever displacement curves recorded on CH_3 and COOH surfaces using CH_3 and COOH terminated probe tips. In these measurements, we monitor the deflection of the cantilever as the sample approaches, contacts and is then withdrawn from the probe tip.[7,9] The deflection is converted to a force using the cantilever spring constant.[18] Hysteresis in the force-displacement curves corresponds to an adhesive interaction between the tip and sample. Qualitatively, the curves in Figure 5.2 show that the adhesive interaction between the functional groups on the modified tip/sample pairs exhibit the following trend: COOH/COOH > CH_3/CH_3 > COOH/CH_3. Results obtained on a number of independent tip/sample combinations are summarized in Table 5.1. The trend in adhesive forces that we have determined for the modified tips and surfaces is consistent with our expectation that the interaction between hydrophilic groups, which can form hydrogen bonds, will be stronger than that between hydrophobic groups,[19] while the cross interaction should be weakest. As shown in Table 5.1, we find that the differences in the adhesive interactions between the same (COOH/COOH or CH_3/CH_3) or different

Figure 5.1. (A) Schematic of the surface modification procedure and a condensation image corresponding to a typical sample. Patterned sample surfaces containing lithographically defined hydrophilic and hydrophobic regions were prepared as previously described.[27] Briefly, Au-coated Si(100) substrates were immersed in 1 mM methylcyclohexane solutions of di-11-(4-azidobenzoate)-1-undecyl disulfide to yield a photosensitive monolayer. Irradiation of these substrates with UV-light ($\lambda > 260$ nm) through a mask and a thin film of ethyl 4-aminobutyrate yielded ethyl ester termination in the irradiated regions of the sample. The sample was then irradiated a second time through a quartz plate and thin film of dioctylamine to yield methyl termination in the previously unreacted areas of the sample. Lastly, the ethyl ester groups were converted to COOH groups by hydrolysis. The condensation image illustrating the spatial pattern of hydrophobic (CH_3) and hydrophilic (COOH) terminated regions in the sample was recorded with an optical microscope while observing the condensation of water vapor onto the cooled sample surface.[28] The water preferentially wets the hydrophilic (COOH) terminated regions of the sample surface. (B) Modification of the cantilever/tip assembly with a specific functional group. Gold-coated Si_3N_4 cantilever/tip assemblies[18] were immersed in 1 mM ethanolic solutions of either octadecylmercaptan or 11-mercapto-undecanoic acid for 2 h to form covalently bound monolayers that were terminated with either hydrophobic (CH_3) or hydrophilic (COOH) functional groups. The specific case of a tip terminating with COOH groups is shown. (C) Schematic views of the experiment. The inset illustrates the interactions between a tip terminating in COOH groups and patterned sample terminating in both CH_3 and COOH groups.

A. Sample Preparation

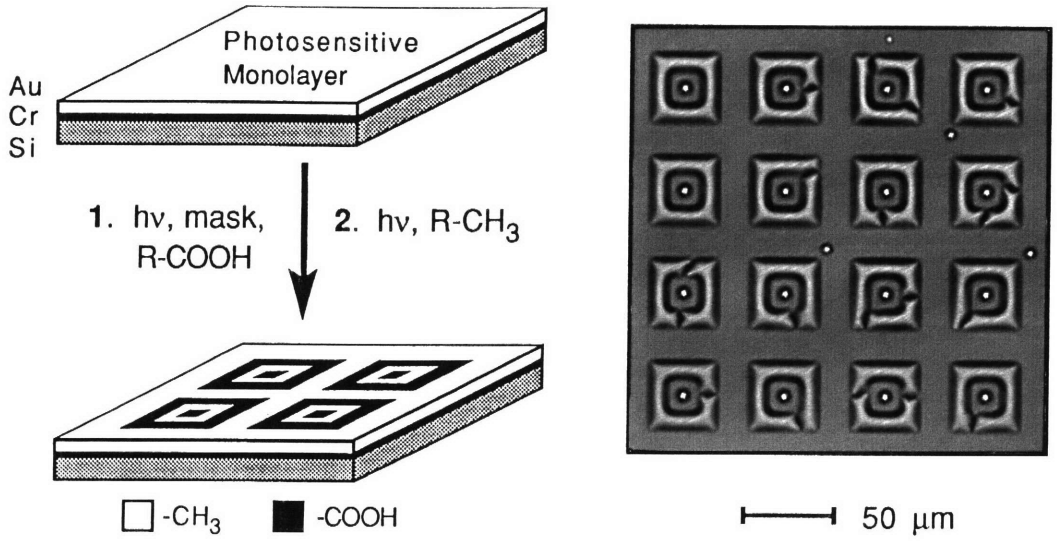

B. Tip Preparation

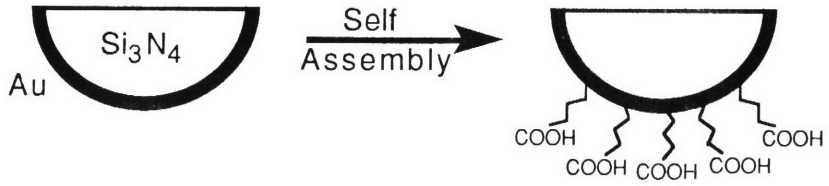

C. Chemical Force Microscopy

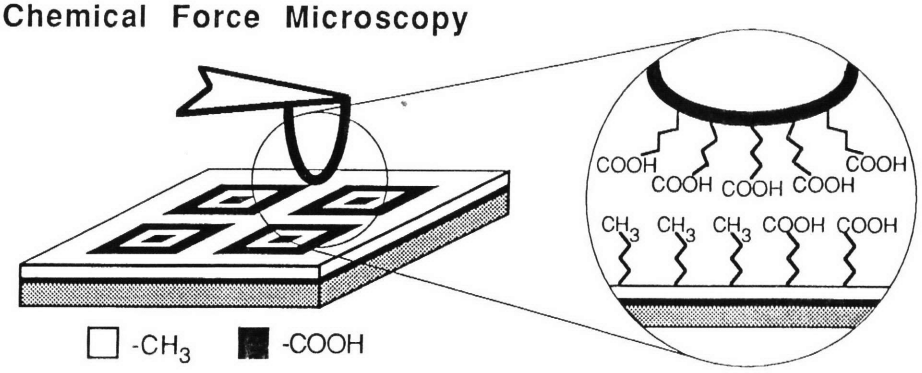

Figure 5.2. Typical force vs. displacement curves recorded between a COOH-terminated tip and sample, a CH_3-terminated tip and COOH-terminated sample, and a CH_3-terminated tip and sample in EtOH using a Nanoscope III LFM.

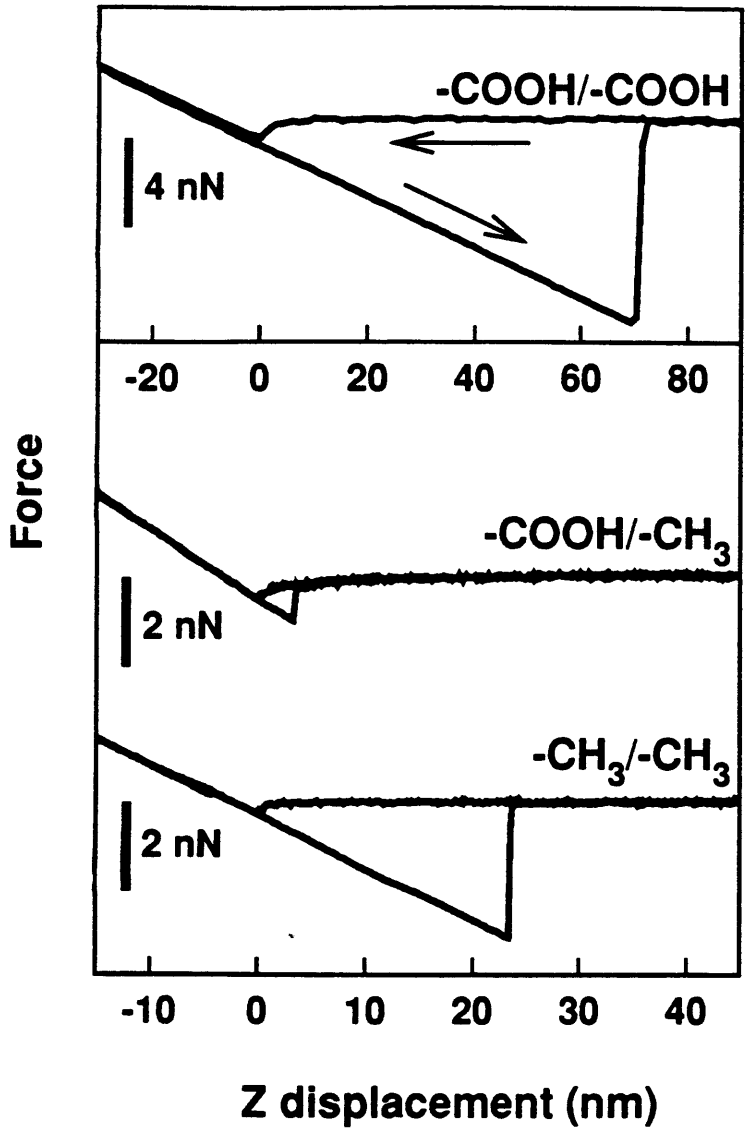
-COOH/-COOH
4 nN
-20
0
20
40
60
80
Force
-COOH/-CH3
2 nN
-CH3/-CH3
2 nN
-10
0
10
20
30
40
Z displacement (nm)

Table 5.1. Summary of adhesive forces (nN) measured between functionalized tips and samples. These data were obtained by averaging the results from at least 300 force vs. displacement curves for each tip/sample combination.

	Tip	
Sample	COOH	CH_3
COOH	8.7 ± 3.2	0.85 ± 0.49
CH_3	0.71 ± 0.35	2.7 ± 0.92

($COOH/CH_3$) functional groups are reproducibly larger than the uncertainty in these measurements, enabling the distinction of these functional groups simply based on the magnitude of the measured adhesive force. We believe that the ability to distinguish the interactions between these simple functional groups is significant since these interactions represent perhaps the most general type of forces that occur between molecules and molecular assemblies.[20] We also find that these modified tips are stable; for example, using a CH_3 terminated tip it is possible to switch repeatedly between COOH and CH_3 terminated samples and obtain the expected differences in adhesive interaction between CH_3/COOH and CH_3/CH_3 groups at each switch.[21] In contrast, measurements made with unmodified probe tips exhibit force-displacement curves that change significantly with time and vary from tip to tip. Finally, it is important to recognize that the measured forces correspond to interactions between a small number of discrete functional groups. Using the Johnson-Kendall-Roberts (JKR) model[2,22] we estimate that the contact area at pull-off is approximately 10 nm^2, and thus, that the measured force results from the interaction between ~50 functional groups on the sample and tip.[23] Our ability to probe such local interaction forces is consistent with other recent AFM studies,[12,13,24] and it would be

interesting to investigate whether the rupture of individual pairs of molecules could be observed as in two recent studies.[12, 24]

Our central result is the spatial mapping of friction forces between the functionalized tips and lithographically patterned samples. Topographic and lateral force images recorded using both CH_3 and COOH functionalized tips on surfaces terminated with CH_3 and COOH groups are shown in Figure 5.3. In general, little or no evidence is seen for the pattern of CH_3 and COOH groups in maps of the surface topography (Figure 5.3B). A relatively featureless topography is expected since the CH_3 and COOH regions of the sample are structurally quite similar. These chemically distinct regions are, however, clearly visible in images of the friction force. As shown in Figure 5.3C, when a CH_3-terminated tip is used for imaging, the CH_3-terminated regions of the sample exhibit a larger friction than the COOH-terminated regions. In contrast, when a COOH-terminated tip is used to image the same sample, the friction contrast is reversed; a low friction force is observed over the CH_3-terminated regions of the sample and a high friction force is observed over those regions terminated with COOH functional groups, as shown in Figure 3D. These observed differences in image contrast agree with chemical intuition and our quantitative adhesion force data since higher friction is observed between similar functional groups (COOH/COOH or CH_3/CH_3) that interact more strongly with each other than dissimilar groups (COOH/CH_3). We find that a minimum applied load of ~3 nN is necessary to observe friction images with good contrast, but this load is well below the threshold load for monolayer damage recently reported.[25] In addition, image contrast using the modified tips is stable and reproducible, but images obtained using unmodified tips do not show reproducible variations in the friction force on the above modified surfaces.

Figure 5.3. (A) Optical condensation image of a patterned sample. The bright, raised areas in this image correspond to liquid H_2O that has condensed on the hydrophilic (COOH-terminated) regions of the sample. (B) Force microscope image of the sample topography of the same surface pattern as in (A) recorded using a probe-tip terminated with hydrophobic (CH_3) functional groups. As expected, there is little difference in the topography observable between the CH_3- and COOH-terminated regions of the sample. Similar topographic images were also recorded using COOH-terminated tips. (C) Image of the friction force recorded simultaneously with the topography in (B). The bright regions correspond a high friction force, while the dark regions correspond to a lower friction force. In this image, which was recorded with a CH_3-terminated tip, high friction is observed over CH_3-terminated regions of the sample. (D) Image of the friction force recorded between a COOH-terminated tip and a similar region of the sample as in (A-C). In this image, high friction is observed over COOH-terminated regions of the sample. Images (B)-(D) were acquired under EtOH with an applied load of 4 nN and a scan rate of 3 Hz. Similar results have been obtained using scan rates between 1 and 10 Hz and applied loads from 3-10 nN.

Condensation Image

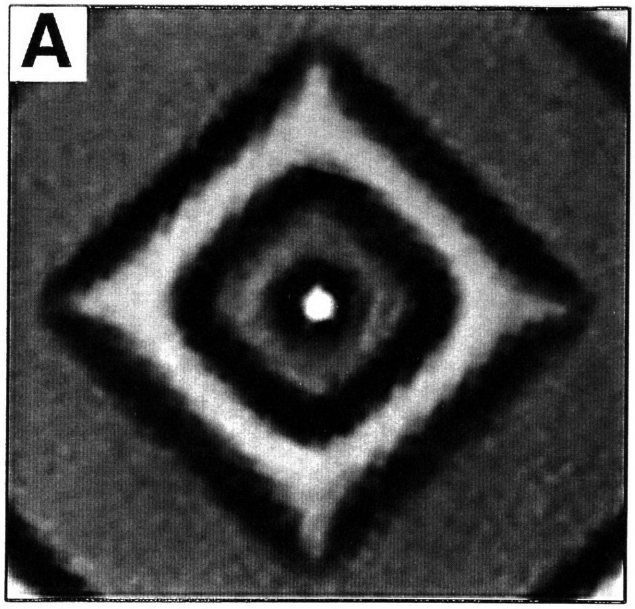

Topographic Image

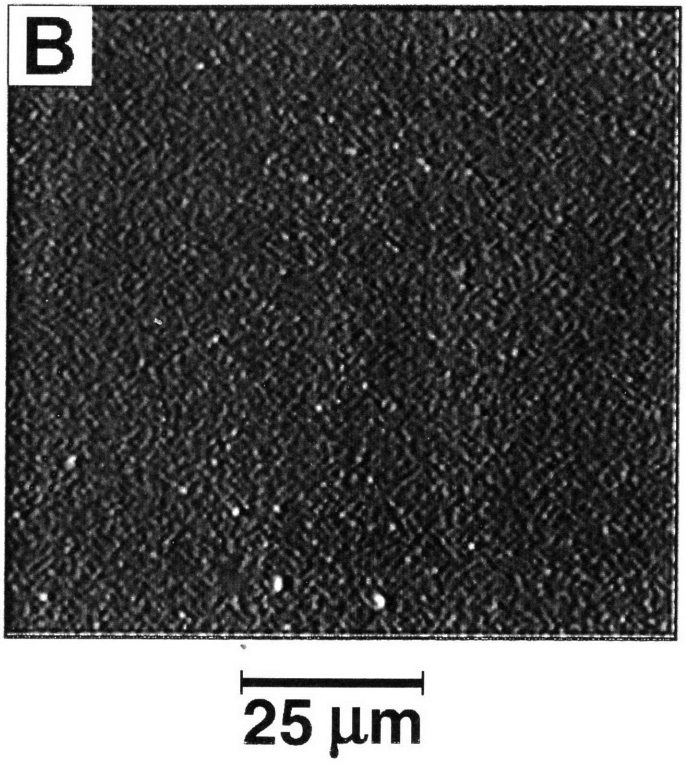

Lateral Force Images

CH_3 Tip

COOH Tip

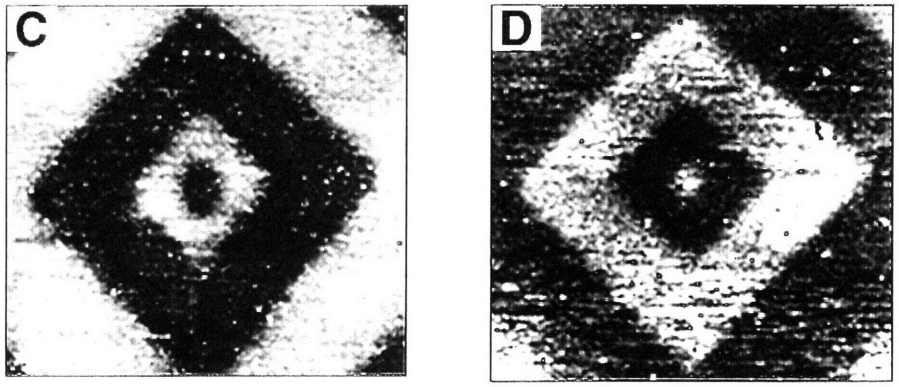

Conclusions

The present results demonstrate clearly that it is possible to map in a predictable manner the spatial distribution of chemically distinct functional groups on a sample surface when using functionalized tips. That is, sample regions that have strong (weak) interactions with the functionalized probe tip will exhibit large (small) friction.[26] We believe that an appropriate description of this imaging technique is *"chemical force microscopy"* since the image contrast is readily interpretable in terms of the chemical interactions between specific functional groups on the modified tips and those being mapped on the sample surface. It is important to consider the lateral resolution provided by this imaging technique. We estimate the resolution of the images in Figure 3 to be approximately 200 nm. However, we believe that the achievable resolution should be on the order of 10 nm (100 Å) based on our estimation of the contact area of the tip on the sample during imaging. Resolution in our present images is believed to be limited by the resolution inherent in our monolayer patterning procedure. Ultimately, the achievable lateral resolution could be improved beyond 10 nm by using sharper probe tips.

In our studies we have demonstrated the concept of chemical force microscopy for the specific case of functional groups exhibiting hydrophobic and hydrophilic character. Using the present techniques it should be possible to map the spatial distribution of other types of functionality such as charged or chemically reactive groups. The ability to map different chemical functionality on surfaces should be of significant utility in studies of adhesion and lubrication. In addition, we believe that more specific interactions, for example those between complimentary/noncomplimentary oligonucleotides and ligand/receptor pairs, could be readily mapped with high resolution. One could thus envision attaching a specific oligonucleotide or receptor to the probe-tip, and then mapping the friction force on a surface that contains an array of different nucleotide sequences or ligands to find those having the strongest interaction. Finally, in cases where the sample surface exhibits significant topographic variations it should still be possible to image with functional group

sensitivity by mapping the adhesive force between a specifically functionalized tip and the unknown sample (determined from force-displacement curves recorded simultaneously with the topographic map) as a function of x-y coordinates.

References

1. Frisbie, C. D.; Rozsnyai, L. F.; Noy, A.; Wrighton, M. S.; Lieber, C. M. *Science* **1994**, *265*, 2071.
2. Israelachvili, J. *Intermolecular & Surface Forces*; Academic: San Diego, 1992.
3. Israelachvili, J. *Acc. Chem. Res.* **1987**, *20*, 415.
4. (a) Yoshizawa, H.; Chen, Y.-L.; Israelachvili, J.; *J. Phys. Chem.* **1993**, *97*, 4128. (b) Chen, Y.-L.; Helm, C. A.; Israelachvilli, J. N. *J. Phys. Chem.* **1991**, *95*, 10736.
5. (a) Ashkin, A.; Dziedzic, J. M.; Bjorkholm, J. E.; Chu, S. *Optics Lett.* **1986**, *11*, 288. (b) Kuo, S. C.; Sheetz, M. P. *Science* **1993**, *260*, 232. (c) Svoboda, K.; Schmidt, C. F.; Schnapp, B. J.; Block, S. M. *Nature* **1993**, *365*, 721.
6. Quate, C. F. *Surf. Sci.* **1994**, *299/300*, 980.
7. Hues, S. M.; Colton, R. J.; Meyer, E.; Güntherodt, H.-J. *MRS Bulletin* **1993**, *18*, 41.
8. Mate, C. M.; McClelland, G. M.; Erlandsson, R.; Chiang, S. *Phys. Rev. Lett.* **1987**, *59*, 1942.
9. Burnham, N. A.; Colton, R. J. *J. Vac. Sci. Technol. A* **1989**, *7*, 2906.
10. Frommer, J. *Angew. Chem. Int. Ed. Engl.* **1992**, *31*, 1298.
11. Rugar, D.; Hansma, P. K. *Phys. Today* **1990**, *43(10)*, 23.
12. Florin, E.-L.; Moy, V. T.; Gaub, H. E. *Science* **1994**, *264*, 415.
13. Lee, G. U.; Kidwell, D. A.; Colton, R. J. *Langmuir* **1994**, *10*, 354.
14. (a) Overney, R. M.; Meyer, E.; Frommer, J.; Brodbeck, D.; Lüthi, R.; Howald, L.; Güntherodt, H.-J.; Fujihira, M.; Takano, H.; Gotoh, Y. *Nature* **1992**, *395*, 133. (b) Overney, R. M.; Meyer, E.; Frommer, J.; Güntherodt, H.-J.; Fujihira, M.; Takano, H.; Gotoh, Y *Langmuir* **1994**, *10*, 1281.
15. Kumar, A.; Biebuyck, H. A.; Whitesides, G. M. *Langmuir* **1994**, *10*, 1498.

16. (a) Thomas, R. C.; Tangyunyong, P.; Houston, J. E.; Michalske, T. A.; Crooks, R. M. *J. Phys. Chem.* **1994**, *98*, 4493. (b) Nakagawa, T.; Ogawa, K.; Kurumizawa, T.; Ozaki, S. *Jpn. J. Appl. Phys.* **1993**, *32*, L294. (c) Barrat, A.; Silberzan, P.; Bourdieu, L.; Chatenay, D. *Europhys. Lett.* **1992**, *20*, 633.

17. (a) Nuzzo, R. G.; Allara, D. L. *J. Am. Chem. Soc.* **1983**, *105*, 4481. (b) Bain, C. D.; Troughton, E. B.; Tao, Y.-T.; Evall, J.; Whitesides, G. M.; Nuzzo, R. G. *J. Am. Chem. Soc.* **1989**, *111*, 321. (c) Whitesides, G. M.; Laibinis, P. E. *Langmuir* **1990**, *6*, 87. (d) Dubois, L. H.; Nuzzo, R. G. *Annu. Rev. Phys. Chem.* **1992**, *43*, 437.

18. The Si_3N_4 catilevers with integrated tips (triangular, 200 μm long, from Digital Instruments, Inc.) were coated with a 30 Å of Cr adhesion layer followed by 1000 Å of Au using an Edwards Auto 306 thermal evaporator. The cantilever force constants were determined using the end-mass resonance detection method (Cleveland, J. P.; Manne, S.; Bocek, D.; Hansma, P. K. *Rev. Sci. Instrum.* **1993**, *64*, 403). We measured the force constants of the uncoated and Au-coated levers to be 0.07 and 0.12 N/m, respectively.

19. The strength of a single hydrogen bond is on the order of 10 kcal/mol, while that of a van der Waals (hydrophobic) bond is about 1 kcal/mol.

20. AFM has been used previously to measure the adhesive interaction between hydrocarbon groups (see reference 16), however, measurements of the adhesive interaction between different types of functional groups (e.g., CH_3/CH_3, CH_3/COOH, and COOH/COOH) have not to our knowledge been reported.

21. Additionally, analysis of the adhesive force as a function of time using tips terminating in COOH showed that the average force dropped only 15% after 400 force-displacement curves. Tips terminating in CH_3 appear to exhibit greater stability.

22. Johnson, K. L.; Kendall, K.; Roberts, A. D.; *Proc. Roy. Soc. London A* **1971**, *324*, 301.

23. The radius of the tip-sample contact area at separation, a_s, is

$$a_s = 1.67\left[\frac{\gamma R^2}{K}\right]^{\frac{1}{3}}$$

where γ is the work of adhesion per unit area of contact, R is the radius of curvature, and K is an elastic constant which is calculated from the Poisson ratio and Young's modulus of Au. For this system γ = 5 mN/m, K = 64 GPa. For our experimental geometry we estimate R = 115 nm. Substituting these values into the above equation yields a_s = 1.7 nm, or a contact area of 9.0 nm^2. This area corresponds to ~50 surface-confined molecules (0.2 nm^2 per molecule—see reference 17). The force per CH_3/CH_3 interaction can be calculated by dividing our experimental value of ~4 nN (Table 1) by 50 which gives 8 x 10^{-11} N. This value is consistent with another, independent calculation of the force between two CH_3 groups, which assumes the interaction can be treated using a Lennard-Jones potential (Noy, A; Frisbie, C. D.; Lieber, C. M. unpublished results).

24. Hoh, J. H.; Cleveland, J. P.; Prater, C. B.; Revel, J.-P.; Hansma, P. K. *J. Am. Chem. Soc.* **1992**, *114*, 4917.

25. Liu, G.; Salmeron, M. B. *Langmuir* **1994**, *10*, 367.

26. It has been suggested on the basis of SFA studies of different hydrocarbon terminated layers that it is the hysteresis in adhesion that will correlate with friction (see reference 4). We believe that in comparisons of chemically distinct functional groups, which exhibit significant differences in adhesive interaction, friction differences are directly related to the variations in the adhesive forces.

27. (a) Wollman, E. W.; Kang, D.; Frisbie, C. D.; Lorkovic, I. M.; Wrighton, M. S. *J. Am.Chem. Soc.* **1994**, *116*, 4395. (b) Rozsnyai, L. F.; Wrighton, M. S. unpublished results.

28. López, G. P.; Biebuyck, H. A.; Frisbie, C. D.; Whitesides, G. M. *Science* **1993**, *260*, 647.

CHAPTER SIX

CHEMICAL FORCE MICROSCOPY: USING CHEMICALLY-MODIFIED TIPS TO QUANTIFY ADHESION, FRICTION, AND FUNCTIONAL GROUP DISTRIBUTIONS IN SELF-ASSEMBLED MONOLAYERS

Introduction

Intermolecular forces are responsible for a wide variety of phenomena in condensed phases extending from capillarity and lubrication at macroscopic length scales, through micelle and membrane self-assembly on a mesoscopic scale, to molecular recognition and protein folding at the nanoscopic scale.[1] Development of a fundamental understanding of such important phenomena, regardless of the length scale, requires detailed knowledge of the magnitude and range of intermolecular forces. For example, macroscopic measurements of friction and adhesion between surfaces are influenced by complex factors such as surface roughness and adsorbed contaminants. Microscopic studies of these forces should, however, be interpretable in terms of fundamental chemical forces such as van der Waals, hydrogen bonding, and electrostatic interactions. In addition, an understanding of intermolecular forces in condensed phases is significant to nanoscale chemistry where noncovalent interactions are important to the manipulation, assembly, and stability of new nanostructures.

Direct experimental measures of the interactions between molecules and molecular assemblies can be achieved using several techniques, including the surface forces apparatus (SFA),[2] optical tweezers[3] and scanning force microscopy.[4-9] The SFA has yielded considerable information about adhesion and friction between molecular assemblies, although these data are an average over large numbers of molecules contained within the ca. 1 mm^2 probing area. On the other hand, force microscopy, which involves measuring the forces on a sharp tip as it is scanned over a sample, has proven to be a useful tool for imaging the structure and dynamics of surface adsorbates at the nanometer scale.[4-24] Few studies have, however, exploited the exquisite force sensing and imaging capabilities of force microscopes to probe the interactions between molecules and macromolecules.[15-23]

A systematic force microscopy study of interactions between molecular groups requires a flexible methodology for attaching molecules to the probe tip. One successful method that we have recently reported[17] involves self-assembly of functionalized organic thiols

onto the surfaces of Au-coated Si_3N_4 probe tips (Figure 6.1). Stable and rugged monolayers of alkyl thiols or disulfides containing a variety of terminal groups can be readily prepared[25] and enables systematic studies of the interactions between basic chemical groups on the probe tip and similarly modified Au substrates. Covalent modification of force probes with thiols and reactive silanes has also been reported by other groups in studies of adhesion[19,20] and contact potential.[21] In addition, nonspecific adsorption has been used to study binding between protein-substrate pairs[22,23] and long-range forces between hydrophobic surfaces.[24]

This chapter describes systematic force microscopy studies of the interactions between different chemical functional groups covalently linked to a force microscope probe tip and sample substrate. The results reported in Chapter Five were discussed only qualitatively—additional data interpretation and instrument calibration are reported in this chapter towards a more quantitative study. Adhesive forces between probe tips and substrates that have been modified with SAMs terminating with COOH, CH_3, and NH_2 functional groups have been measured in EtOH and H_2O solvents. The measured adhesive forces are found to agree with predictions of the Johnson, Kendall, and Roberts (JKR) theory, and thus show that the observed interactions correlate with the surface free energy. In addition, lateral force imaging studies demonstrate that the friction force between different functional groups correlates directly with the adhesion forces between these same groups. The dependence of friction forces on the tip and sample functionality is shown to be the basis for chemical force microscopy in which lateral force images are interpreted in terms of a spatial distribution of different functional groups.

Figure 6.1. Schematic drawing of a CFM setup. The sample rests on a piezoelectric tube which can be finely moved laterally (x and y) and vertically (z). A laser beam is reflected from the backside of the tip into a photodiode to measure two types of tip-surface interactions: As the sample is rastered under the tip, the tip will move up and down in response to surface topography, resulting in the atomic force (height) signal. The tip will also rock back and forth in response to friction, yielding the lateral force (friction) signal. The inset illustrates the chemically specific interactions presented in this report. An Au-coated COOH-terminated tip contacts the boundary of CH_3- and COOH-terminated region of the sample.

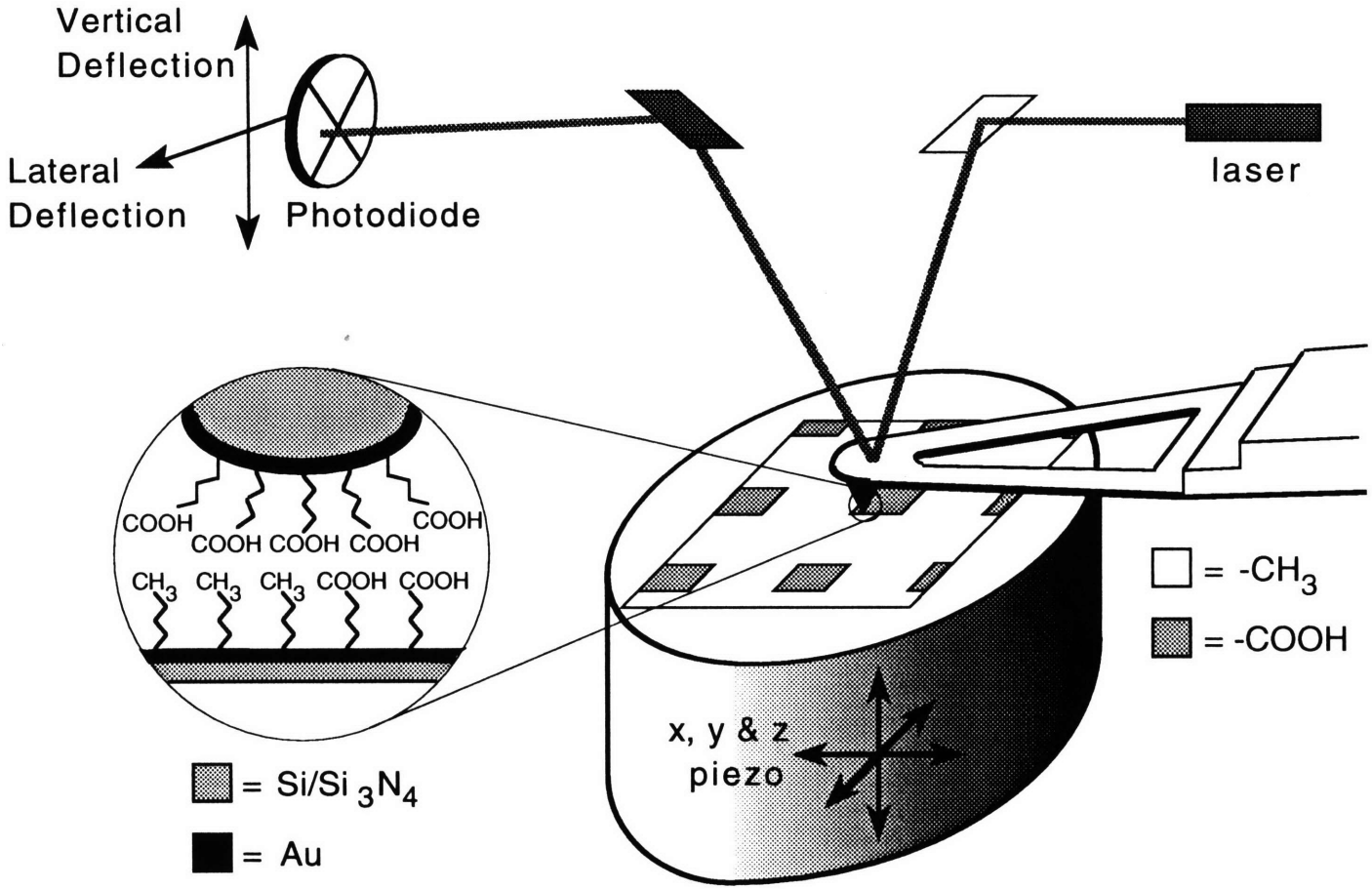
Vertical
Deflection
Lateral
Deflection
Photodiode
laser
COOH
COOH COOH COOH
COOH
CH3 CH3 CH3 COOH COOH
= -CH3
= -COOH
x, y & z
piezo
= Si/Si 3N4
= Au

Experimental Section

Materials. Di-11-(4-azidobenzoate)-1-undecyl disulfide, **I**, (see Chapter One and references therein) and 11-mercaptoundecanoic acid were used from previous studies.[17] Octadecanethiol, 3-aminopropyltriethoxysilane, and K(t-Bu)OH were available commercially (Aldrich) and used as received. Dioctylamine (Aldrich) was distilled under reduced pressure and stored under N_2. The free amine of ethyl-4-aminobutyrate hydrochloride (Aldrich) was obtained by a method adapted from the literature.[26] Briefly, 10 g of the compound was dissolved in 25 ml of warm EtOH to which 300-400 ml of Et_2O was added, maintaining solubility with EtOH as necessary. Anhydrous NH_3 was bubbled through the solution for 30-45 min and the resulting fine white precipitate was removed by filtration. The remaining clear oil was dried, distilled under reduced pressure, and stored under N_2 at 20 °C until use in substrate functionalization. Solvents used in chemical manipulations were of reagent grade or better; solvents used in substrate and probe tip functionalization were HPLC grade to reduce the amount of particulate matter. All water was deionized with a Barnstead NANOpure II filtration unit to 18 MΩ·cm resistivity.

Au-coated Substrates and Probe Tips. Substrates of the desired size were cut from Si (100) wafers (Silicon Sense, Nashua, NH; test grade, 500 μm thick). These substrates and commercial Si_3N_4 tip-cantilever assemblies (Digital Instruments, Santa Barbara, CA) were coated by thermal evaporation (Edwards Auto 306 Cryo evaporator) with a 20 Å adhesion layer of Cr followed by 1000 Å of Au. Care was taken to avoid heating the Si_3N_4 probes during evaporation. We suspect that heating caused the cantilevers to bend permanently, making them unusable. This bending was presumably due to differences in the thermal expansion coefficients of Au and Si_3N_4. The Au wire (99.99%) was cleaned in 3:1 HCl:HNO_3, rinsed with deionized H_2O, EtOH, and oven dried immediately prior to evaporation.

Substrate and Tip Derivatization. Monolayers were formed immediately after Au evaporation. Monolayers of **I** were formed by immersion of the Au samples in 2-3 mM

methylcyclohexane solutions for at least 12 hours. Monolayers of 11-mercaptoundecanoic acid and octadecanethiol were formed by immersion of the freshly coated substrates and probe tips in 2-3 mM EtOH solutions for a least 2 hours. Before use or characterization, all SAM substrates were rinsed in EtOH (SAM substrates of **I** were first rinsed with methylcyclohexane, then EtOH) and dried with a stream of dry Ar. Amine-terminated monolayers were prepared by immersing freshly cleaned Si(100) substrates (1:1:5 NH_4OH:H_2O_2:H_2O, 70 °C, 10 min) in a 2% toluene solution of 3-aminopropyltriethoxy-silane for 1 hour. Silane monolayer formation was verified by X-ray photoelectron spectroscopy.

SAM Photopatterning. Amines were covalently attached to Au-**I** SAM substrates in high yield by UV-irradiation as previously reported.[27] SAMs terminating in two distinct functional groups were formed by double irradiation using a mask to define the pattern in the first step. To obtain a patterned surface terminating in COOH and CH_3, a drop of ethyl-4-aminobutyrate was first placed on a freshly rinsed and dried Au-**I** substrate. A Cr-on-quartz mask was then placed on top of the substrate, Cr-side down, forcing the amine to spread evenly across the sample. The assembly was irradiated for 2 min through the mask using a filtered (10 cm quartz cell filled with 1:1:1 H_2O:EtOH:EtOAc) 200 W Hg lamp ($\lambda >$ 260 nm). After rinsing with a copious amount of EtOH and drying with a stream of dry Ar, a drop of dioctylamine was applied to the sample. A clear quartz plate was placed on the sample and the assembly was uniformly irradiated for 2 min, rinsed, and dried.

The surface-confined ethyl ester was hydrolyzed following a procedure for the hydrolysis of hindered esters.[28] A solution of 25 ml ethyl ether, 1.33 mg K(t-Bu)OH, and 60 μl H_2O was cooled on ice. The solution was transferred to a vial containing the samples and left at room temperature for 2-4 hours. Contact angle titration on homogeneous COOH-terminated SAM samples hydrolyzed in this manner were consistent with measurements taken on SAMs of 11-mercaptoundecanoic acid on Au. Condensation figures of the patterned substrates revealed H_2O condensation only on the acid-terminated

regions; no H_2O droplets were found on the hydrophobic areas of the sample. Before CFM imaging, the samples were cut to 1.2 cm x 1.2 cm squares, rinsed with deionized H_2O, and dried with a stream of dry Ar or N_2. Freshly prepared samples were used for each set of experiments.

Chemical Force Microscopy. Adhesion and friction measurements were made with a Digital Instruments (Santa Barbara, CA) Nanoscope III lateral force microscope (LFM) equipped with a fluid cell. Measurements were done under absolute EtOH except where noted. Derivatized tips were rinsed in EtOH and dried under N_2 just prior to mounting them in the fluid cell.

Cantilever Calibration. Triangular, 200 μm long Si_3N_4 cantilevers were calibrated using a resonance detection method:[29] Small endmasses consisting of W spheres (~10 μm diameter, ~4 ng) were placed on the end of the lever using a glass micropipet. The W spheres stuck to the end of the lever by capillary adhesion. The diameters of the spheres were determined with an optical microscope and used to calculate the added mass. The end-loaded lever was mounted into the scan head of the microscope, and the resonance frequency of thermal vibrations was determined by monitoring the signal from the photodiode detector with a spectrum analyzer (HP-3561A Dynamic Signal Analyzer).

Results and Discussion

Probe Tip Modification. Quantitative interpretation of force microscopy data requires detailed knowledge of the tip radii and spring constants of the Au-coated tip-cantilever assemblies. The tip radius affects the tip/surface contact area—in effect, the number of molecular interactions—and thereby is an important parameter in the quantitative interpretation and comparison of force microscopy data. A scanning electron microscopy image of a Si_3N_4 cantilever-tip assembly coated with 1000 Å of Au is shown in Figure 6.2. No charging effects were observed during SEM imaging, indicating complete Au coating of the tip. Charging did occur on uncoated Si_3N_4 tips. We observed significant variations in radii of curvature for the tips from different batches supplied by the manufacturer. Radii for Au-coated tips range from ~60 nm ("sharp tips", Figure 6.2) to ~150 nm ("blunt tips"). These differences represent typical variations that can be observed for commercial Si_3N_4 tips.[30]

All adhesion and friction force data presented in this report were taken using sharp tips coated with ~1000 Å of Au and functionalized with the appropriate SAM. In our previous report[17] (Chapter Five), blunt tips were used. The differences in adhesion forces between the present and previous reports are attributed principally to the differences in tip radii.

Cantilever force constants, k, have been determined by measuring the cantilever resonance frequency, ν, as a function of spherical tungsten masses added to the end of the tip.[29] Representative data obtained for both uncoated and Au-coated Si_3N_4 cantilevers are shown in Figure 6.3. The plots of the added mass vs. $1/\nu^2$ yield straight lines with slopes proportional to k. As expected, the thicker Au-coated cantilevers exhibit larger force constants (~0.12 N/m) than the bare Si_3N_4 cantilevers (~0.07 N/m). Also, the observed k for the uncoated cantilevers is 40% smaller than that reported by the manufacturer. This deviation represents the typical variation for nominally similar batches of cantilevers and is in agreement with previous reports.[29] Hence, although it is possible to calculate k for the Au-coated cantilevers from the manufacturer's value for the Si_3N_4 cantilever and the

Figure 6.2. Scanning electron microscopy images of an Au-coated force microscopy probe tip. The inset shows the high magnification image of the area near the end of the tip.

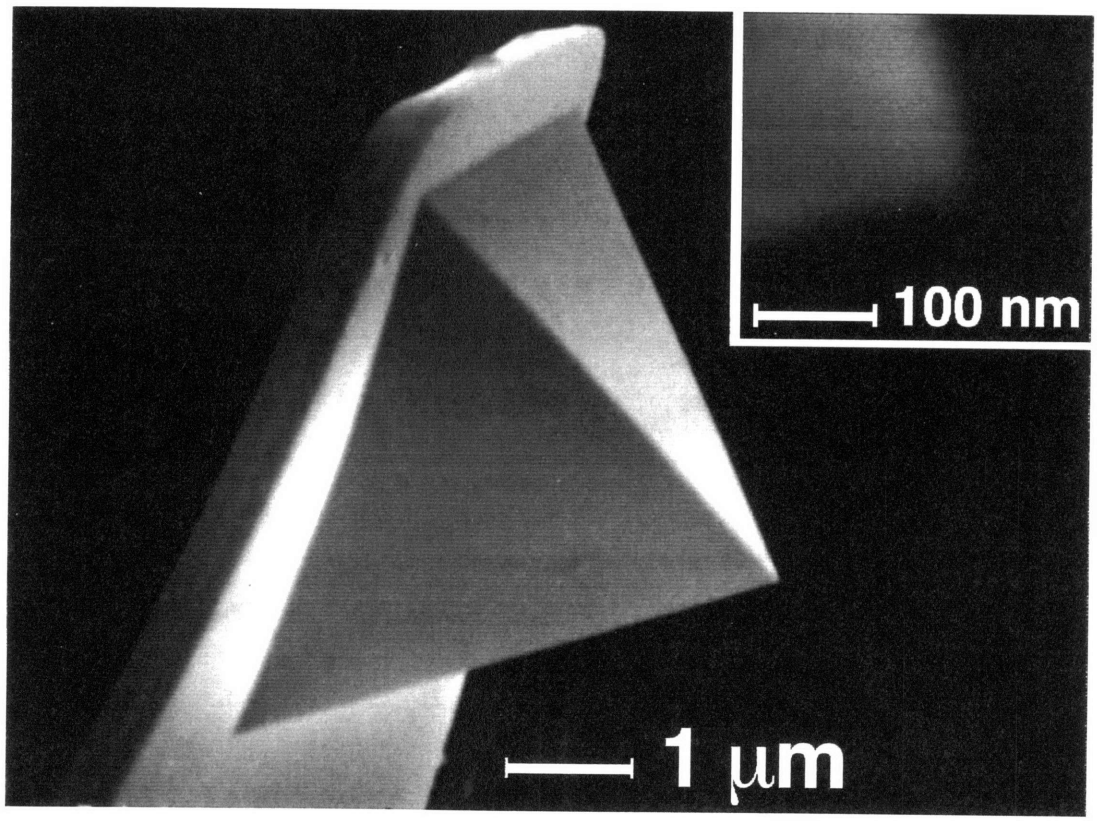
100 nm
1 μm

Figure 6.3. Plot of the load mass vs. $1/(2\pi\nu)^2$ of tip/cantilever assemblies using adsorbed W balls of varying size. The force constants are 0.07 and 0.12 N/m for native and Au-coated cantilevers, respectively.

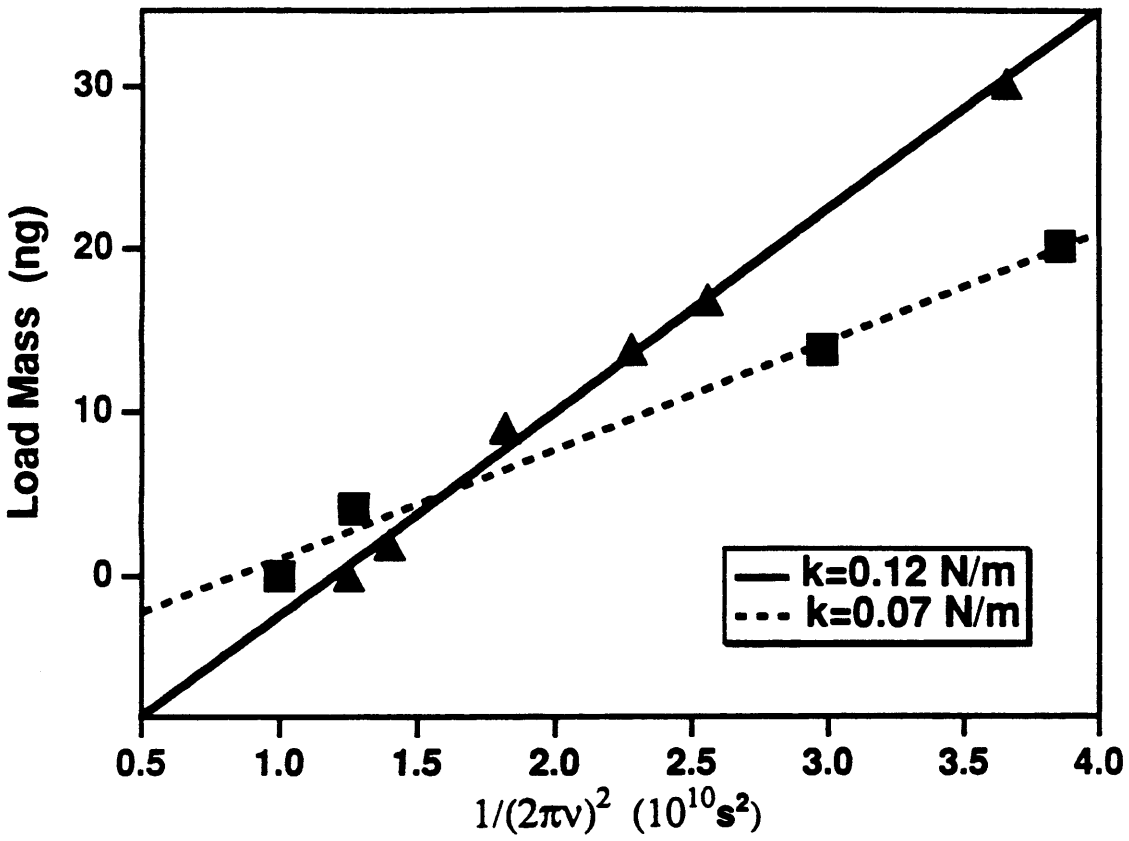
Load Mass (ng)
30
20
10
0
0.5
1.0
1.5
2.0
2.5
3.0
3.5
4.0
1/(2πν)² (10¹⁰s²)
k=0.12 N/m
k=0.07 N/m

thickness and elastic constants of Au,[31] we have used direct measurements of k in our studies to minimize this source of uncertainty. We also found that the variations in spring constant value for the cantilevers from the same wafer do not exceed 20%.[32]

Adhesive Measurements between Uncharged Functional Groups. The adhesive interaction between different functional groups was determined from force vs. cantilever displacement curves. In these measurements the deflection of the cantilever is recorded as the sample approaches, contacts, and is then withdrawn from the probe tip.[33] (See Chapter Four.) The observed cantilever deflection is converted into a force value using the cantilever spring constant. These measurements were carried out in solution rather than air to eliminate uncertainties arising from capillary forces.[34,35]

Representative force-displacement curves obtained in EtOH using Au-coated tips and samples that were functionalized with SAMs terminating in either CH_3 or COOH groups are shown in Figure 6.4. The hysteresis in the force displacement curves (approach vs. withdrawal) corresponds to the adhesion between functional groups on the tip and sample surface. The magnitude of the adhesive interactions between tip/sample functional groups decreases in the following order: COOH/COOH > CH_3/CH_3 > CH_3/COOH. This observed trend in adhesive force agrees with qualitative expectations that interaction between hydrogen bonding groups (COOH/COOH) will be greater than nonhydrogen bonding groups (CH_3/CH_3). The same trend was observed in our previous study for measurements made with blunt tips,[17] although the magnitudes of the adhesion forces were larger by a factor of ~3, owing to the increase in contact area.

To quantify the differences and uncertainties in the adhesive interactions between different functional groups, we have recorded multiple force curves (≥300) for each type of intermolecular interaction. These data are plotted as histograms—adhesive force vs. the number of times that this force is observed for the COOH/COOH, CH_3/CH_3, and CH_3/COOH interactions—and are shown in Figure 6.5. The mean value of the interaction and its experimental uncertainty were determined by fitting the histograms to Gaussian

Figure 6.4. Representative force versus displacement curves recorded for CH_3/COOH, CH_3/CH_3, and COOH/COOH tip/sample termini using sharp tips ($R \approx 60$nm.). All data were obtained in EtOH solution using the fluid cell.

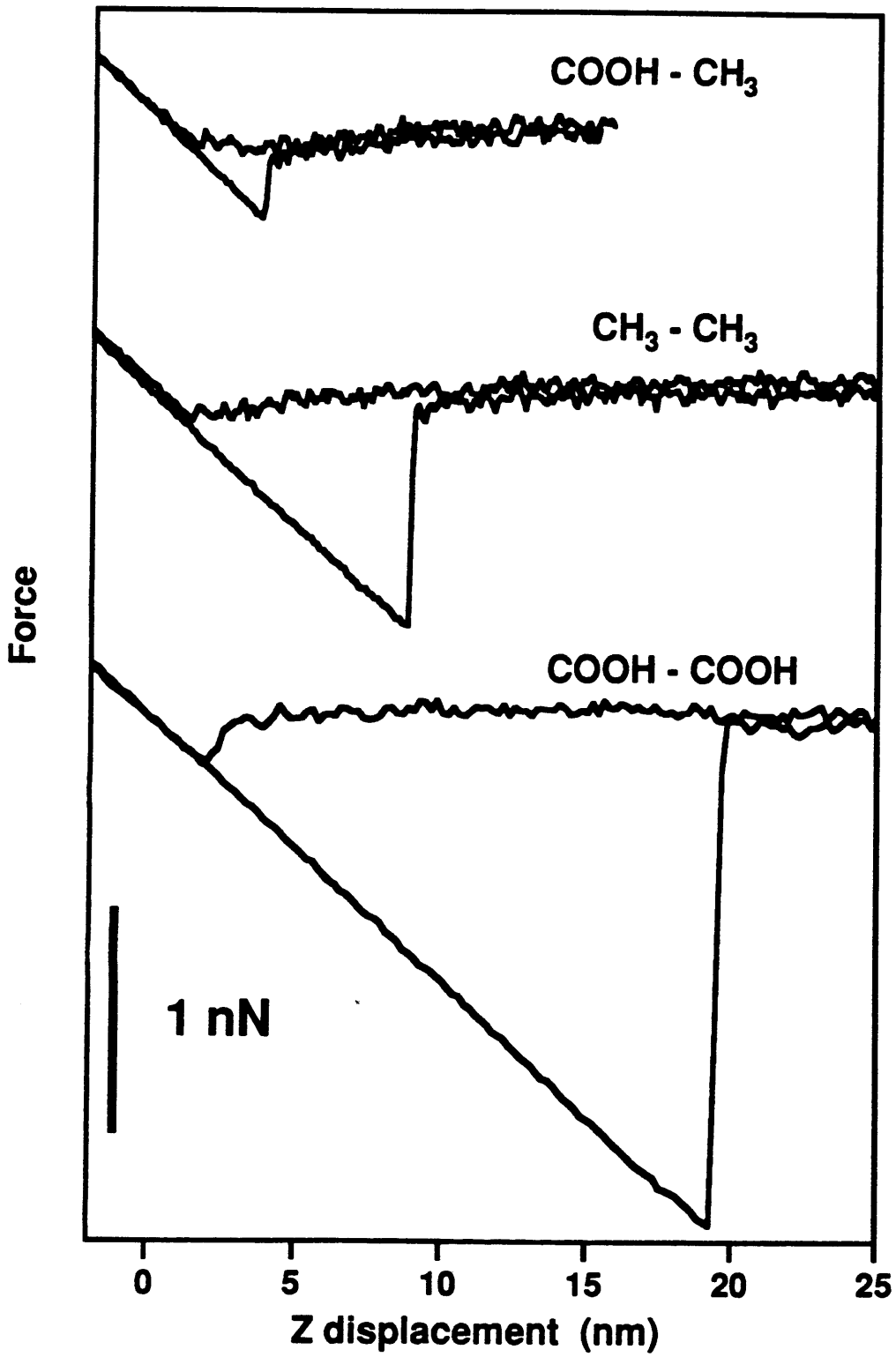
COOH - CH3
CH3 - CH3
COOH - COOH
1 nN
Force
0
5
10
15
20
25
Z displacement (nm)

Figure 6.5. Histograms showing the number of times that a given adhesion force was observed in repetitive measurements using functionalized samples and "sharp" tips (~60 nm radii) terminating in (a) COOH/COOH, (b) CH_3/CH_3, and (c) CH_3/COOH. Each histogram represents more than 300 repetitive tip-sample contacts for one functionalized tip. All measurements were made in EtOH solution.

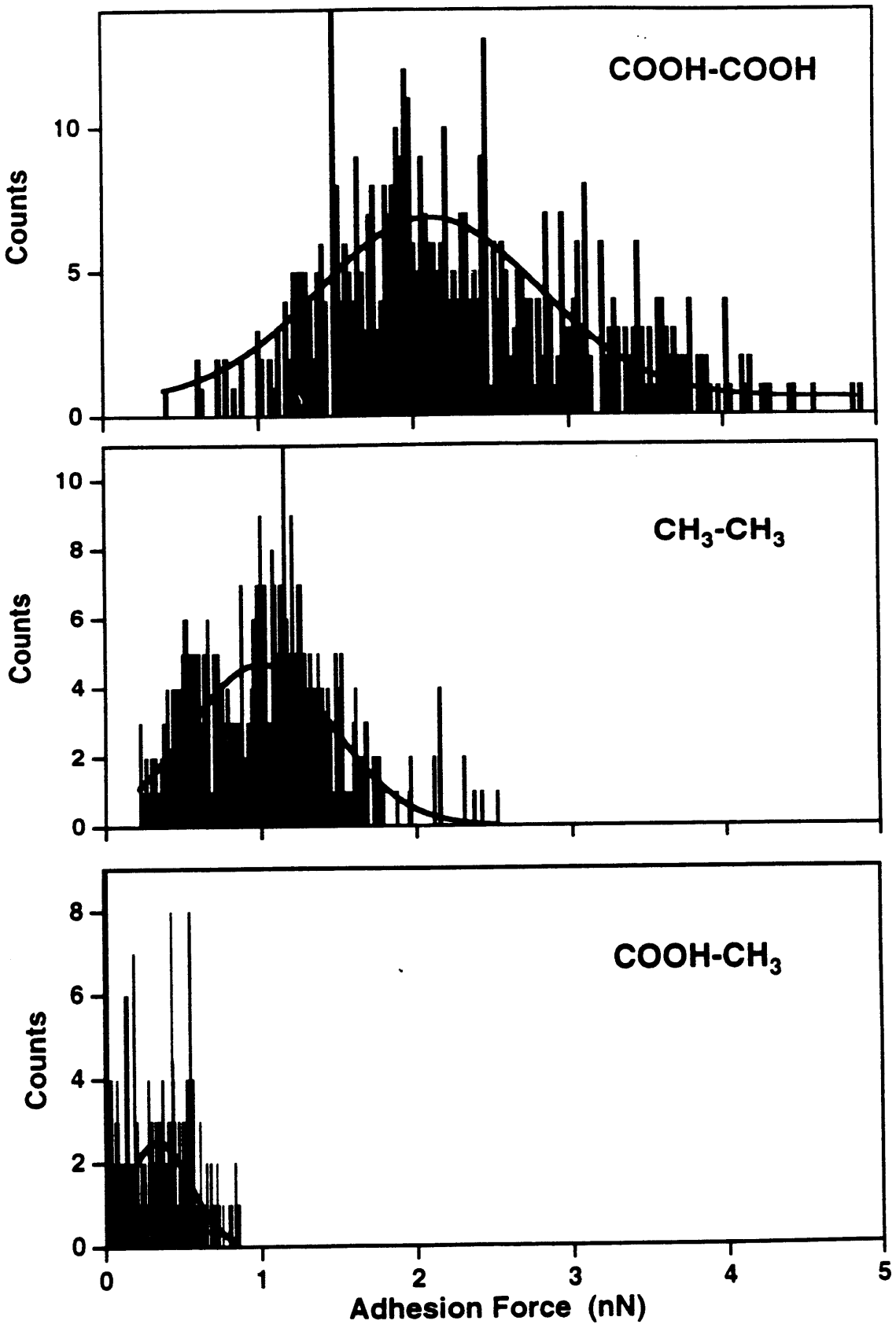
COOH-COOH
CH3-CH3
COOH-CH3
Counts
Counts
Counts
Adhesion Force (nN)
0
1
2
3
4
5
0
5
10
0
2
4
6
8
10
0
2
4
6
8

curves. This analysis yields mean adhesive forces ± 1σ uncertainties of 2.3 ± 0.8, 1.0 ± 0.4, and 0.3 ± 0.2 nN for the interactions between COOH/COOH, CH_3/CH_3, and CH_3/COOH groups, respectively.[36] Since the mean value for each type of interaction is outside the uncertainty range for the other interactions, these results show that we can reproducibly differentiate between chemically distinct functional groups by measuring the adhesion force.

In addition, these adhesion data can be used to assess the energetics of the different intermolecular interactions and the absolute number of functional groups that contribute to the experimentally observed forces. We have quantitatively addressed these two points using the JKR theory of adhesion mechanics.[1a,37] The JKR model predicts that the adhesion force, F_{ad}, or force required to separate a tip of radius R[38] from a planar surface at pull-off is given by

$$F_{ad} = \frac{3}{2}\pi R W_{st} \tag{6.1}$$

where W_{st} is the work of adhesion for separating the sample and tip. (We report F_{ad} as a positive value, however, since the tip is being pulled away from the sample, a negative force is actually being applied.) The work of adhesion, W_{st}, ("γ" in Chapters Four and Seven) can be estimated using the Young-Dupré equation[37]

$$W_{st} = \gamma_s + \gamma_t - \gamma_{st} \tag{6.2}$$

where γ_s and γ_t are the surface free energies of the sample and tip, and γ_{st} is the interfacial free energy of the two contacting surfaces. If we consider sample and tip combinations that have the same surface functional groups (CH_3/CH_3 and COOH/COOH), then $\gamma_{st} = 0$ and $\gamma_s = \gamma_t$, and it is possible to simplify eq 6.2 to $W_{st} = 2\gamma$, where γ in this case corresponds to the free energy of the surface in equilibrium with solvent. Hence, it is simply this surface free energy that should determine the adhesive force between tip and sample covered with the same functional groups.

We have checked the validity of this approach by estimating the expected value of F_{ad} for CH_3 terminated surfaces and tips. Previous measurements of the contact angle of EtOH

on CH_3-terminated SAMs yielded a value of $\gamma = 2.5$ mJ/m^2.[25c] The value of F_{ad} calculated using this value of γ and the radius of the tip, R, is 1.3 nN, in good agreement with the experimentally determined value of 1.0 nN for sharp tips (see Figure 6.5). Similar agreement was also found in calculations made using the radii of the blunt tips.[17] These results thus demonstrate that the continuum JKR approach provides a reasonable interpretation of our nanoscopic measurements.

Another interpretation of these data can yield important information about the free energies of surfaces. Since high free energy surfaces are readily wet by liquids, it is difficult to use contact angle measurements to extract γ_S. This disadvantage turns out to be an advantage in our measurements because high surface energies lead to larger adhesion forces. For example, in the case of COOH-terminated SAMs, which are completely wet by EtOH, we found $F_{ad} = 2.3$ nN for the sharp probe tips. The value of γ(COOH) in EtOH obtained using this force and the same tip radius as in the CH_3 calculation is 4.5 mJ/m^2. We believe that our value represents the most direct measure of this quantity to date. Furthermore, this approach can obviously be extended to other functional group pairs and different solvent systems. Such studies should provide of wealth of useful thermodynamic data.

We have also used the JKR model to estimate the number of molecular interactions contributing to the measured adhesive forces. The contact radius at pull-off, a_S, for surfaces terminating in the same functional groups is

$$a_S = \left[\frac{3\pi\gamma R^2}{K} \right]^{1/3} \tag{6.3}$$

where K is the elastic modulus of the tip and sample. The value of K can be reasonably approximated using the bulk value for gold, 64 GPa, assuming that SAMs do not change significantly the elastic behavior of the solids. For the CH_3/CH_3 interaction we calculate that $a_S = 1.0$ nm, and thus that the contact area is 3.1 nm^2. This corresponds to an interaction between only 15 molecules on the tip and sample.[39] Importantly, if the tip

radius could be reduced to ~10 nm, the contact area at pull-off would correspond to interaction between only single molecular pairs! Measurements in this molecular-scale regime could be especially interesting since they would provide truly microscopic data addressing solvated intermolecular interactions and could test for a breakdown of continuum theories such as JKR.

Friction Measurements and Imaging. Recently, we proposed that friction and adhesive forces between structurally similar SAMs should correlate directly with each other since microscopically both forces originate from the breaking of intermolecular interactions.[17] To test this hypothesis quantitatively, we have studied the friction force between functional groups on a sample surface and tip by recording the lateral deflection of the tip cantilever while the sample was scanned back and forth along the x-direction. The resulting curve is called a friction loop (Figure 6.6).[40] The values of the lateral force plotted in these loops were determined from the lateral spring constant of the cantilever and lateral sensitivity of the optical detector in our force microscope.[29,41] The friction force corresponds to one half of the difference between upper and lower lateral forces plotted in the loop.

Friction loops were recorded and analyzed as a function of the applied load and the functional groups terminating the surface and tip SAMs. Data recorded with sharp tips are summarized in Figure 6.7. We found that the friction force increases linearly with the applied load for each combination of chemically modified tip and surface, and that for a fixed applied load the friction force decreases as follows: COOH/COOH > CH_3/CH_3 > $COOH/CH_3$. The same trend was observed for data recorded with blunt tips, although again, the magnitude of the friction values were larger due to the greater contact areas.[42] The coefficients of friction, μ, which were determined from the slopes of friction vs. load plots, are 2.5, 0.8 and 0.4 for COOH/COOH, CH_3/CH_3, and $COOH/CH_3$ interactions, respectively. Notably, the trend in the magnitudes of the friction forces and coefficients is the same as that observed for the adhesion forces (see Figure 6.5): COOH/COOH

Figure 6.6. A typical friction loop recorded on a COOH-terminated sample using COOH-modified probe tip in EtOH solution. The applied load was 17 nN.

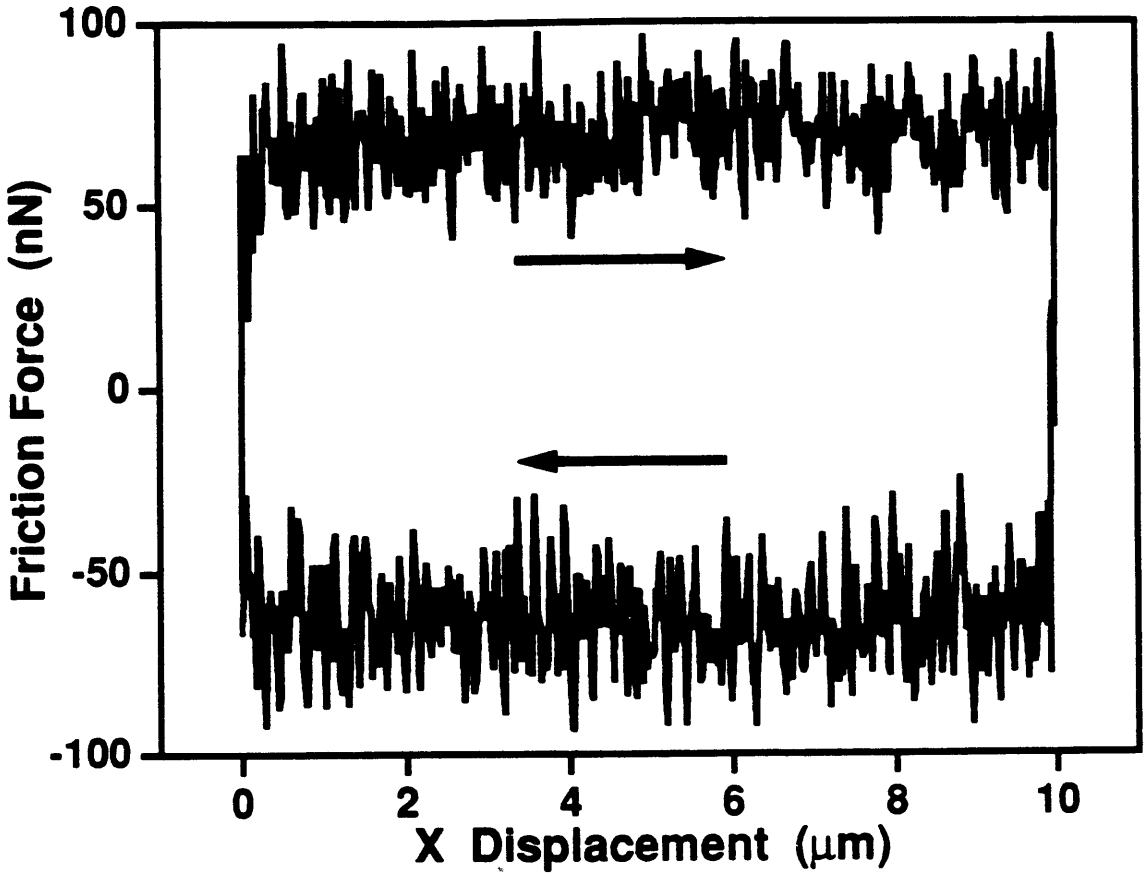
100
50
0
-50
-100
Friction Force (nN)
0
2
4
6
8
10
X Displacement (μm)

Figure 6.7. Summary of the friction force vs. applied load data recorded for functionalized samples and tips terminating in COOH/COOH, CH_3/CH_3 and $COOH/CH_3$ in EtOH.

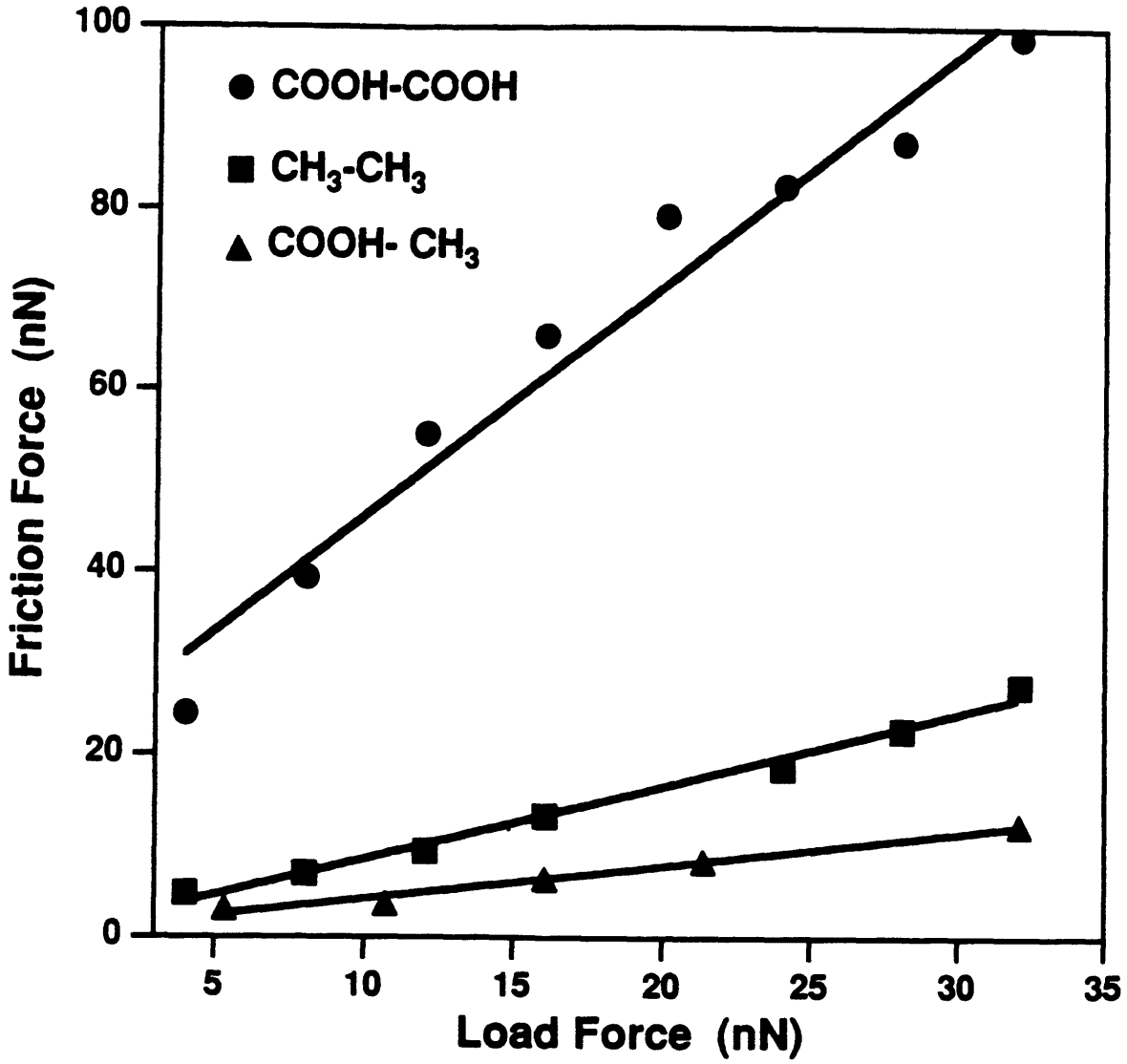
COOH-COOH
CH3-CH3
COOH- CH3
Friction Force (nN)
Load Force (nN)
0
20
40
60
80
100
5
10
15
20
25
30
35

terminated tips/samples yield large friction and adhesion forces, while COOH/CH_3 functionalities yield the lowest friction and the smallest adhesion.

These new results confirm our earlier suggestion[17] that the friction and adhesion forces between structurally similar but chemically distinct SAMs correlate directly with each other. In contrast, SFA studies of different hydrocarbon surfactants found that the friction force correlated with adhesion hysteresis and not the adhesion force.[2b,43] These studies focused on structurally dissimilar phases (i.e., crystalline, amorphous and liquid-like), and thus differ from the present studies in which the structurally similar (nearly crystalline[44]) SAMs were probed. More recent SFA studies of structurally similar layers show, however, that friction force correlates with the force of adhesion.[45] In addition, independent force microscopy studies[20] have recently observed results similar to our investigations. Hence, we believe that this is a manifestation of a general relationship between adhesion and friction on a microscopic scale.[46]

The differences in friction shown in Figure 6.7 can be used to produce lateral force images of patterned surfaces with predictable contrast. Using the photochemical patterning method described above, we have produced SAMs having 10 μm x 10 μm square regions that terminate with COOH groups and repeat every 30 μm in a square pattern; the regions of the SAM surrounding these hydrophilic squares terminate with hydrophobic CH_3 groups (Figure 6.8). Figure 6.9 shows topography and lateral force images of the patterned SAMs recorded using tips modified with SAMs terminating in either COOH or CH_3 groups. The surface exhibits a flat topography across the CH_3 and COOH terminated regions of the sample (Figure 6.9A). Though several small adventitious particles are detected on the sample surface, no chemical information is revealed. Figures 6.9B and 6.9C show a friction maps of the same area as in Figure 6.9A, and in these figures chemical information about the surface is readily apparent. Friction maps recorded with the COOH terminated tips (Figure 6.9B) exhibit high friction (light shades) in the square area of the sample that contains the COOH terminated SAM and low friction in the CH_3

terminated regions. Images recorded with CH_3 terminated tips (Figure 6.9C) exhibit a reversal in the friction contrast: low friction (dark shades) in the square area of the sample that contains the COOH terminated SAM and higher friction over the surrounding CH_3 terminated regions. Note that the contrast in Figure 6.9B is greater than that in Figure 6.9C. This difference in friction contrast is consistent with the friction vs. load curves obtained on homogenous SAM samples (see Figure 6.7). Namely, at a given applied load the difference in friction between the two surface functionalities and a COOH tip is always greater than the difference between the two groups and a CH_3-terminated tip.

The reversal in image (friction) contrast occurs only with changes in the probe tip functionality, and thus we can conclude that we are imaging with sensitivity to chemical functional groups. For this reason we have previously called this approach to imaging—imaging with chemically functionalized tips—chemical force microscopy.[17] Predictable image contrast using chemically derivatized tips has also been observed in a recent independent study,[20] and thus we believe this approach is viable and may serve as a method for mapping more complex and chemically heterogeneous surfaces. Other researchers have previously used differences in friction forces to map different domains of phase segregated Langmuir-Blodgett films,[15] however, contrast in these images is believed to arise predominantly from differences in the elastic properties of the domains and not the chemical functionality at the film surface.[15b]

The friction force on these patterned SAMs has also been determined in air. We find that "acid-tip contrast" (i.e., high friction in the hydrophilic regions of the surface) is always observed in air regardless of whether the tip is bare Si_3N_4, coated with Au, or derivatized with COOH or CH_3 functional groups. Similar images of patterned SAMs using unmodified Si_3N_4 tips have been reported by Whitesides and coworkers.[47] The mechanism of contrast in these images is not unambiguously determined, but is likely due to differences in capillary forces in the hydrophilic and hydrophobic portions of the surface. Capillary forces are typically 10 times stronger than the adhesion forces that were

Figure 6.8. Condensation image of H_2O on a photopatterned SAM substrate showing the repeat pattern of 10 x 10 μm^2 squares terminating in COOH on a background terminating in CH_3. H_2O condenses only on the hydrophilic COOH-terminated regions of the sample.

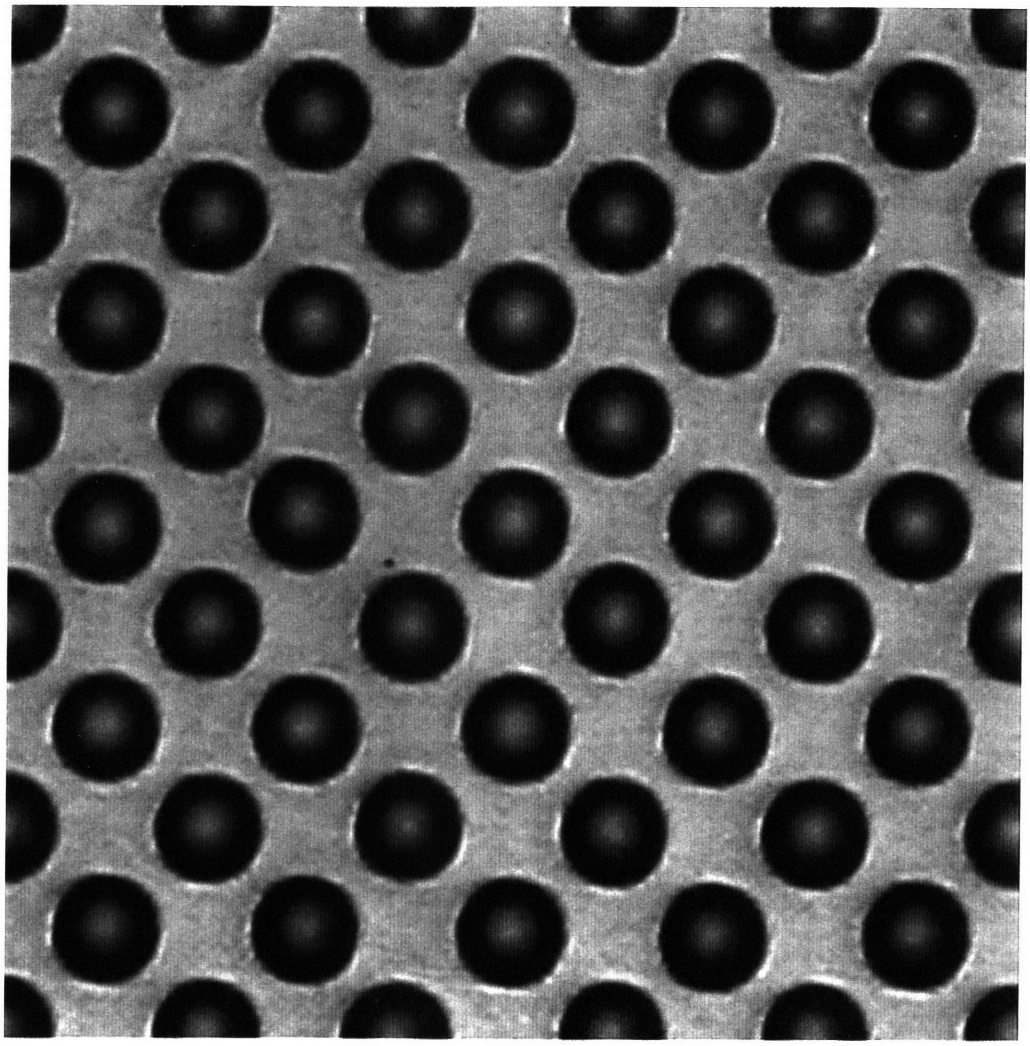

30 μm

Figure 6.9. Force microscopy images on one square of a photopatterned sample identical to that shown in Figure 6.8 of (A) topography, (B) friction force using a tip modified with a COOH-terminated SAM, and (C) friction force using a tip modified with a CH_3-terminated SAM. The apparent stretch in vertical direction observed in image (C) is due to the strain of the O-ring in the fluid cell during imaging.

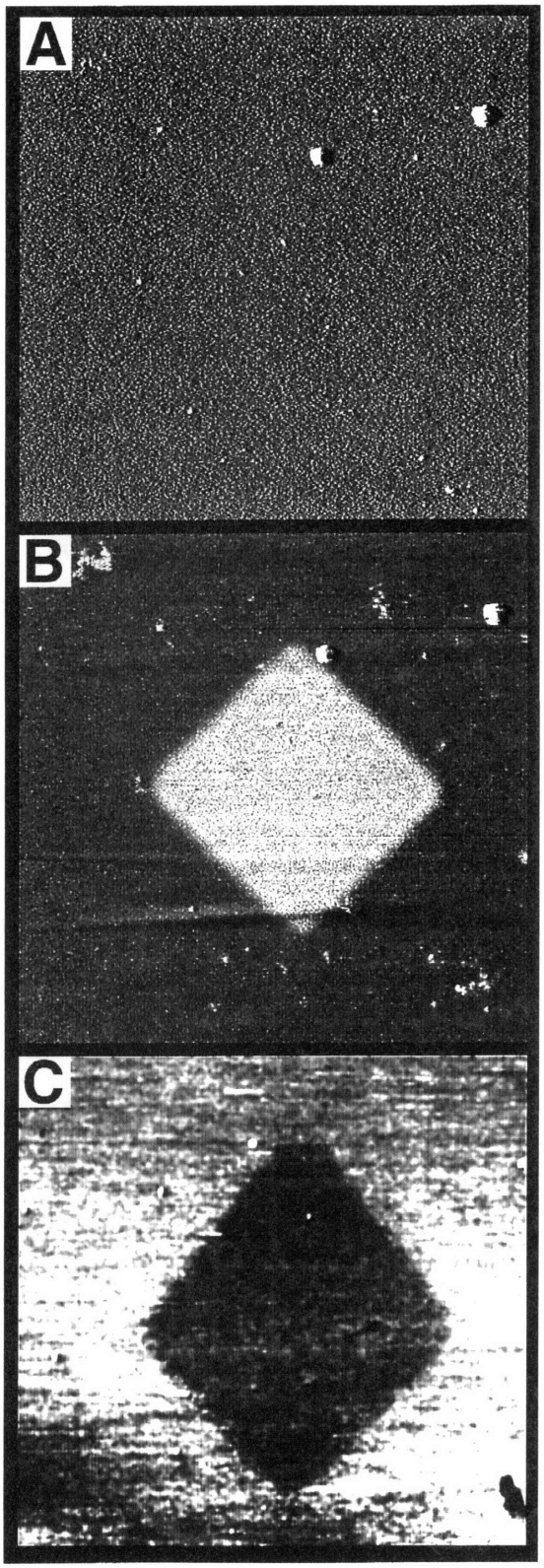
A
B
C
10 μm

measured in EtOH,[35] and thus overwhelm small differences in the intermolecular interactions in air.[48] Force microscopy studies in solution not only eliminate this problem, but are most relevant to structure and function determination of chemical, biological, and materials systems. We present our approach as one fruitful towards these applications.

Electrostatic Interactions. Finally, we present initial results in measuring adhesive interactions between oppositely charged monovalent functional groups. The electrostatic contribution to the attractive and repulsive forces between charged surfaces has been studied previously using the SFA and force microscopy.[2,24,49] These studies have probed the long-range coulombic interactions that occur between two charged surfaces as they approach one another. In the present study, we were concerned with the role that electrostatic interactions play as two surfaces just separate (i.e., the contribution to adhesion), rather than the effects at long distances.

To study this electrostatic interaction we utilized monolayers of 11-mercaptoundecanoic acid on the probe tip and 3-aminopropyltriethoxysilane on a Si substrate. Simple amines and carboxylic acids are well known to form zwitterionic pairs under neutral conditions. The pK_a's of acidic and basic groups on SAM surfaces, however, are shifted by approximately 2 pH units higher and lower, respectively.[50] These acidic and basic groups still should form zwitterionic pairs in solution. Histograms of adhesion force values recorded in deionized H_2O (18 MΩ·cm) at pH = 6 and a 0.3 M aqueous NaCl solution (also at pH = 6) are shown in Figure 6.10. The mean adhesive force between these oppositely charged groups is 14 nN in H_2O, but decreases to 4.5 nN in 0.3 M NaCl. This salt concentration reduces the characteristic length scale (the Debye length, λ_D) for the electrostatic interaction to only 5.5 Å ($\lambda_D \approx 1$ μm in deionized H_2O[1a]). Along with the significant drop in the length scale of the interaction we found that the adhesive force drops by a factor of three to 4.5 nN. The strong decrease in the measured force with increasing ionic strength suggests that in pure H_2O a significant component of the total force arises from charge-charge interactions between groups outside of the area of physical contact

Figure 6.10. Histograms of force vs. displacement curves recorded between functionalized samples terminating in COO^- groups and tips terminating in NH_3^+ in (upper histogram) deionized H_2O (18 MΩ·cm, pH = 6.5) and (lower histogram) 0.3 M NaCl aqueous solution (pH = 6.5).

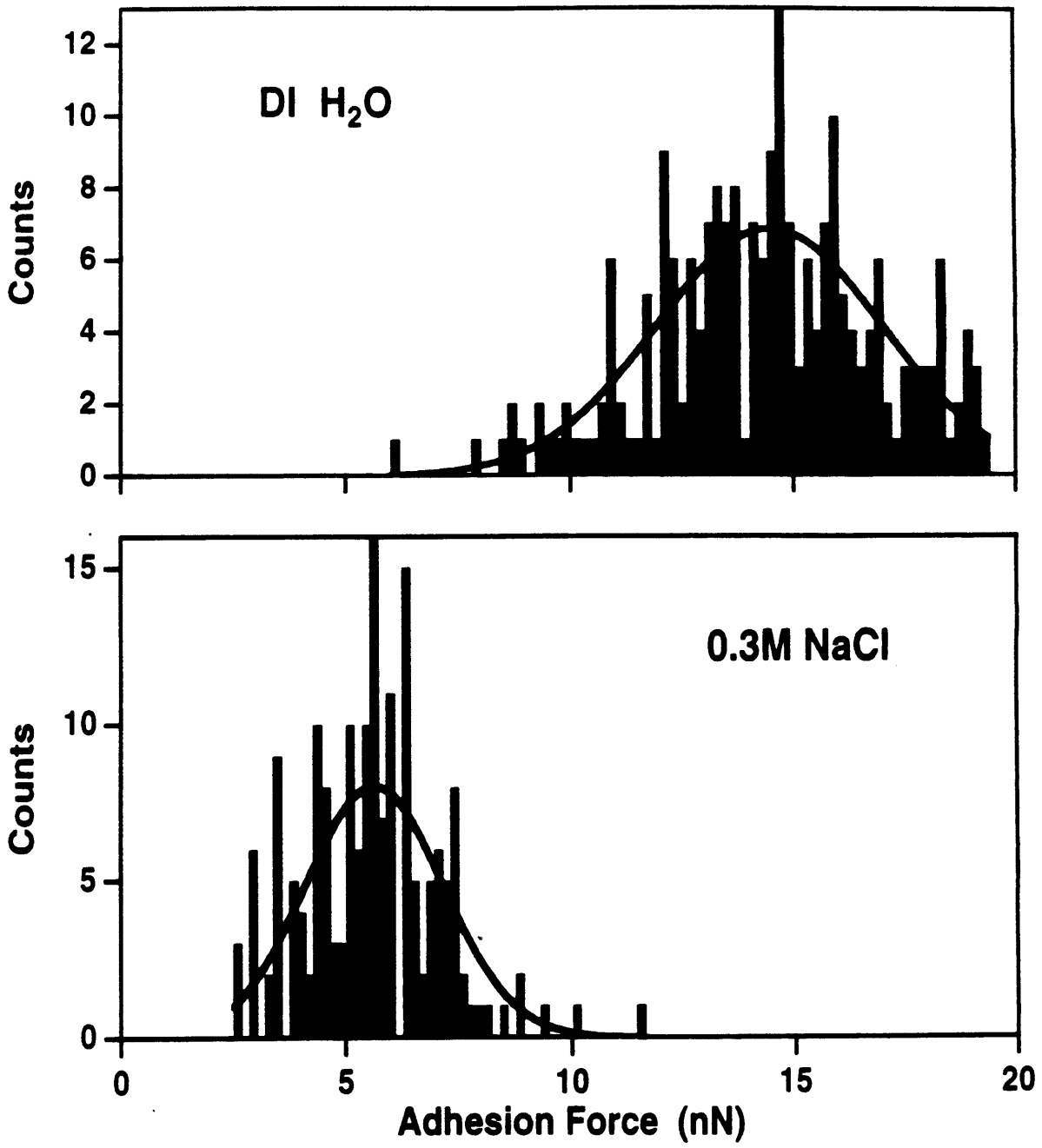
DI H_2O
Counts
12
10
8
6
4
2
0
0.3M NaCl
Counts
15
10
5
0
0
5
10
15
20
Adhesion Force (nN)

between the tip and sample.[51] Also, the adhesive interactions in H_2O are a factor of 5 to 10 stronger than those measured in EtOH. It is evident from these measurements that future studies and comparisons of adhesive interactions between charged and uncharged functional groups, from simple functionalities to, for example, more complex charge transfer systems, will necessitate studies of solvent and ionic strength to investigate the various contributions to adhesion and friction.

Conclusions

We have shown that molecules may be attached to Au-coated force microscope probe tips using the well established affinity of thiols for Au, and that the chemically modified tips produced by this method may be used to quantitatively measure adhesion and friction forces between the functional groups terminating the SAMs on the tip and sample. Adhesion studies between SAMs which terminate in COOH and CH_3 functional groups have shown that the interaction strength between these groups follows a trend: COOH/COOH > CH_3/CH_3 > COOH/CH_3. These adhesion forces agree well with forces predicted by the JKR theory of adhesive contact. Using this model we were also able to show that the contact area between sharp (~60 nm radii) tips and the sample corresponds to an interaction between only 15 molecular pairs, and that by reducing the tip radii to ~10 nm it may be possible to measure the interactions between single molecular pairs. Our analyses of these data also show how it should be possible using CFM to determine surface free energies for organic surface/liquid interfaces that are unobtainable by contact angle measurements.

In addition, the friction force between tips and samples modified with COOH and CH_3 groups has also been measured as a function of applied load. The magnitude of the friction force was found to be COOH/COOH > CH_3/CH_3 > COOH/CH_3, thus demonstrating that friction forces between different chemical functional groups correlate directly with adhesion forces between the same groups. The predictable dependence of friction forces on the tip and sample functionalities is the basis for chemical force microscopy, where lateral force images are interpreted in terms of the strength of adhesive interactions between functional groups.

We believe that these studies open up significant areas of research for the future. For example, (1) a host of different types of molecular interactions can be studied since the modification of probe tips with SAMs provides a general way to introduce chemical functionality onto probe tips; (2) basic thermodynamic information that will be relevant to

chemists and biologists can be extracted from the analysis of CFM data obtained in different solvent media; (3) CFM imaging of other systems such as polymers and biomolecules could lead to new insights into the spatial distribution of functional groups and/or hydrophobic vs. hydrophilic domains.

Appendix

Calculation of the Lateral Spring Constant for a V-shaped Cantilever. A V-shaped cantilever can be approximated by two identical rectangular beams made of a material with Young's modulus E, shear modulus G, and Poisson ratio ν. If the total torque applied to the cantilever is T, then the torque applied to one of the beams is T/2. Also, the strain energy stored in one beam is equal to one half of the total strain energy, S.E.

Scheme 6A.1. Cantilever/tip geometry showing components of torque.

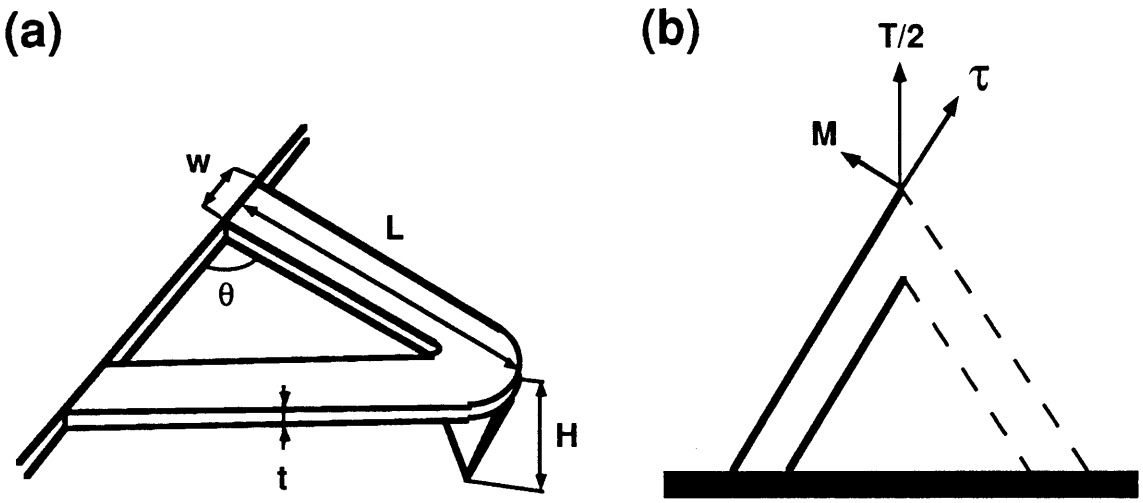

The beam length width and height are denoted respectively as L, w and h. The angle between cantilever beam and the substrate is θ (Scheme 6A.1a). Let M and τ be the bending and twisting components of torque (Scheme 6A.1b). The strain energy stored in one beam is:

$$\frac{1}{2}\text{S.E.} = \int_0^L \frac{M^2}{2EI}dx + \frac{\tau^2 L}{2GJ} = \frac{M^2 L}{2EI} + \frac{\tau^2 L}{2GJ} = \frac{\frac{T^2}{4}L\cos^2\theta}{2E\left(\frac{1}{12}wh^3\right)} + \frac{\frac{T^2}{4}L\sin^2\theta}{2\left[\frac{E}{2(1+\nu)}\right]J}; \quad (6A.1)$$

where I and J are the moments of inertia for a rectangular beam. For the case when w >> h, expressions for J and I are as follows:[31]

$$I = \frac{wh^3}{12}$$
$$J = \frac{wh^3}{16}\left(\frac{16}{3} - 3.36\frac{h}{w}\right) \approx \frac{wh^3}{3}; \tag{6A.2}$$

Therefore, the total strain energy is:

$$S.E. = 2 \times \left[\frac{1}{2}\frac{T^2}{4}L\left(\frac{\cos^2\theta}{\frac{1}{12}wh^3E} + \frac{\sin^2\theta}{\frac{1}{3}wh^3G}\right)\right] = \frac{T^2L}{2Ewh^3}\left[6\cos^2\theta + 3(1+\nu)\sin^2\theta\right] \tag{6A.3}$$

The torsional spring constant k_t can be obtained as a reciprocal of the second derivative of the total strain energy with respect to T:

$$k_t^{-1} = \frac{\partial^2(S.E.)}{\partial T^2} \tag{6A.4}$$

Therefore

$$k_t = \frac{Ewh^3}{L}\left[\frac{1}{6\cos^2\theta + 3(1+\nu)\sin^2\theta}\right] \tag{6A.5}$$

The values of h and E are not well known and may vary significantly due to poor reproducibility of the materials growth process. Therefore, we have related the value of k_t to the experimentally determined normal spring constant, k_n. For a V-shaped tip, k_n can be approximated as a sum of normal spring constants for two rectangular beams:[31]

$$k_n = 2 \times \frac{3EI}{L^3} = \frac{Ewh^3}{2L^3} \tag{6A.6}$$

Then the ratio for the torsional spring constant to normal spring constant is

$$\frac{k_t}{k_n} = \frac{\frac{Ewh^3}{L}\left[\frac{1}{6\cos^2\theta + 3(1+\nu)\sin^2\theta}\right]}{\frac{Ewh^3}{2L^3}} = \frac{2L^2}{\left[6\cos^2\theta + 3(1+\nu)\sin^2\theta\right]} \tag{6A.7}$$

The torsional spring constant can be converted to the lateral spring constant k_{lat} (related to lateral displacement) according to the following formula:

$$k_{lat} = \frac{k_t}{H^2} \tag{6A.8}$$

where H is the tip vertical height. Therefore, the final formula for the lateral spring constant of a V-shaped cantilever-tip assembly is

$$k_{lat} = \frac{2}{\left[6\cos^2\theta + 3(1+\nu)\sin^2\theta\right]}\left(\frac{L}{H}\right)^2 \times k_n \tag{6A.9}$$

The only elastic parameter that this formula contains is the relatively well-known Poisson ratio for silicon nitride.[41] All other parameters can be determined directly by measurement.

References

1. (a) Israelachvili, J. *Intermolecular & Surface Forces*; Academic: San Diego, 1992. (b) Ulman, A. *Introduction to Ultrathin Organic Films*; Academic: San Diego, 1991. (c) Fersht, A. *Enzyme Structure and Mechanics*; W.H. Freeman: New York, 1985.
2. (a) Israelachvili, J. *Acc. Chem. Res.* **1987**, *20*, 415. (b) Yoshizawa, H.; Chen,Y.-L.; Israelachvili, J. *J. Phys. Chem.* **1993**, *97*, 4128. (c) Chen, Y.-L.; Helm, C. A.; Israelachvili, J. *J. Phys. Chem.* **1991**, *95*, 10736. (d) Israelachvili, J. *J. Vac. Sci. Technol. A* **1992**, *10*, 2961.
3. (a) Ashkin, A.; Dziedzic, J. M.; Bjorkholm, J. E.; Chu, S. *Optics Lett.* **1986**, *11*, 288. (b) Kuo, S. C.; Sheetz, M. P. *Science* **1993**, *260*, 232. (c) Svoboda, K.; Schmidt, C. F.; Schnapp, B. J.; Block, S. M. *Nature* **1993**, *365*, 721. (d) Perkins, T.; Smith, D.E.; Chu, S. *Science* **1994**, *264*, 819. (e) Finer, J. T.; Simmons, R. M.; Spudich, J. A. *Nature* **1994**, *386*, 113.
4. Quate, C. F. *Surf. Sci.* **1994**, *299/300*, 980.
5. Hues, S. M.; Colton, R. J.; Meyer, E.; Güntherodt, H.-J. *MRS Bulletin* **1993**, *18*, 41.
6. Mate, C. M.; McClelland, G. M.; Erlandsson, R.; Chiang, S. *Phys. Rev. Lett.* **1987**, *59*, 1942.
7. Burnham, N. A.; Colton, R. J. *J. Vac. Sci. Technol. A* **1989**, *7*, 2906.
8. (a) Marti, O.; Ribi, H. O.; Drake, B.; Albrecht, T. R.; Quate, C. F.; Hansma, P. K. *Science* **1988**, *239*, 50. (b) Frommer, J. *Angew. Chem. Int. Ed. Engl.* **1992**, *31*, 1298.
9. Rugar, D.; Hansma, P. K. *Phys. Today* **1990**, *43*, 23.
10. (a) Ducker, W. A.; Senden, T. J.; Pashley, R. M. *Nature* **1991** *353*, 239. (b) Ducker, W. A.; Senden, T. J. *Langmuir* **1992**, *8*, 1831. (c) Biggs, S.; Mulvaney, P. *J. Chem. Phys.* **1994**, *100*, 8501.

11. (a) Blackman, G. S.; Mate, C.M.; Philpott, M. R. *Phys. Rev. Lett.* **1990**, *65*, 2270. (b) Joyce, S. A.; Thomas, R. C.; Houston, J. E.; Michalske, T. A.; Crooks, R. M. *Phys. Rev. Lett.* **1992**, *68*, 2790. (c) Burnham, N. A.; Dominguez, D. D.; Mowery, R. L.; Colton, R. J. *Phys. Rev. Lett.* **1990**, *64*, 1931.

12. (a) Haugstad, G.; Gladfelter, W. L.; Weberg, E. B.; Weberg, R. T.; Weatherill, T. D. *Langmuir* **1994**, *10*, 4295. (b) Radmacher, M.; Fritz, M.; Cleveland, J. P.; Walters, D. A.; Hansma, P. K. *Langmuir* **1994**, *10*, 3809.

13. Radmacher, M.; Fritz, M.; Hansma, H. G.; Hansma, P. K. *Science* **1994**, *265*, 1577.

14. Cai, H.; Hillier, A.; Franklin, K. R.; Nunn, C. C.; Ward, M. D. *Science* **1994**, *266*, 1551.

15. (a) Overney, R. M.; Meyer, E.; Frommer, J.; Brodbeck, D.; Luthi, R.; Howald, L.; Guntherodt, H.-J.; Fujihira, M.; Takano, H.; Gotoh, Y. *Nature* **1992**, *395*, 133. (b) Overney, R. M.; Meyer, E.; Frommer, J.; Guntherodt, H.-J.; Fujihira, M.; Takano, H.; Gotoh, Y. *Langmuir* **1994**, *10*, 1281.

16. (a) Hoh, J. H.; Cleveland, J. P.; Prater, C. B.; Revel, J. P.; Hansma, P. K. *J. Am. Chem. Soc.* **1992**, *114*, 4917. (b) Weisenhorn, A. L.; Maivald, P.; Butt, H.-J.; Hansma, P. K. *Phys. Rev. B.* **1992**, *45*, 11226.

17. Frisbie, C. D.; Rozsnyai, L. F.; Noy, A.; Wrighton, M. S.; Lieber, C. M. *Science* **1994**, *265*, 2071.

18. Lee, G. U.; Chrisey, L. A.; Colton, R. J. *Science* **1994**, *266*, 771.

19. Nakagawa, T.; Ogawa, K.; Kurumizawa, T.; Ozaki, S. *Jpn. J. Appl. Phys.* **1993**, *32*, L294.

20. Green, J.-B. D.; McDermott, M. T.; Porter, M. D.; Siperko, L. M. manusctipt in preparation.

21. Thomas, R. C.; Tangyunyong, P.; Houston, J. E.; Michalske, T. A.; Crooks, R. M. *J. Phys. Chem.* **1994**, *98*, 4493.

22. Lee, G. U.; Kidwell, D. A.; Colton, R. J. *Langmuir* **1994**, *10*, 354.

23. (a) Florin, E. L.; Moy, V. T.; Gaub, H. E. *Science* **1994**, *264*, 415. (b) Moy, V. T.; Florin, E. L.; Gaub, H. E. *Science* **1994**, *266*, 257.

24. Tsao, Y.-H.; Evans, D. F.; Wennerström, H. *Science* **1993**, *262*, 547.

25. (a) Nuzzo, R. G.; Allara, D. L.; *J. Am. Chem. Soc.* **1983**, *105*, 4481. (b) Porter, M. D.; Bright, T. B.; Allara, D. L.; Chidsey, C. E. D. *J. Am. Chem. Soc.* **1987**, *109*, 3559. (c) Bain, C. D.; Troughton, E. B.; Tao, Y.-T.; Evall, J.; Whitesides, G. M.; Nuzzo, R. G. *J. Am. Chem. Soc.* **1989**, *111*, 321. (d) Whitesides, G. M.; Laibinis, P. E. *Langmuir* **1990**, *6*, 87. (e) Dubois, L. H.; Nuzzo, R. G. *Annu. Rev. Phys. Chem.* **1992**, *43*, 437. (f) Bain, C. D.; Evall, J.; Whitesides, G. M. *J. Am. Chem. Soc.* **1989**, *111*, 7155. (g) Delamarche, E.; Michel, B.; Kang, H.; Gerber, Ch. *Langmuir* **1994**, *10*, 4103.

26. Kossel, A. *Hoppe-Seyler's Z. Physiol. Chem.* **1912**, 303.

27. (a) Wollman, E. W.; Kang, D.; Frisbie, C. D.; Lorkovic, I. M.; Wrighton, M. S. *J. Am. Chem. Soc.* **1994**, *116*, 4395. (b) Rozsnyai, L. F.; Wrighton, M. S. *J. Am. Chem. Soc.* **1994**, *116*, 5993. (c) Lawrence F. Rozsnyai and Mark S. Wrighton *Langmuir*, in press.

28. Gassman, P. G.; Schenk, W. N. *J. Org. Chem.* **1977**, *42*, 918.

29. Cleveland, J. P.; Manne, S.; Bocek, D.; Hansma, P. K. *Rev. Sci. Instr.* **1993**, *64*, 403.

30. The variations in tip radius of curvature arise from nonuniform microfabrication steps used to produce the Si_3N_4 catilever-tip assemblies.

31. Liu, Y.; Wu, T.; Evans, D.F. *Langmuir* **1994**, *10*, 2241.

32. The error of ±20% does not exceed the accuracy of the resonance-endmass calibration method. (Cleveland, J. P., personal communication, 1994).

33. Burnham, N. A.; Colton, R. J.; Pollock, H. M. *J. Vac. Sci. Technol. A* **1991**, *9*, 2548.

34. Under ambient conditions the SAM surfaces are covered with thin films of adsorbed H_2O and contaminants. These species give rise to relatively large capillary forces that can obscure weak intermolecular interactions (see reference 35). The contribution of capillary forces to measured data can be eliminated by carrying out experiments in ultrahigh vacuum or fluid solution.

35. Grigg, D. A.; Russel, P. E.; Griffith, J. E. *J. Vac. Sci. Tech. A.* **1992**, *10*, 680.

36. The Gaussian fits are believed to provide a good means for estimating the uncertainty in these experiments but may not represent the best model for fitting this type of data. For example, a Gaussian fit assumes a symmetric distribution of force between $\pm\infty$, while in reality all forces are >0.

37. Johnson, K. L.; Kendall, K.; Roberts, A. D. *Proc. R. Soc. London, A.* **1971**, *324*, 301.

38. The radius of the tip (R_t) determined from the analysis of electron microscopy images is 60 nm. The value of R used in eq 6.1 is, however, reduced by the effective curvature of the gold islands that make up the sample surface (R_S). We have measured R_S to be approximately 500 nm by contact AFM.

$$R = \frac{R_t R_s}{R_t + R_s} = 54 \text{ nm.}$$

39. The area per functional group of close-packed self-assembled monolayers of thiols on Au is 0.2 nm^2.[1b]

40. Overney, R. M.; Takano, H.; Fujihira, M.; Paulus, W.; Ringsdorf, H. *Phys. Rev. Lett.* **1994**, *72*, 3546.

41. The lateral spring constant, k_{lat}, for a triangular cantilever is $k_{lat} = \frac{2}{6\cos^2\theta + 3(1+\nu)\sin^2\theta}\left(\frac{L}{H}\right)^2 k_n$ where θ is the angle between the base arms of the triangular cantilever, ν is the Poisson ratio for Si_3N_4, L is the length of the cantilever beam, H is the length of the tip, and k_n is the normal spring constant. (For

the derivation of this formula, see the Appendix.) Substituting the measured values of k_n, L, H and θ, and the literature value of ν (*CRC Handbook of Materials Science,v.II*, Lynch, C.T., Ed.; CRC Press: Boca Raton, 1975, p 382) yields k_{lat} = 225. This value is similar to that reported in previous studies.[10]

42. The contact radius, a, for an applied load of F is given by $a^3 = \frac{R}{K}\left[F + 3\pi RW_{12} + \left(6\pi RW_{12}F + \left(3\pi RW_{12}\right)^2\right)^{1/2}\right]$ where R is the tip radius. Hence, as the tip radius increases, the contact area and number of intermolecular interactions increases for a given applied load.

43. Chaudhury, M. K.; Owen, M. J. *Langmuir* **1993**, *9*, 29.

44. Adhesion and friction force measurements were made with samples composed of homogeneous long-chain alkylthiols (see Experimental Section) which have a nearly crystalline structure (see reference 25). In the case of functional group imaging, SAMs terminating in a relatively bulky phenylazide group were used, and the desired terminal groups were subsequently attached photochemically. Though the same trend in friction is observed in these SAMs as with the simpler homogeneous monolayers, the same arguement for crystalline structure cannot be made.

45. Yoshizawa, H.; Israelachvili, J. *Thin Solid Films* **1994**, *246*, 71.

46. It is important to recognize, however, several caveats that must be considered in making comparisons of friction data obtained with functionalized surfaces and tips. First, similar radii tip must be used since the friction force depends on contact area (see reference 42). Secondly, the surface solvation must be controlled since the capillary force can dominate other contributions. In this regard, we believe that imaging in solution or ultrahigh vacuum represents the only unambiguous control of the surface solvation; an uncontrolled layer of adsorbates such as H_2O will be present on a surface even in a "dry" and inert atmosphere.

47. Wilbur, J. L.; Biebuyck, H. A.; MacDonald, J.C.; Whitesides, G.M. *Langmuir*, in press.

48. Binggeli, M.; Mate, C.M *Appl. Phys. Lett.* **1994**, *65*, 415.

49. Butt, H.-J. *Biophys. J.* **1991**, *60*, 1438.

50. Lee, T. R.; Carey, R. I.; Biebuyck, H. A.; Whitesides, G. M. *Langmuir* **1994**, *10*, 741.

51. (a) Derjaguin, B.V.; Muller,V.M.; Toporov, Yu.P. *J. Coll. Interfac. Sci.* **1975**, *53*, 314. (b) Maugis, D. *J. Coll. Interfac. Sci.*, **1992**,*150*, 243.

CHAPTER SEVEN

CHEMICAL FORCE MICROSCOPY: MEASURING ADHESION, FRICTION, AND FUNCTIONAL GROUP DISTRIBUTIONS IN AQUEOUS MEDIA

Introduction

The development of scanning probe microscopy, and atomic force microscopy (AFM) in particular, has advanced our understanding of surface science and tribology, and has allowed forces to be measured quantitatively on the molecular and atomic scale. We have recently introduced an advance in AFM that chemically specifies the type of interaction between the tip and sample. Coating the tip and surface with self-assembled monolayers (SAMs) ending in one of a variety of known functional groups allows the type and strength of force to be identified and selected. Patterns of two different functional groups are fabricated on the surface to generate images based on known chemical interactions. This technique, chemical force microscopy (CFM), has been used to measure and quantify van der Waals and hydrogen bonding forces between functional groups in ethanol, to correlate adhesion forces with friction forces, and to generate functional group images of chemically patterned samples[1] (see Chapters Five and Six).

The advantages of immersing the AFM probe tip and sample in a liquid such as water have been described quantitatively,[2] and the ability to use aqueous solvents is especially important when studying biological samples.[3] Forces between the tip and substrates (soft, easily damaged biological samples) are at least an order of magnitude lower in water that in air, decreasing the physical influence of the tip (damage) on the substrate. Experiments in water also allow most biological samples to be studied in their native environment.

Recent experiments report the measurement of adhesion forces between inorganic tips (i.e., Si_3N_4, WC) and surfaces (i.e., mica, glass, Au, surfactant monolayers) in water.[4] Most of these reports comment on the difficulty in obtaining reliable data and interpreting them, reflecting the challenges of working in water. Measurements between Si_3N_4 tips and monolayer surfaces terminating in acidic and basic groups have also been reported using AFM[5] and interfacial force microscopy.[6] Probe tips have been modified using glass[7] or latex[4c] spheres, and silane[8] or thiol[6] monolayers. Functionalized Si_3N_4 tips[9] and attached microspheres[10] have also been used to measure the binding forces between DNA

strands[10b] and avidin/biotin groups[9,10a] representing important quantitative investigations of biological recognition processes.

In this study we use CFM to measure adhesion and friction between ionizable groups in water as a function of ionic strength and pH. Alkanethiol monolayers were used to derivatize the tip and sample with COOH or CH_3 groups; silanes were used to terminate Si surfaces in NH_2. Adhesion and friction forces between COOH groups on the tip and sample are modulated with the pH of the surrounding water. There changes have been interpreted in terms of monolayer structure and tip/surface interaction. Friction force images of functional group patterns (COOH/NH_2) fabricated on the surface were obtained with a COOH tip. Contrast in these images follows chemical intuition, with friction greater between COOH/NH_2 tip/sample functional groups than COOH/COOH, and depends greatly on the pH of the surrounding medium.

Experimental Section

All measurements and images were obtained with a Nanoscope III AFM (Digital Instruments, Santa Barbara). In general, Si_3N_4 tips and Si (100) wafer substrates (Silicon Sense, Nashua, NH; test grade, 500 μm thick) were coated with Au by e-beam or thermal evaporation. Freshly evaporated tips and samples were derivatized immediately after use for 2-24 hours from mM solutions. Functional group patterning was performed using di-11-(4-azidobenzoate)-1-undecyl disulfide,[11] (see Chapter One and references therein) as previously reported, and 11-mercaptoundecanoic acid were synthesized using literature procedures.[12] Octadecanethiol was available commercially (Aldrich) and used as received. The free amine of ethyl-4-aminobutyrate hydrochloride (Aldrich) used in the generation of COOH patterns was obtained as previously reported,[1b] while the diaminopropane (Aldrich), used to generate NH_2 patterns, was used as received. Solvents used in chemical manipulations were of reagent grade or better; solvents used in substrate and probe tip functionalization were HPLC grade to reduce the amount of particulate matter. Water was deionized with a Barnstead NANOpure II filtration unit to 18 MΩ·cm resistivity (pH = 6.5-7.0); buffers were made using $NaHPO_4$ or Na_2PO_4 and adjusting using HCl and/or NaOH to a constant total salt concentration of 0.01 M using a pH meter.

Adhesion is calculated from force-distance curves by measuring the magnitude of tip deflection just before pull-off. Each adhesion force value reported is the average of values taken from at least 200 force-distance curves. Friction forces were measured by taking half the difference between the lateral deflection of a tip scanning in the +X and –X directions over a 10 μm length. Each scan results in ~400 deflection points. The friction force measurement constitutes an average value of force at a certain applied normal load, which is controlled by the feedback system. Both the normal and lateral force constants of the tip were known from previous work.[1b] Consult reference 1b for additional experimental details. (See also Chapter Six.)

Results and Discussion

Adhesion in Deionized Water. Adhesion between functional groups was first measured in deionized water (DI H_2O, pH 6.5-7.0). The averages of multiple force-distance curves (at least 200 individual force-distance curves were taken to measure each force value) indicate that the adhesion force between COOH/COOH, CH_3/CH_3, $COOH/NH_2$ tip/surface functional groups are 3.8, 27, and 14 nN, respectively. The adhesion theory introduced by Jackson, Kendall, and Roberts (JKR)[13] can be used to corroborate these values. Equation 7.1 can be used to estimate the pull-off, or adhesion force, F_{ad}, between similar groups on a tip of radius R and the sample in a third medium.

$$F_{ad} = \frac{3}{2}\pi R\gamma \tag{7.1}$$

The work of adhesion, γ, is given by the Dupré equation for two surfaces 1 and 2 in a medium 3. (The work of adhesion between the tip and sample is symbolized by W_{st} in Chapter Six.)

$$\gamma = \gamma_{13} + \gamma_{23} - \gamma_{12} \tag{7.2}$$

In the case of COOH groups in H_2O, the solid-liquid interfacial energy (γ_{i3}) can be estimated at 5 nN/m.[14] The value of γ_{12} in this case is zero. Using a tip with a radius of 60 nN,[15] the adhesion force is 2.8 nN, which agrees nicely with the measured value of 3.8 nN. The same analysis can be applied to the case of the CH_3/CH_3 interaction. The γ_{i3} value in this case is ~46 nN/m,[16] giving an adhesion force of 26 nN, almost identical to the experimentally determined value of 27 nN. In both of these cases, the principles of JKR theory work very well. While in principle the JKR theory can be used to estimate adhesion forces between surfaces with dissimilar functional groups, the calculations are complicated by non-zero γ_{12} values, which are often difficult to measure or compute. In addition, while JKR theory seems to work well for van der Waals, electrostatic, or even hydrogen bonding forces, it does not address chemical interactions. Using recently reported data on the

$COOH/NH_2$ interaction in a dry N_2 atmosphere,[6] the equations of JKR theory would yield an adhesive force an order of magnitude larger than what we measure. The measured value of 14 nN seems to indicate that the predominant interaction between $COOH/NH_2$ groups is electrostatic rather than chemical. The COOH and NH_2 termini are at least partially charged at pH 6.5-7.0.[17] Although other interactions (i.e., van der Waals) may contribute to the total adhesion force, an significant electrostatic component is strongly supported by a diminution of the adhesive force in a salt solution—we have previously measured the adhesion force between COOH and NH_2 groups to be 14 nN in deionized H_2O and 4.5 nN in 0.3 M NaCl.[1b]

Adhesion between COOH Groups as a Function of Ionic Strength. The adhesion (pull-off) forces between Au-coated tips and samples ending in COOH groups was studied as a function of ionic strength to investigate electrostatic interactions further. Figure 7.1 shows adhesion force values measured in water at different NaCl concentrations. As the salt concentrations increase from 0.0001 M to 0.1 M, the adhesion force decreases from 3.7 nN to 1.3 nN. The COOH groups in this solution (pH 6.5-7.0) are partially ionized[17] (see below) and the interaction is probably a combination of short-range hydrogen bonding, and longer-range van der Waals and ionic interactions. Long-range electrostatic interactions are screened in electrolyte solution with a characteristic decay length, the Debye length.[18] The lower plot in Figure 7.1 clearly shows that up to a certain salt concentration the adhesion force varies linearly with the square root of the salt concentration, which is proportional to the reciprocal of the Debye length. So although a hydrogen-bonding interaction is expected intuitively, the screening effect indicates the presence of a longer-range interaction. As the ionic strength increases from 0.1 M to 1.0 M, adhesion increases from 1.3 nN to ~4 nN. At these higher ion concentrations, the Debye length decreases further,[19] and the interactions become quite complex and difficult to calculate or predict. For these reasons the total salt concentration in subsequent experiments was limited to 0.2 M. The adhesion dependence on salt concentration shows

Figure 7.1. The adhesion force between COOH groups on the tip and surface is plotted as a function of salt concentration. The lower graph shows that the adhesion force scales linearly with the square root of salt concentration (proportional to reciprocal of the Debye length) for salt concentrations up to 0.05 M.

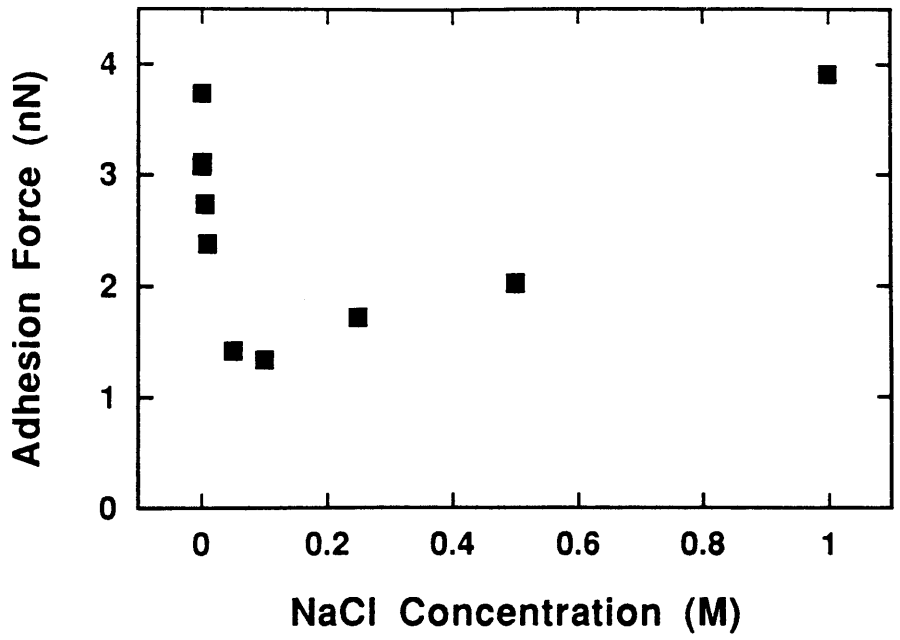
Adhesion Force (nN)
0
1
2
3
4
0
0.2
0.4
0.6
0.8
1
NaCl Concentration (M)

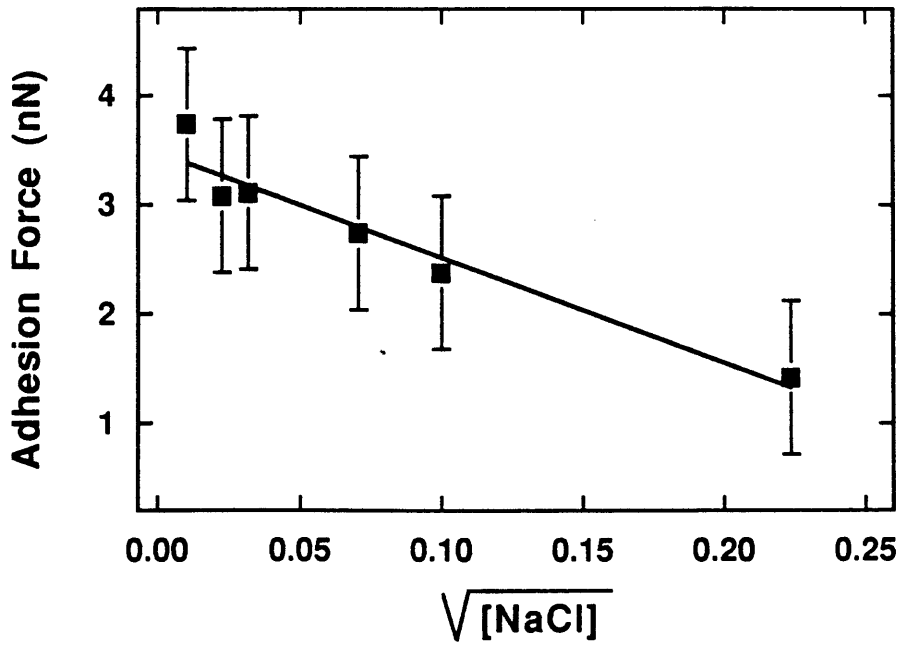
Adhesion Force (nN)
1
2
3
4
0.00
0.05
0.10
0.15
0.20
0.25
√[NaCl]

that the tip/surface interaction is due at least partially to an electrostatic interaction. We are currently investigating these interactions in greater detail; from these data it is apparent that the exact ionic strength of the surrounding solvent must be known before any experimental results can be interpreted quantitatively.

Adhesion Force Measurements as a Function of pH. Force-distance measurements have also been used to measure the pull-off force between functional groups in buffered solutions as a function of pH. Figure 7.2 shows the pH dependence of the COOH/COOH interaction. At low pH, COOH groups on the tip and surface are fully protonated and can interact via hydrogen bonds. Therefore, adhesion in acidic solution is high (pH < 5, F_{ad} > 0.8 nN). These values are in good agreement with those reported above and in Figure 7.1: at 0.2 M ionic strength $F_{ad} \approx 1.3$ nN. At high pH (pH > 6.5), deprotonated groups repel each other electrostatically and no adhesion is observed. The transition between high and low adhesion occurs near pH 6. The appearance of the titration curve is very similar to a classical acid-base titration curve, and the midpoint of the drastic change in adhesion can be taken as an estimate of the surface pK_a of COOH groups. Notably, the surface pK_a of 11-mercaptoundecanoic acid has been determined from contact angle measurements to be 5-6,[17] in agreement with our measurements.

The pH dependence of other acidic and basic groups is currently being investigated. If adhesion forces correlate with protonation and deprotonation, the adhesion behavior should be similar to that of COOH: compared to the curve shown in Figure 7.2, titration curves of acidic groups should be shifted by the appropriate difference in surface pKa, while titration curves of basis groups should be reversed. Adhesion titration data on NH_2 groups and other ionizable surface functionalities will be reported in the near future.

Friction Force Measurements as a Function of pH. By measuring the lateral deflection of the tip, chemical force microscopy can be used to measure the friction force between molecular groups. We have previously shown that the friction force between certain molecular groups correlates with the adhesion force between the same groups in

Figure 7.2. A plot of adhesion between COOH groups on the tip and sample as a function of pH using buffered (0.01 M total salt concentration) aqueous solutions. Each adhesion value was taken from an average of at least 200 force-distance measurements.

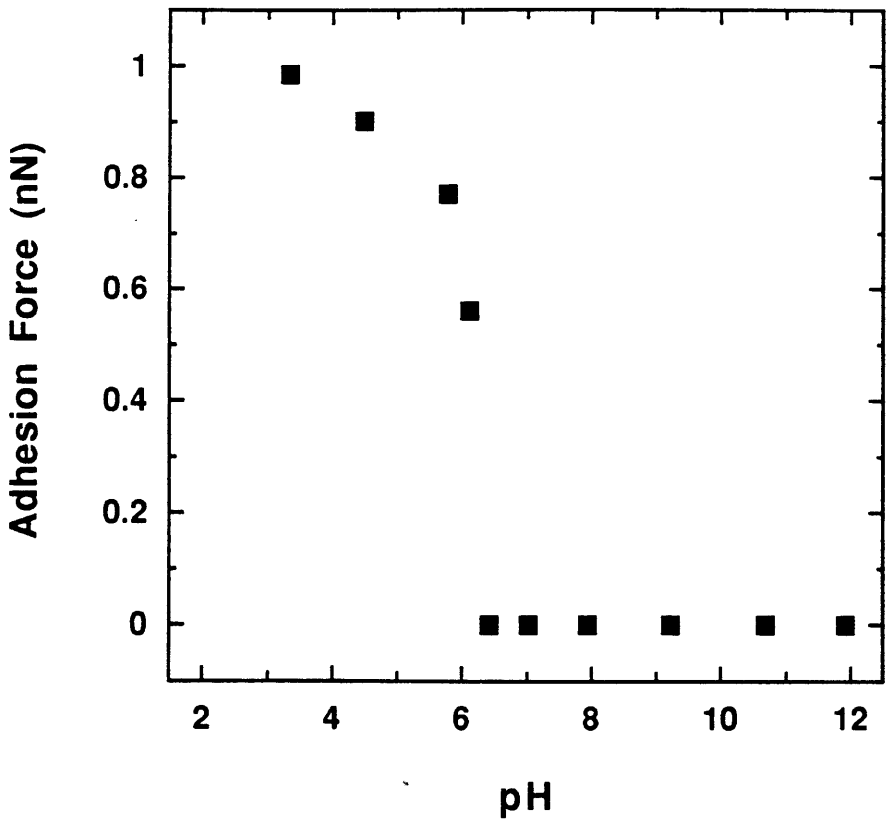
Adhesion Force (nN)
1
0.8
0.6
0.4
0.2
0
2
4
6
8
10
12
pH

EtOH.[1] Here, the friction force between COOH groups on the tip and sample is investigated as a function of pH in aqueous solution.

Classically, fiction force is proportional to applied load. We[1b] and others[20] have shown that friction force between a functionalized probe tip and surface is proportional to surface free energy, and increases linearly with applied normal loads between 1 and 35 nN. Figure 7.3 shows friction vs. load curves between COOH groups at three different pH values. Again, friction force increases linearly with applied load. The friction coefficient μ is given by the slope of each line. Importantly, the friction coefficient is higher at low and high pH, and decreases at intermediate pH. This trend can be clearly seen in Figure 7.4 as a plot of friction coefficient, μ, vs. pH. Note that the minimum friction coefficient (pH 5.8) and the adhesion transition (pH 5.8-6.2, Figure 7.2) occur at the same pH region.

The data presented in Figures 7.2 and 7.4 support a structural model of SAMs terminating in COOH groups recently proposed from contact angle titrations:[17] Monolayers of 11-mercaptoundecanoic acid are protonated at low pH (pH < 3) and deprotonated at high pH (pH > 8). In these completely protonated and deprotonated forms, hydrophilic portions of the COOH or COO^- groups are fully exposed at the surface; these surfaces are completely wet by droplets of acidic and basic H_2O. In aqueous solutions of intermediate pH however (pH = 4-7), hydrogen bonding between neighboring groups exposes the more hydrophobic carbonyl or methylene groups. Contact angles under these conditions increase to a maximum of ~40° at a droplet pH of ~6. Both our adhesion data (Figure 7.2) and friction data (Figure 7.4) agree with these contact angle data and support the structural model hypothesized. At low pH, COOH groups on the tip and surface can interact via hydrogen bonds. Adhesion and friction are therefore relatively high. At intermediate pH, hydrogen bonding occurs between neighboring groups decreasing the adhesion between the tip and surface.[21] The increased exposure of methylene groups at the surface causes the SAMs to be more hydrophobic[22], and thus decreases the friction coefficient. In basic solution, tips and surfaces ending in carboxylate anions do not adhere

Figure 7.3. Plots of friction force vs. normal load force of the tip between COOH groups at three different pH values. The slope of each line is the friction force coefficient, μ.

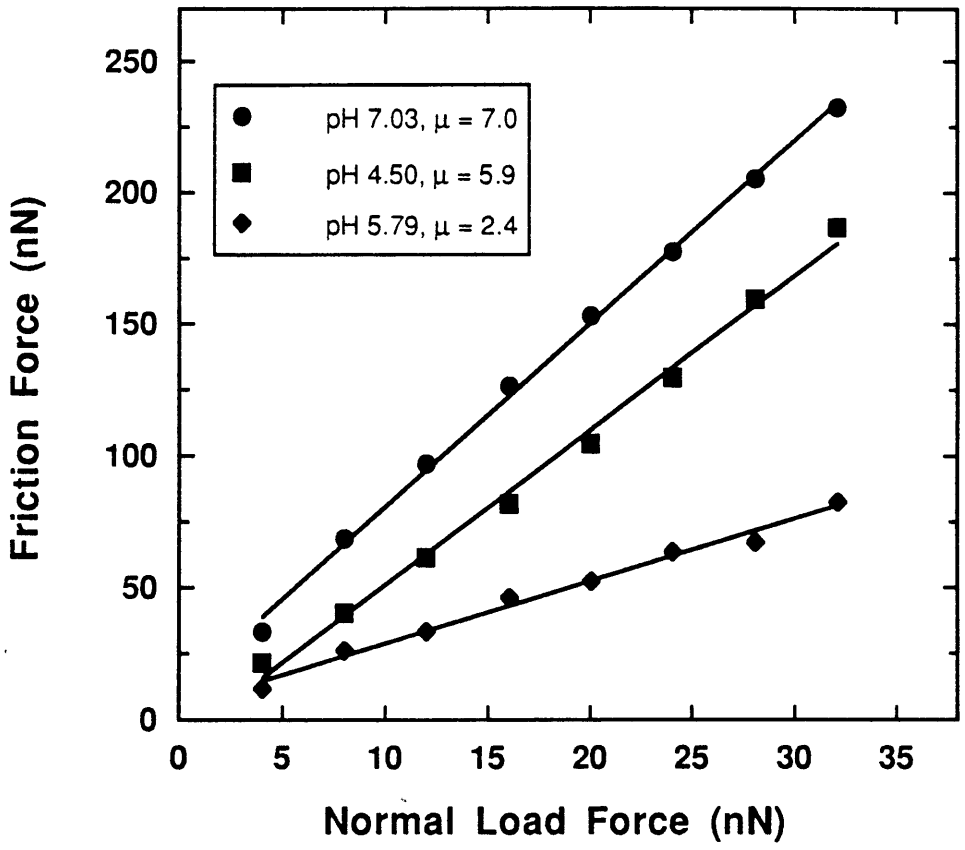
pH 7.03, μ = 7.0
pH 4.50, μ = 5.9
pH 5.79, μ = 2.4
Friction Force (nN)
Normal Load Force (nN)
0
50
100
150
200
250
0
5
10
15
20
25
30
35

Figure 7.4. A plot of friction coefficients vs. pH between tips and surfaces terminating in COOH groups. Each point is taken from the slope of a friction force vs. load curve.

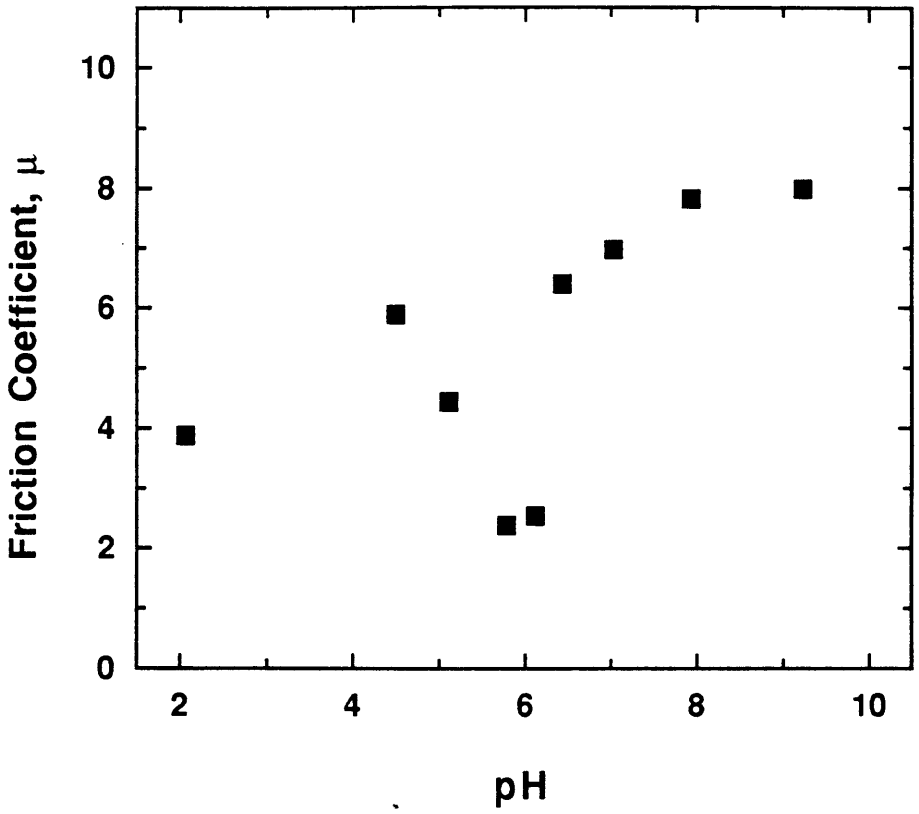
Friction Coefficient, μ
0
2
4
6
8
10
2
4
6
8
10
pH

due to electrostatic repulsion. The friction force ceases to correlate with adhesion force at high pH (pH > 6.5). Since the tip and substrate are charged, the relatively high friction may be caused by disruption of ion layers built up on these surfaces.[23]

Imaging Functional Groups in Water. Though the friction forces between the tip and sample in chemical force microscopy may not always be related to adhesion forces, they can always be modulated by chemical changes in functional groups. Chemical force microscopy has the powerful ability to generate images of chemically patterned surfaces, and therefore to map the distribution of known functional groups. This ability may soon be used in force microscopy investigations of unknown, chemically heterogeneous samples.

Figure 7.5 shows the first image to our knowledge of functional groups in H_2O that can be explained in terms of specific chemical interactions between the tip and surface. The tip was coated with a COOH-terminated SAM, and the surface was patterned with COOH and NH_2 terminal groups using a photosensitive SAM terminating in aryl azide. The image shown was taken in a buffered solution (0.01 M total salt) at pH 7. The bright regions indicate high friction and correspond to regions terminating in NH_2 while the dark regions indicate low friction on areas terminating in COOH. Although a detailed understanding of adhesion and friction behavior between COOH and NH_2 groups is not yet complete, the image in Figure 7.5 is clear and agrees with our chemical intuition: COOH and NH_2 groups may interact via an electrostatic attraction or a proton-transfer reaction and should interact more strongly than the COOH/COOH tip/surface combination.

The image contrast depends greatly on pH. High-contrast images were obtained with COOH tips in solutions at or below pH 7, whereas images taken under basic conditions showed poor contrast. We believe that as more COOH groups on the tip become deprotonated, the electrostatic double-layer on the tip surface becomes more pronounced and dominates the interaction between surface groups. Any difference in friction between the different functional groups on the surface is concealed by the charged double-layer and the corresponding image contrast is very low, if perceptible at all. In solutions where the

tip is neutral or only slightly charged, the difference in interactions between different surface functionalities is readily detected. Thus, we realize that the surrounding medium has a profound effect on the predominant type and relative intensity of various functional group interactions and is an additional parameter that can be used in adhesion and friction studies. The image in Figure 7.5 demonstrates the ability of CFM to successfully map chemically different functional groups in H_2O, a complex but ubiquitous solvent important to biological samples.

Figure 7.5. A friction force image of a sample patterned with COOH and NH_2 groups taken with a tip functionalized with COOH groups. Patterns were fabricated by selectively irradiating SAMs terminating in aryl azide in the presence of a liquid film of the appropriate functionalized amine. Light regions indicate high friction and correspond to area on the surface exposing NH_2 groups. Dark shades indicate low friction forces and represent surface areas ending in COOH. The image was acquired in a buffered solvent at pH 7.

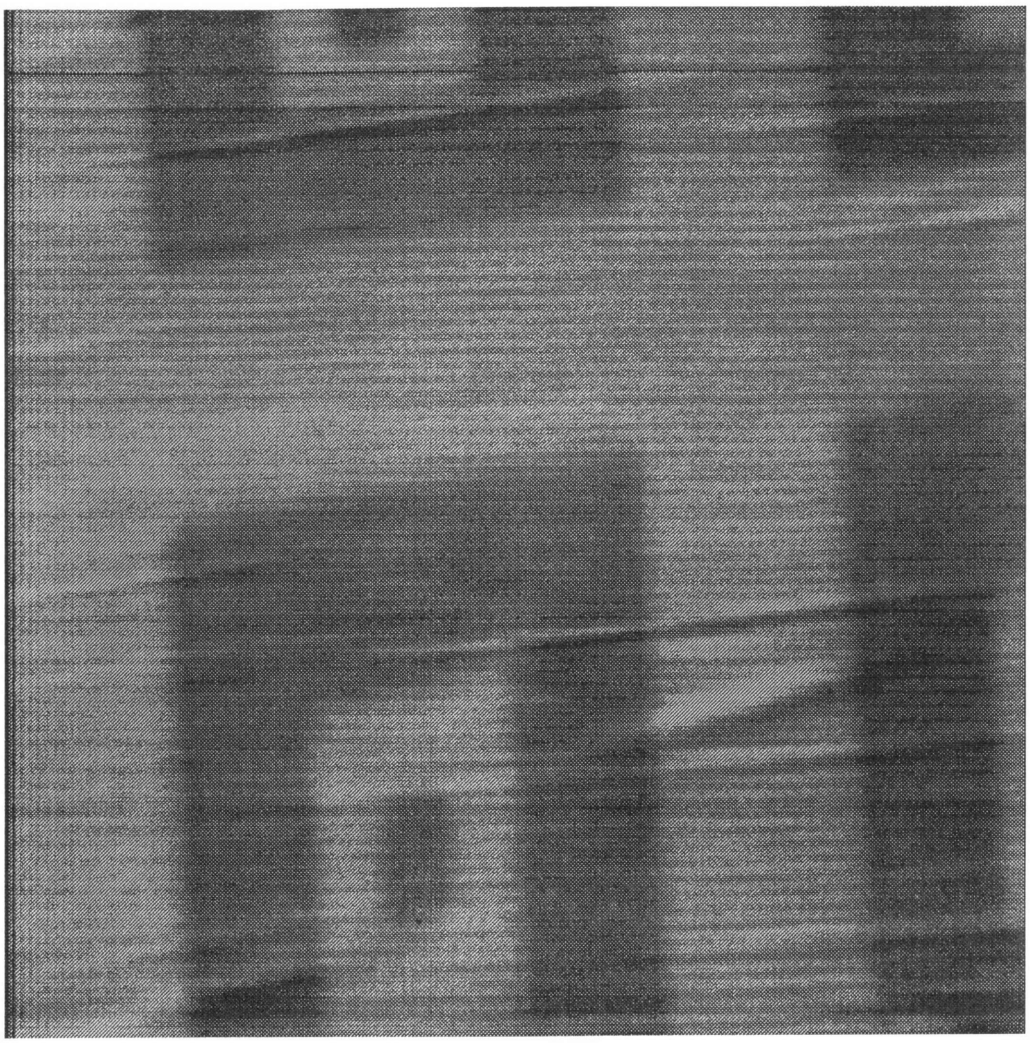

Conclusions

Adhesion and friction forces between known molecular groups have been measured quantitatively by CFM by altering the interacting molecular groups and surrounding medium systematically. This report presents our first experiments in probing specific interactions in H_2O. Notably, the friction coefficient does not always correlate with adhesion strength between the same groups on the tip and surface. We believe that in EtOH, the interactions between functional groups are relatively simple and easy to identify compared to those in H_2O. Friction is seen to correlate with adhesion in EtOH and in H_2O at low and intermediate pH. The lack of correlation under basic conditions can be related to chemical properties on the tip and sample. Although adhesion and friction are most often related, they represent physical processes that may depend differently on complex and subtle factors such as surface molecular structure and electrostatic screening and charging effects. Future investigations in this area will continue to advance fundamental understanding of supramolecular behavior and the role of solvent in intermolecular interactions. This knowledge will be critical in defining new abilities of CFM as a quantitative measurement and imaging tool.

References

1. (a) Frisbie, C. D.; Rozsnyai, L. F.; Noy, A.; Wrighton, M. S.; Lieber, C. M. *Science* **1994**, *265*, 2071. (b) Noy, A; Frisbie, C. D.; Rozsnyai, L. F.; Wrighton, M. S.; Lieber, C. M. *J. Am. Chem. Soc.*, in press.
2. (a) Goodman, F. O.; Garcia, N. *Phys Rev. B* **1991**, *43*, 4728. (b) Hutter, J. L.; Bechhoefer, J. *J. Appl. Phys.* **1993**, *73*, 4123.
3. *STM and SFM in Biology*; Marti, O.; Amrein, M. Eds.; Academic: San Diego, 1993; Chapters 7 and 8.
4. (a) Butt, H.-J. *Biophys. J.* **1991**, *60*, 1438. (b) Weisenhorn, A. L.; Maivald, P.; Butt, H.-J.; Hansma, P. K. *Phys Rev. B* **1992**, *45*, 11262. (c) Li, Y. Q.; Tao, N. J.; Pan, J.; Garcia, A. A.; Lindsay, S. M. *Langmuir* **1993**, *9*, 637. (d) Biggs, S.; Mulvaney, P. *J. Chem. Phys.* **1994**, *100*, 8501.
5. Ishino, T.; Hieda, H.; Tanaka, K.; Gemma, N. *Jpn. J. Appl. Phys.* **1994**, *33*, 4718.
6. Thomas, R. C.; Houston, J. E.; Crooks, R. M.; Kim. T.; Michalske, T. A. *J. Am. Chem. Soc.* **1995**, *117*, 3830.
7. Rabinovich, Y. I.; Yoon, R.-H. *Langmuir* **1994**, *10*, 1903.
8. Barrat, A.; Silberzan, P.; Bourdieu, L.; Chatenay, D. *Europhys. Lett.* **1992**, *20*, 633.
9. Moy, V. T.; Florin, E. L.; Gaub, H. E. *Science* **1994**, *266*, 257.
10. (a) Lee, G. U.; Kidwell, D. A.; Colton, R. J. *Langmuir* **1994**, *10*, 354. (b) Lee, G. U.; Chrisey, L. A.; Colton, R. J. *Science* **1994**, *266*, 771.
11. Wollman, E. W.; Kang, D.; Frisbie, C. D.; Lorkovic, I. M.; Wrighton, M. S. *J. Am. Chem. Soc.* **1994**, *116*, 4395.
12. Bain, C. D.; Troughton, E. B.; Tao, Y.-T.; Evall, J.; Whitesides, G. M.; Nuzzo, R. G. *J. Am. Chem. Soc.* **1989**, *111*, 321.

13. Johnson, K. L.; Kendall, K.; Roberts, A. D. *Proc. R. Soc. London, A.* **1971**, *324*, 301.

14. In general, solid-liquid interfacial energy (γ_{SL}) values can be estimated using Young's equation, $\gamma_{SV} = \gamma_{SL} + \gamma_{LV}\cos\theta$, where θ is the contact angle. Liquid-vapor intefacial energies are generally known (H_2O = 72 nN/m) but both solid-liquid and solid-vapor values are difficult to measure. A value of γ_{SL} = 5 nN/m is reasonable based on contact angle measurements and solubility of carboxylic acids in water and can be used as a good estimate.

15. Tip radii were measured by scanning electron microscopy. Tips used in this study have an average radius of ~60 nm.

16. Young' equation is used confidently in this case. The γ_{SV} value of COOH-terminated *n*-alkanethiols has been measured to be 19 nN/m (see reference 12) with a water contact angle of 112°.

17. Lee, T. R.; Carey, R. I.; Biebuyck, H. A.; Whitesides *Langmuir*, **1994**, *10*, 741.

18. Israelachvili, J. *Intermolecular & Surface Forces*; Academic: San Diego, 1992, pp 125, 199.

19. In solutions of monovalent salts, the Debye length is ~1 nm at 0.1 M and ~0.3 nm at 1.0 M. (See reference 18, p 238.)

20. (a) Liu, Y.; Evans, D. F. *Langmuir* **1994**, *10*, 2241. (b) Green, J.-B. D.; McDermott, M. T.; Porter, M. D.; Siperko, L. M. manusctipt in preparation.

21. Based on the adhesion data in deionized water presented above, a hydrophobic interaction between molecular groups in should result in stronger adhesion than a hydrogen bonding interaction. An increase in adhesion force at intermediate pH has not been detected, however.

22. Though "more hydrophobic" these partially deprotonated COOH groups will still be partially charged. The adhesion force between the tip and surface will still have an electrostatic component, as shown by the data in Figure 7.1.

23. See reference 18, chapter 12.

LIST of PUBLICATIONS

Lawrence F. Rozsnyai, David R. Benson, Stephen P. A. Fodor, Peter G. Schultz "Photolithographic Immobilization of Biopolymers on Solid Supports" *Angew. Chem. Int. Ed. Engl.* **1992**, *31*, 759.

Lawrence F. Rozsnyai, Mark S. Wrighton "Selective Electrochemical Deposition of Polyaniline via Photopatterning of a Monolayer-Modified Substrate" *J. Am. Chem. Soc.* **1994**, *116*, 5993.

C. Daniel Frisbie, Lawrence F. Rozsnyai, Aleksandr Noy, Mark S. Wrighton, Charles M. Lieber "Functional Group Imaging by Chemical Force Microscopy" *Science* **1994**, *265*, 2071.

Lawrence F. Rozsnyai, Mark S. Wrighton "Selective Electrodeposition of Conducting Polymers via Monolayer Photopatterning" *Langmuir*, in press.

Aleksandr Noy, C. Daniel Frisbie, Lawrence F. Rozsnyai, Mark S. Wrighton, and Charles M. Lieber "Chemical Force Microscopy: Exploiting Chemically-Modified Tips to Quantify Adhesion, Friction, and Functional Group Distributions in Molecular Assemblies" *J. Am. Chem. Soc.*, in press.

Christopher H. McCoy, Lawrence F. Rozsnyai, Mark S. Wrighton, "Direct Chemical Tuning of the Electrical Properties of Poly(3-methylthiophene) by Chlorination" Manuscript in preparation.

Lawrence F. Rozsnyai, Mark S. Wrighton "Controlling the Adhesion of Conducting Polymer Films with Patterned Self-Assembled Monolayers" Manuscript in preparation.

Aleksandr Noy, Dmitri Vezenov, Lawrence F. Rozsnyai, Mark S. Wrighton, and Charles M. Lieber "Chemical Force Microscopy: Measuring Adhesion, Friction, and Functional Group Distributions in Aqueous Media" Manuscript in preparation.

BIOGRAPHICAL NOTE

Lawrence F. Rozsnyai was born on December 26, 1968 in Livermore, California. Raised there by two parents with a strong scientific background, he progressed through the public school system with a natural leaning towards math and the sciences. He first conducted research while in high school with the help of Dr. Paul Daley from Lawrence Livermore National Laboratory on the effects of simulated acid rain on plant growth. He then attended the University of California at Berkeley to study chemistry, and returned to LLNL the summer of his junior year to conduct research in scanning tunneling microscopy. This position allowed him to continue research at Lawrence Berkeley Laboratory, and later in the department of chemistry on campus. Work in his senior year with professor Peter Schultz led to a collaboration with the Affymax Research Institute, and his first publication. Larry began graduate school at the Massachusetts Institute of Technology after graduating from the College of Chemistry at Berkeley in 1991. Interested in applied and materials chemistry, he began work with professor Mark Wrighton. While on his way to a vacation in California in 1994, he met professor George Whitesides and established an opportunity to work under his direction as a postdoctoral associate. Larry completed his thesis work and graduated from MIT in June, 1995. He plans to enjoy a relaxing summer and to begin work with professor Whitesides at Harvard University in the fall. While the east coast has given him an increased appreciation of staying indoors and reading, Larry enjoys a variety of outdoor activities including running, cycling, photography, and backpacking—when time and weather allow.